THOU SHALL NOT FLOW: ASSESSING MAGNITUDES AND PROCESSES OF DISSOLVED REACTIVE PHOSPHORUS (P) REMOVAL BY P-SORBING MATERIALS

BY

TAYLOR BERKSHIRE

THESIS

Submitted in partial fulfillment of the requirements
for the degree of Master of Science in Crop Sciences
in the Graduate College of the
University of Illinois Urbana-Champaign, 2021

Urbana, Illinois

Master's Committee:

Assistant Professor Andrew J. Margenot, Chair
Research Assistant Professor Reid Christianson
Assistant Professor Laura Christianson

ABSTRACT

Agricultural phosphorus (P) losses continue to contribute to eutrophication globally. There are currently best management practices that target particulate P losses but are not specifically designed to reduce dissolved reactive phosphorus (DRP) losses. A novel practice is the use of P removal structures. Phosphorus removal structures are designed to intercept surface runoff at the edge of agricultural fields to capture DRP losses. Phosphorus-sorbing media (PSM), waste by-products with high P removal potential, are the basis of P removal structures. The ability of PSM to remove DRP depends on the physical and chemical properties of the PSM, but the estimated DRP removal potential depends on the method used for evaluation.

This M.S. thesis addresses how physical and chemical traits of PSM can differ by PSM type, source, and particle size fractions, how DRP is removed by PSM, and the extent to which methodological differences challenge comparison of DRP removal potential of PSMs. The first chapter evaluates the traits of PSM that influence DRP removal, assesses how DRP is removed by PSM using sequential fractionation, and to what extent these traits vary by PSM type, source, and particle size fraction. These traits are hydraulic conductivity, particle size, reactive metal element composition (total Ca, Mg, Fe, Al, water-soluble Ca and Mg, ammonium-oxalate extractable Fe and Al, and citrate-bicarbonate-dithionite extractable Fe and Al). The second chapter examines how the methodology used to assess DRP removal potential impacts comparability of magnitude and processes of DRP removal. The methodologies used are batch isotherms and flow-through columns.

PSM type played an important role in DRP removal and the hydraulic conductivity of a PSM is a key factor to consider for feasibility in a P removal structure. A larger particle size

fraction such as 4 – 6.3 mm or 6.3 – 8 mm should be used in a P removal structure to maximize DRP removal while maintaining a sufficient hydraulic conductivity. This study showed that differences in metal cation concentrations among PSM type and source are more influential in DRP removal than the difference among particle size fractions. Sequential extraction revealed that certain PSM, specifically steel slag (SS), may be removing DRP differently than commonly assumed with Al contributing to DRP removal and also the Ca removal mechanism including adsorption and not strictly precipitation. This work reveals the importance of accounting for inherent P when determining how DRP is removed by PSM. As demonstrated by sequential extraction of PSM after exposure to DRP, if inherent P is not accounted for, then the magnitude of DRP recovered is not interpretable as inherent P can account for 100% of DRP recovered for some fractions. High inherent P in PSM does not appear to impact the ability to remove P, but is important to quantify to accurately measure which metal cation is responsible for removing P.

This study also highlighted the need for a standard method used for evaluating PSM to increase comparability. In batch sorption isotherms, changing the DRP concentration range and whether an electrolyte solution is used affected DRP removal potential of PSM. The use of an electrolyte solution generally decreased the DRP removal potential, as well the DRP range ≤ 20,000 mg kg^{-1}. Evaluation of the flow-through columns showed that a retention time > 20 s and inflow solution DRP concentration > 0.5 mg L^{-1} would provide the most consistent DRP removal on a mass basis for both types of PSM type for a P removal structure in the field. Batch isotherms and flow-through columns provide different metrics to evaluate DRP removal potential for PSM, but the highest DRP removing PSM remained the same. Testing PSM with flow-through columns revealed that some PSM can have a net P loss as they release previously sorbed DRP as well as additional inherent P. This work also shows that the chemical and

physical traits of PSM are important to their DRP removal potential and that the methods by which PSM are assessed need to be standardized to promote comparability.

ACKNOWLEDGMENTS

First and foremost, I would like to thank my adviser, Dr. Andrew Margenot, for his willingness to accept me into the Soils Lab, his guidance throughout my project, and his patience with my questions and learning adventures. I would like to thank the other members of my research committee: Thank you to Dr. Laura and Reid Christianson for allowing me to work on my project in your lab and all of your support and feedback. The work was supported by the Department of Crop Sciences at the University of Illinois at Urbana-Champaign, including a Samuel R. Aldrich Fellowship to T.B. and a Graduate College Conference Travel Award to T.B.

Thank you to my Soils Lab colleagues and my I-DROP colleagues who not only supported me by answering research questions or helping take samples, but also became dear friends who kept my spirits high and encouraged me throughout my degree. Thank you Kristian Akers for your wonderful support and funny title suggestions. Finally, thank you to my family and friends for supporting me through the ups and down, even if you didn't quite understand what I was doing all the time.

This thesis is dedicated to my mom, thank you for pushing me to be my best and always believing in me, I wish you could be here to see it; and to my son, thank you for being a bright light in my life that keeps me pushing forward.

TABLE OF CONTENTS

CHAPTER 1: EVALUATING RELATIONSHIPS AMONG PHYSICAL AND CHEMICAL PROPERTIES OF PHOSPHORUS-SORBING MATERIALS TO OPTIMIZE PHOSPHORUS REMOVAL FOR PHOSPHORUS REMOVAL STRUCTURES

1.1 Introduction

Eutrophication of surface waters by phosphorus (P) continues to impair global water quality [1] and is predicted to worsen if actions are not taken to reduce P losses [2]. Losses of P from point and non-point (agricultural) sources are a well-known contributor to eutrophication. The P losses contributed by agricultural fields is a combination of surface runoff and subsurface drainage from fields to water bodies as dissolved P and particulate P. Particulate P is the P bound to soil particles [3], and is exported from agricultural fields via erosion. Dissolved orthophosphate P, measured as molybdate-reactive P after 0.45 μm filtration, is known as dissolved reactive P (DRP) and is more bioavailable than particulate P, making DRP a driver for eutrophication [4]. The high water solubility of orthophosphate increases potential DRP loss via surface runoff or tile drainage effluent, particularly during storm events [5].

The Gulf of Mexico hypoxic zone is one of the largest eutrophication hotspots in the world, caused by the nutrient losses to the Mississippi River Basin [6]. Agricultural contributions to total P export average 49% [7] and range 32 – 80% among the states in the Mississippi River Basin [8,9]. To decrease the size of the hypoxic zone to less than 5000 km^2, the U.S. Environmental Protection Agency (EPA) Hypoxia Task Force created the Gulf Hypoxia Action Plan in 2008 that seeks to reduce riverine loads of P (and nitrogen) [6,10]. By 2015, twelve of the 31 states in the Mississippi River Basin developed nutrient reduction strategies [11]. These state-specific but overall similar strategies outline best management practices (BMP) to reduce nutrient losses from both point and agricultural sources [12]. As the leading state contributor of

total P to the Mississippi River Basin, Illinois is a priority state for DRP loss reduction [13]. The estimated annual average total riverine P export from Illinois during 2013-2017 was 19.5 million kg, 48% of which was estimated to be from agricultural sources [14] and 50% of the total P loads were estimated to be DRP [15], making DRP a target for P loss mitigation.

The BMPs for non-point sources, notably cover crops, reduced tillage, and fertilizer management [8,14,16], outlined in state nutrient loss reduction strategies to mitigate P losses do not specifically target DRP reduction. Cover crops and conservation tillage chiefly reduce particulate P losses from agricultural fields, but may not necessarily reduce DRP losses and under some conditions may even increase DRP losses [17,18]. Off-field BMPs include bioreactors, buffers (saturated or riparian), and constructed wetlands [14]. Bioreactors are designed to reduce nitrogen losses [19,20], buffers limit nitrogen and particulate P losses [21,22], and wetlands remove nitrate and particulate P [23,24]. However, none of these are designed to reduce DRP transfer to surface waters, and there are variable results on how well these practices mitigate DRP losses. For example, DRP removal for wetlands can range from 7 – 99% [25-27]. For some buffers, DRP loss reductions of 30 – 85% have been reported [28-31]. A BMP that can consistently reduce agricultural DRP export would offer a management tool to meet nutrient loss reduction goals.

Phosphorus removal structures are an emerging, edge-of-field P loss mitigation practice that employ a P-sorbing medium (PSM) to remove DRP from water exiting agricultural fields as run-off or tile drainage effluent. Limited evaluations of P removal structures located in Task Force states of Oklahoma [32], Ohio [33], and Indiana [34] have shown promise of 27 – 55% DRP removal. However, P removal structures are not currently included as a BMP in any of the twelve Task Force states' nutrient reduction strategies [12,16,35]. Along with the benefit of

providing a management tool that targets DRP losses, PSM also allow for the reuse of material that would otherwise be discarded. Phosphorus-sorbing materials used in P removal structures are industrial by-products or waste materials [36] and readily available across the Mississippi River Basin [37-39], offering a low-cost to source. Candidate PSM have been evaluated typically based on their high concentrations of total Ca (< 1 – 38.6%), Mg (< 1 – 9.1%), Fe (< 1 – 50.9%), and Al (< 1 – 10.5%) [37-39]. Common PSM candidates include fly ash [40,41], gypsum [42,43], drinking water treatment residuals [44,45], zeolite [41,46], acid mine drainage treatment residuals (AMDR) [47,48], and steel slag (SS) [20,49]. However, AMDR and SS generally have the highest DRP removal potential [47,50].

An ideal PSM maximizes DRP removal and saturated hydraulic conductivity (K_{sat}). Hydraulic conductivity strongly tracks with particle size distribution and determines the maximum transmission rate of water through the PSM matrix. As DRP exports are highest during and directly after rain events [5], it is important that a P removal structure is effective during high water flow. Small particle size diameter (< 2 mm) generally entails a low K_{sat} and thus transmission rate. If the rate of transmission is slower than the rate of inflow, the P-loaded water will bypass the P removal structure. In contrast, a high K_{sat} allows percolation of water and DRP removal during a storm event. Decreasing particle size generally entails greater surface area and thus a greater P sorption capacity, albeit at a cost of lower K_{sat} [51,52]. Previous studies generally evaluated either the smallest (< 2 mm) to identify maximum P removal [38,47] or a large (> 6.3 mm) particle size fraction to prevent clogging in P removal structures [49,50,53]. However, these studies have not evaluated the relationship between DRP removal and particle size fractions of PSM [38,50,54].

Two properties of PSM that interact to determine DRP removal are particle size distribution and composition. DRP removal is inversely related to particle size diameter due to the availability of surface binding sites [52,55]. Dissolved reactive P removal is impacted by the variation in PSM particle size distribution, but concurrent shifts in metal cation concentrations could also contribute to DRP removal. Two types of PSM are commonly conceptualized based on metal cation composition and thus expected DRP removal mechanisms: (1) Ca- and/or Mg-rich PSMs such as SS, and (2) Fe- and/or Al-rich PSMs such as AMDR [38]. Dissolved reactive P precipitates with Ca and Mg at pH > 7 or is sorbed by Fe and Al at pH < 6.5 [56]. Characterizations of PSM generally entail a combination of total Fe, Al, Ca, and Mg; water-soluble (WS) Ca and Mg; ammonium-oxalate (AO) Fe and Al; or citrate-bicarbonate-dithionite (CBD) Fe and Al concentrations (e.g. [37,39,47]). However, total concentrations are not necessarily indicative of the reactive pools, the readily soluble concentrations of the metal cation (WS, AO), that react with phosphate in solution. Reactive pools better predict DRP removal [36,57,58]. To complement measurements of total and reactive metal cation pools thought to explain and predict PSM removal of DRP, Fourier transform infrared spectroscopy (FTIR) offers characterization of PSM functional group composition. Fourier transform infrared spectroscopy measures the relative abundance of polar bonds and thus functional groups of mineralogical constituents of PSM, as well as metal-P bonds that are expected to form during PSM removal of DRP. The proposed compositional differences in AMDR and SS and mechanisms of P removal can therefore be characterized by FTIR spectroscopy.

Sequential chemical fractionation of P can be used to test hypothesized removal of DRP by PSM type according to metal cation composition. Sequentially extracted P fractions can be interpreted to approximate P pools based on solubility-based extraction of discrete compounds of

Al, Fe, and Ca [59]. A commonly employed fractionation of inorganic P is that of Chang and Jackson [60] as modified by Zhang and Kovar [59], which separates P into five fractions: NH_4Cl-P (soluble and loosely bound P), NH_4F-P (Al-P), NaOH-P (Fe-P), $Na_3C_6H_5O_7$, $NaHCO_3$, $Na_2S_2O_4$ or CBD-P) (reductant-soluble P), or H_2SO_4-P (Ca-P) [59]. Steel slag would be expected to recover DRP as NH_4Cl-P and H_2SO_4-P, whereas AMDR should recover DRP as NH_4Cl-P, NH_4F-P, and NaOH-P. Previous studies have conducted sequential fractionation of PSM following P saturation, but did not evaluate P already present (i.e., inherent P) or how P binding may change with different P concentrations [38,61]. Determining P extracted from P-untreated PSM is necessary as a background to accurately determine how much of an added amount of P is recovered in a given fraction. Sequentially extracted P fractions (mg P kg^{-1} PSM) can be evaluated based on metal cations and/or degree of crystallinity to identify the fate of DRP removed. Additionally, comparing P removal fate inferred by sequential fractionation with independently determined measures of PSM metal cation concentrations (e.g., total, WS, AO, CBD) can be used to test to what extent metal cation concentrations are an accurate predictor of DRP removal in PSM. Phosphorus pools proxied by sequentially extracted P fractions approximately can correspond to the metal cations thought to be responsible for PSM removal of DRP. For example, NaOH-P is interpreted as Fe-P which would correspond with the metal cation composition of Fe_{ao} because it is interpretable as a reactive pool of Fe.

This study examined how physical and chemical traits of PSM changed among PSM type, source, and particle size fractions. The first objective was to test the hypothesized tradeoff between DRP removal and K_{sat} by PSM type, source, and particle size fractions to identify the relative importance of these in maximizing K_{sat} and P removal. We hypothesized PSM type to have a greater role than source or particle size fractions, and larger (> 4 mm) particle size

fractions to maximize the tradeoff. The second objective was to determine the extent to which PSM composition (total, WS, AO, CBD concentrations, functional group chemistry) differed among PSM type, source, and particle size fractions. We hypothesized the greatest difference in metal cation concentration between SS and AMDR, then between the smallest and largest particle size fraction for a given PSM, and the least difference by source. The third objective was to determine to what extent and which metal cation reactive pools (WS, AO, and CBD) drive DRP removal by PSM as assessed by sequential fractionation. We hypothesized that Ca_{ws}, Mg_{ws} would be associated with NH_4Cl-P and H_2SO_4-P and would best explain DRP removal across SS sources and particle size fractions. In contrast, we hypothesized that Fe_{ao}, Al_{ao}, Fe_{cbd}, and Al_{cbd} would be associated with NH_4Cl-P, Al-P, Fe-P, and CBD-P and would best explain DRP removal across AMDR sources and particle sizes.

1.2 Materials and Methods

1.2.1 Filter Media and General Characterization

This study examined two sources of SS and two sources of AMDR, two common PSM with demonstrated potential for P sorption [39,41,62]. Steel slag is a granular Ca-rich by-product of steel production with metal cation concentrations reported to range 21.7 – 38.6% Ca, < 1 – 9.1% Mg, < 1 – 24.3% Fe, < 1 – 8.5% Al and 6.4 – 18.8% Si [38,54,61,63,64]. Steel slag can have a high P-sorption capacity (160 – 44,250 mg P kg^{-1} PSM) and can be rejuvenated with an aluminum sulfate solution to precipitate Al hydroxide minerals [49] to extend the lifespan of the P removal structures [37,39,65]. Steel slag was obtained from two sources, TMS International Corporation in Parkhill, PA (SS1) and the US Steel Corporation in Granite City, IL (SS2). Acid mine drainage treatment residuals (AMDR) are the product of processing mine drainage waste. This acidic waste (pH < 4) [66] is typically neutralized (to pH ~7) with alkaline materials such as calcium carbonate, which results in metal hydroxide precipitation [37,47]. Neutralization is done to improve the water quality

of surrounding streams by reducing the pollution of toxic metals and sulfates with mine drainage [67]. Acid mine drainage residuals used in this study are a fine (< 2 mm diameter) material with varying composition depending on the source from < 1-30.1% Ca, < 1-3.8% Mg, 8.4-50.9% Fe, < 1-10.5% Al, and 1.8-20.9% Si [20,38,47,48]. Acid mine drainage residuals can have high P-sorption capacity (1,820 – 157,000 mg P kg^{-1} AMDR), higher than SS [37,47]. The two AMDRs tested were sourced from the Pennsylvania EPA (AMDR1) and the Blue Valley Mine Drainage Treatment and Fish Culture Station in Brandy Camp, PA (AMDR2).

1.2.2 Particle Size Determination

Particle size fractions of PSM were quantified by dry sieving and hydrometer [68]. An oven-dry equivalent of 400 g ± 5 g of sample was dry sieved through a set of 10, 8, 6.3, 4, and 2 mm sieves. The mass of each particle size fraction was determined to calculate PSM particle size distribution. The particle size fraction < 2 mm was further separated into < 0.002 mm, 0.002 – 0.05 mm, and 0.05 – 2 mm fractions by hydrometer. Briefly, 40.00 g ± 0.05 g of oven-dry < 2 mm PSM was shaken for 16 h at 120 rev min^{-1} in 100 mL 5% (m/v) sodium hexametaphosphate solution to disperse particles [69]. The suspension was brought to a final volume of 1.000 L with 18.2Ω·cm water at 25 °C. A control was also made for temperature and solution viscosity corrections consisting of 100 mL 5% (m/v) sodium hexametaphosphate solution brought to the same volume as the samples, thoroughly mixed by inverting the cylinder three times. A hydrometer was used to measure the settling rates of particles in suspension at 40 sec and 6 h to estimate 0.05 – 2 mm and < 0.002 mm diameter particle sizes respectively. The particle size fractions were divided into six fractions of < 2 mm ($PSM_{<2}$), 2-4 mm ($PSM_{2\text{-}4}$), 4-6.3 mm ($PSM_{4\text{-}6.3}$), 6.3-8 mm ($PSM_{6.3\text{-}8}$), 8-10 ($PSM_{8\text{-}10}$) mm, and bulk (PSM_{bulk}) which is a non-sieved, bulk sample containing all particle size fractions. If there is only one particle size fraction for the

PSM, then no subscript was used. When comparisons are made between the PSM types and SS sources, SS_{bulk} was used.

1.2.3 pH

The pH of all PSM particle size fractions was measured with a 1:1 PSM mass to 18.2Ω·cm water volume ratio [70]. They were equilibrated for 30 min with two stirrings and allowed to settle for an additional 10 min. The pH was measured after equilibration of 24 h in the batch sorption isotherm extracts.

1.2.4 Batch sorption isotherms

Phosphorus removal of all PSM particle size fractions was determined via batch sorption isotherm experiments. For consistency with previous evaluations of PSM [61,71], a solid to solution ratio of 1:20 using 1.50 ± 0.05 g air-dry mass of PSM to 30 mL of a gradient concentration of PO_4^{3-}-P L^{-1} was selected. This ratio was also chosen because a lower ratio requires a longer equilibration time, potentially introducing discrepancies between P removal determined by batch isotherms of PSM versus field-scale P removal structures [39].

The equilibration time for batch sorption tests was first established by conducting batch sorption at varying shaking intensities of 100, 200 and 250 rev min^{-1} with an initial DRP concentration of 20 mg PO_4^{3-}-P L^{-1} as potassium monophosphate in an 18.2Ω·cm water background. Supernatant was sampled at 4, 8, 12, 24, 36, and 48 h by centrifugation and filtration (0.45 μm cellulose filter). The supernatant was analyzed for molybdate-reactive P (MRP) by colorimetry [72]. The equilibration time for 20 mg P L^{-1} was 48 h at 100 rev min^{-1}, 24 h at 200 rev min^{-1}, and 20 h at 250 rev min^{-1}. Multiple evaluations of steel slag have identified a 24 h equilibration time for batch isotherms [20,36,38]. An oscillation frequency of 200 rev min^{-1} was selected because it resulted in similar DRP removal as for 100 rev min^{-1}, but at a shorter

duration. Additionally, there was no visual evidence of particle slaking at 200 rev min^{-1}, but there was for 250 rev min^{-1} which could lead to an overestimation of P removal by increasing the availability of metal cations for sorption (Fe, Al) or precipitation (Ca, Mg).

Batch sorption tests were then conducted in quadruplicate using an initial DRP concentration of 0, 100, 200, 400, 600, 800, and 1000 mg kg^{-1} (0 – 50 mg L^{-1}) as potassium monophosphate in 18.2 MΩ·cm water. At the end of equilibration, the supernatant was immediately filtered (0.45 µm cellulosic filter), DRP was quantified as MRP by colorimetry [72] to calculate the filtrate final concentration of P (mg kg^{-1}). With the initial DRP concentration added and the final DRP concentration remaining in the filtrate known, the percent DRP removal was calculated:

$$\text{Percent DRP removed: } \left(\frac{DRP\ added - Final\ DRP\ Concentration}{DRP\ added}\right) * 100 \quad (1)$$

1.2.5 Saturated hydraulic conductivity

A constant head tank (65 cm) was constructed to supply water to a PSM-packed column (26 cm length; 5.1 cm diameter). The outflow from the column was collected in a graduated cylinder over 15 sec. The K_{sat} was determined using Darcy's law:

$$K_{sat} = \frac{Q}{iA} \quad (2)$$

where K_{sat} is the saturated hydraulic conductivity (cm s^{-1}), Q is the discharge (cm^3 s^{-1}), i is the hydraulic gradient (cm cm^{-1}), which is the change in head over the length of the packed PSM in the column, and A is the cross-sectional area (cm^2) of the column. The values for A and i remained constant for all materials.

1.2.6 Total metal cation analysis

Total Fe (Fe_{tot}), Mg (Mg_{tot}), and Ca (Ca_{tot}) concentrations of all PSM particle size fractions were determined according to the U.S. Environmental Protection Agency (USEPA) method 3050B [73] using inductively coupled plasma mass spectrometry. Total Al was not measured due to detection issues with ICP-MS. In brief, 1.0 g oven-dry weight was digested at 95°C ± 5°C with 15 mL concentrated nitric acid and 2 mL 30% hydrogen peroxide, and the digestate as analyzed for Fe, Mg, and Ca.

1.2.7 Reactive Fe and Al

Ammonium oxalate extractable Fe (Fe_{ao}) and Al (Al_{ao}) were determined for PSM particle size fractions as a metric of amorphous Fe and Al oxides known to have high P sorption capacity. To determine Fe_{ao} and Al_{ao}, 0.2 M 30 mL ammonium oxalate solution (pH 3.0) was added to an oven-dry equivalent of 0.50 g ± 0.05 g PSM, wrapped with aluminum foil and shaken horizontally for 2 h, centrifuged at 3724 *g* for 15 min, and filtered using 0.45 µm cellulosic filter paper [74]. The filtrate was analyzed for Fe and Al via ICP-MS.

The CBD extraction was sequentially performed on the residual PSM following the ammonium-oxalate extraction, it represents crystalline Fe and Al oxides. The CBD extractable Fe (Fe_{cbd}) and Al (Al_{cbd}) were determined for PSM particle size fractions. The CBD extraction was performed by combining 0.5 g $Na_2S_2O_4$ and 6.0 g $Na_3C_6H_5O_7$ with the residual PSM following ammonium oxalate extraction and with 30 mL DI water. The mixture was shaken for 16 h at 120 rev min^{-1}, centrifuged at 3724 *g* for 15 min, and filtered using a 0.45 µm cellulosic filter paper [74]. Filtrate Fe and Al concentrations were quantified by ICP-MS.

1.2.8 Reactive Ca and Mg

To determine water-soluble Ca (Ca_{ws}) and Mg (Mg_{ws}), 20 mL 1 M NH_4OAc, pH 7.0, extracting solution was added to 2.0 g PSM and shaken for 30 min at 200 rev min^{-1} on a reciprocating shaker. The extract was filtered through 0.45 µm cellulosic filter paper and concentrations of Ca and Mg in the filtrate were quantified via ICP-MS.

1.2.9 Attenuated total reflectance Fourier transform infrared (ATR-FTIR) spectroscopy

Fourier transform infrared spectroscopy was used to determine relative abundance of polar bonds relevant to PSM mode of action, including P and the metal cation binding partners thought to operate in removal of P by PSMs. Two regions of the infrared spectrum were used: mid-infrared (MIR) and far-infrared (FIR). A portion of the spectrum overlaps between the MIR and FIR, but both offer a range of the infrared spectrum that the other does not. The MIR allows for evaluation of higher wavenumbers (> 1800 cm^{-1}), while the FIR allows for evaluation of lower wavenumbers (< 400 cm^{-1}).

For each PSM (bulk and fractions), a DRP-untreated and DRP-treated sample were analyzed by FTIR. The DRP-treated sampled was obtained by equilibrating 1.50 ± 0.05 g of PSM with a solution of potassium monophosphate equivalent to 1000 mg P kg^{-1} PSM (24 h), following the methods of the batch sorption isotherms. Spectra were collected on a subsample of < 2 mm ground, air-dry PSM used for the sequential fractionation. Spectra were collected on a Nicolet iS50 spectrometer with a deuterated triglycine sulfate (DTGS), single-bounce attenuated total reflectance (ATR) (ThermoFisher, Madison, WI) across the mid-infrared (MIR) region of 4000 – 400 cm^{-1}. Spectra were also collected in the partial MIR and far-infrared (FIR) region of 1800 – 100 cm^{-1} using the same approach as MIR to capture the full range of functional groups present in the PSM. A total of 128 co-added scans were collected to produce one spectrum. Each

PSM sample was scanned and the three replicates for the specific PSM were averaged and produced one spectrum per sample. Spectral subtractions were used in order to enhance features in the phosphate absorbance band (800-1300 cm^{-1} [75]) in DRP-treated PSM. Spectral subtractions were done by subtracting the average DRP-untreated spectrum the average DRP-treated spectrum to produce one spectrum for each PSM. Some limitations of subtraction include peak convolution, inconsistencies in the fineness of the < 2 mm, and low absorbance with low concentrations of elements [76].

Spectra were interpreted based on the characteristic vibrational frequencies (cm^{-1}) of minerals previously identified for AMDR and SS. Minerals commonly present in SS include portlandite [37,77,78], dicalcium silicate [79-84], tricalcium silicate [79-85], dicalcium ferrite [79,82,83], lime [79,80,83,86], periclase [77,79,83,87], and merwinite [77,81,85,87]. Minerals commonly present in AMDR include calcite [38,88,89], goethite [37], brucite [88,89], and hematite [37,90]. FTIR spectra of these minerals were used to interpret PSM spectral features.

1.2.10 Sequential Fractionation for Al-, Fe-, and Ca-P

PSM were equilibrated with 100 mg DRP kg^{-1} or 1000 mg DRP kg^{-1} for 24 h. The supernatant was filtered through 0.45 µm cellulosic filter paper and then the remaining PSM were air-dried and ground to < 2 mm. The Chang and Jackson [60] sequential fractionation as modified by Zhang and Kovar [59] was used to estimate 1) NH_4Cl-P (soluble and loosely bound P), 2) NH_4F-P (Al-P), 3) NaOH-P (Fe-P), 4) $Na_3C_6H_5O_7$, $NaHCO_3$, $Na_2S_2O_4$ or CBD-P) (reductant-soluble P), and 5) H_2SO_4-P (Ca-P). The two P treatments, +100 and 1000 mg kg^{-1}, underwent sequential fractionation, as well as a no P added control (i.e., inherent P). First, 0.4 g air-dried and ground PSM were extracted in 20 mL 1 M NH_4Cl for 30 min, centrifuged, and decanted. Twenty mL 0.5 M NH_4F were added to the residuals, shaken for 1 h, centrifuged,

decanted, and washed twice with 10 mL 6.8M NaCl that was combined with the extract. Then, 20 mL 0.1 M NaOH was added to the residuals, shaken for 17 h, centrifuged, decanted, and washed twice with 10 mL 6.8 M NaCl that was combined with the extract. Next, 10 mL 0.3M $Na_3C_6H_5O_7$and 2 mL 1 M $NaHCO_3$ were added to the residuals and heated for 15 min at 85°C. Next, 0.4 g $Na_2S_2O_4$ was added with rapid stirring to mix and heated at 85°C for another 15 min. The samples were then centrifuged, decanted, and washed twice with 10 mL 6.8 M NaCl that was combined with the extract. Finally, 20 mL 0.25 M H_2SO_4 were added to the residuals, shaken for 1 h, centrifuged, decanted, and the residuals washed twice with 10 mL 6.8 M NaCl that was combined with the extract. The P in the extracts was quantified via ICP-MS.

The NH_4Cl-P was interpreted as soluble and loosely bound P and the metal cation responsible could be Fe, Al, Ca, or Mg (total and/or water-soluble). The NH_4F-P was interpreted as Al-P, corresponding to the metal cation composition of Al_{ao} , the reactive pool of Al. NaOH-P was interpreted as Fe-P, corresponding to Fe_{ao}. The CBD-P was interpreted as reductant-soluble P or occluded P, corresponding to Fe_{cbd} and Al_{cbd}. The H_2SO_4-P was interpreted as Ca-P, corresponding to the insoluble Ca_{tot} and Mg_{tot} as these are the metal cation related pools, including Mg as there is not a fraction that is interpreted specifically for Mg.

Phosphorus recovery was determined as a percent of the DRP added. Phosphorus recovery was calculated as:

$$\frac{Extracted\ P - Inherent\ P}{DRP\ added} * 100 \quad (3)$$

where extracted P is the concentration of DRP removed as a particular fraction, inherent P is the extractable P from the PSM (+0 mg kg^{-1}), and DRP added is either +100 or 1000 mg kg^{-1}. The P recovery was determined both by the fraction and the sum of fractions and for both +100 and 1000 mg kg^{-1}.

1.2.11 Total P

Every PSM particle size fraction was evaluated to determine the total P within the PSM (i.e., total inherent P) by digesting 0.25 g air-dried PSM ground to < 2 mm diameter in 2 mL glacial HNO_3 at room temperature for 16 h. The mixture was then heated to 100°C for 1 h. Next, an additional 2 mL glacial HNO_3 was added and the mixture was digested for 2 h at 100°C. Digestates were allowed to cool for 30 min before adding 0.125 mL H_2O_2. The samples were vortexed to homogenize and heated for an additional 30 min. Once more, digestates were cooled for 30 min, 0.125 mL H_2O_2 was added, samples were vortexed to homogenize, and then heated for 30 min. Finally, the digestates were cooled again for 30 min, 0.25 mL H_2O_2 was added and digested for 1 h. The digestates were cooled and diluted to 10 mL with 18.2Ω·cm water. A 1 mL aliquot was diluted 5-fold with 18.2Ω·cm water and colorimetrically analyzed for total P as MRP.

1.2.12 Statistical Analyses

Analyses were performed using SAS v9.4 (Cary Institute, NC). Response variables were evaluated for the assumptions of normality of residuals and homogeneity of variances. Mean differences between particle size fractions of the same PSM and among particle size fractions of different PSM were evaluated using Tukey's test with significance at $p \leq 0.05$. This was done for K_{sat}, Fe_{tot}, Ca_{tot}, Mg_{tot}, Ca_{ws}, Mg_{ws}, Fe_{ao}, Al_{ao}, Fe_{cbd}, and $Al_{cbd.}$ For the PSM_{bulk} comparisons, Al_{cbd} was log-transformed to achieve normality before evaluation using Tukey's test.

Mean differences for each fraction of the sequential fractionation for +0, 100, and 1000 mg kg^{-1} within each particle size fraction and across particle size fractions for either +0, 100, or 1000 mg kg^{-1} were evaluated using Tukey's test with significance at $p \leq 0.05$. For NH_4Cl-P, both AMDR2 and $SS1_{4\text{-}6.3}$ were log-transformed to achieve normality within the PSM to evaluate

DRP treatments of +0, 100 and 1000 mg kg^{-1} using Tukey's test with significance at $p \leq 0.05$. Welch's ANOVA (non-homogenous) was used for the NH_4Cl fraction of SS2 for +0 and 1000 mg kg^{-1} comparisons across all particle size fractions to test significance of mean differences. For NH_4F-P, SS1 particle size fractions for +1000 mg kg^{-1} were log-transformed to achieve normality. For H_2SO_4-P, $SS2_{4\text{-}6.3}$ required a non-parametric test (Kruskal-Wallis) for mean difference comparisons within the particle size fraction for +0, 100, and 1000 mg kg^{-1}.

1.3 Results

1.3.1 Particle Size Determination

The AMDR was finer than SS_{bulk}. Both AMDR samples consisted only of < 2 mm diameter particles whereas SS had up to five particle size fractions, depending on the source. While $AMDR1_{<0.002}$ was 9-fold higher than $AMDR2_{<0.002}$, $AMDR2_{0.05\text{-}2}$ was nearly 8-fold higher than AMDR1 (Figure 1). Though SS2 had a greater distribution across particle size diameters than SS1, the < 2 mm fraction was a similar proportion for both SS. The proportion of $SS2_{<0.002}$ was more than double that of $SS1_{<0.002}$ but both fractions constituted a relatively minor component of particle size distribution. Steel slag $1_{0.05\text{-}2}$ was greater than $SS2_{0.05\text{-}2}$ (9.1% vs. 8.5%). Steel slag 1 particle size distribution was dominated by the 2 – 4 mm (48%) and 4 – 6.3 mm (42%) particle size fractions. Steel slag 2 particle size distribution included 6.3 – 8 mm (29%) as well 8 – 10 mm (17%) that was not present in SS1.

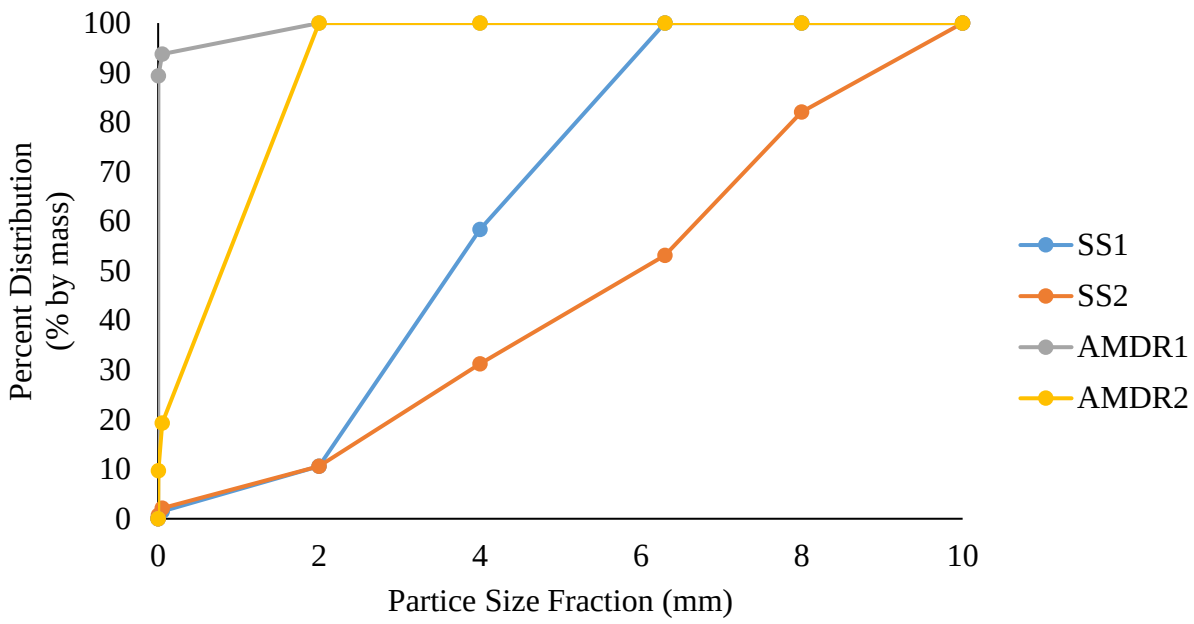

Figure 1. Cumulative total of particle size fraction distribution by mass for steel slag 1 (SS1), steel slag 2 (SS2), acid mine drainage residuals 1 (AMDR1), and acid mine drainage residuals 2 (AMDR2). The particle size fractions were measured by dry sieving (10 - 2 mm) and hydrometer (< 2 mm).

1.3.2 pH

Steel slag were strongly alkaline (pH > 9.0) whereas AMDR were slightly acidic to slightly alkaline (6.3-7.9) (Table 1). The mean pH of AMDR1 (7.9) was over one unit higher than AMDR2 (6.3). The mean pH of $SS2_{bulk}$ was two units higher than $SS1_{bulk}$ (11.2 vs 9.3). SS1 particle size fractions exhibited similar pH, except for $SS1_{2\text{-}4}$ that had a slightly lower pH (10.8). The pH of SS2 particle size fractions were overall similar, with the exception of a higher pH for $SS2_{<2}$ (12.8).

The pH after equilibration of 24 h in batch isotherms increased or decreased as the initial DRP concentration (0-1000 mg P kg^{-1} PSM) increased. Compared to the pH of the material itself, the pH of AMDR1 (+0 mg kg^{-1}) dropped from 3.8 units after equilibration and increased 1.5 units for AMDR2 (+0 mg kg^{-1}). For all SS1 particle size fractions, pH decreased up to 1.6 units as initial DRP concentration increased. For each SS2 particle size fraction, except $SS_{8\text{-}10,}$

the pH following batch sorption was similar across all DRP concentration treatments. The $SS2_{8\text{-}10}$ decreased 3 units from the +0 mg kg^{-1} to +1000 mg kg^{-1}.

1.3.3 Batch Sorption Isotherms

Dissolve reactive P removal by AMDR and SS_{bulk} was greater than 99% at +100 mg kg^{-1} (Table 2). Acid mine drainage residuals DRP removal was greater than SS_{bulk} at higher initial DRP concentrations. Source influenced P removal for SS_{bulk}, but not AMDR, which had > 99% P removal across all initial DRP concentrations. The $SS2_{bulk}$ had greater P removal than $SS1_{bulk}$ across all DRP concentrations and particle size fractions.

As SS particle size fraction increased, DRP removal decreased. All PSM had > 90% removal at the initial DRP concentration of +100 mg kg^{-1}. Phosphorus removal decreased to < 90% at +1000 mg kg^{-1} by $SS1_{<2}$, +600 mg kg^{-1} by $SS1_{2\text{-}4}$, and +400 mg kg^{-1} by $SS1_{4\text{-}6.3}$. The $SS1_{4\text{-}6.3}$ had the lowest DRP removal rate (58%) at +1000 mg kg^{-1}. Steel slag 2 fractions < 6.3 mm removed more than 90% of P. Both $SS2_{6.3\text{-}8}$ and $SS2_{8\text{-}10}$ removed > 90% up to +400 and 200 mg kg^{-1} respectively. The lowest DRP removal exhibited at was $SS2_{8\text{-}10}$ at +1000 mg kg^{-1} of 39%.

Table 1

The pH of steel slag 1 (SS1), steel slag 2 (SS2), acid mine drainage residuals 1 (AMDR1), acid mine drainage residuals 2 (AMDR2) after a 1:1 protocol and after the batch isotherm equilibration with a gradient of initial dissolved reactive phosphorus concentrations.

	1:1		Post-equilibration isotherm pH													
			+0 mg kg^{-1}		+100 mg kg^{-1}		+200 mg kg^{-1}		+400 mg kg^{-1}		+600 mg kg^{-1}		+800 mg kg^{-1}		+1000 mg kg^{-1}	
	mean	se	mean	se	mean	se	mean	se	mean	se	mean	se	mean	se	mean	se
SS1 <2	11.1	0.08	11.2	0.07	10.8	0.07	10.8	0.07	10.2	0.11	10.1	0.15	9.7	0.08	9.6	0.10
SS1 2-4	10.8	0.01	10.3	0.18	10.6	0.16	10.3	0.18	9.9	0.23	9.1	0.32	9.2	0.35	8.8	0.14
SS1 4-6.3	11.5	0.01	11.2	0.07	10.8	0.07	10.8	0.07	10.2	0.11	10.1	0.15	9.7	0.08	9.6	0.10
SS1 Bulk	9.3	0.06	11.4	0.05	11.3	0.06	11.2	0.07	11.0	0.06	10.6	0.18	10.5	0.06	10.0	0.13
SS2 <2	12.8	0.01	12.8	0.04	12.8	0.07	12.9	0.04	12.9	0.03	12.9	0.02	12.8	0.02	12.7	0.02
SS2 2-4	12.0	0.04	12.6	0.03	12.6	0.05	12.4	0.07	12.5	0.05	12.5	0.08	12.5	0.08	12.4	0.04
SS2 4-6.3	12.1	0.07	11.8	0.13	11.8	0.09	11.7	0.07	11.9	0.12	11.8	0.10	11.7	0.06	11.8	0.10
SS2 6.3-8	12.1	0.05	11.3	0.13	10.9	0.28	11.0	0.15	11.0	0.28	9.3	0.78	9.9	0.77	10.9	0.22
SS2 8-10	12.0	0.05	11.0	0.10	10.5	0.63	10.4	0.35	10.5	0.74	9.5	0.73	8.1	0.16	8.0	0.03
SS2 Bulk	11.2	0.04	12.1	0.16	11.8	0.22	12.0	0.23	11.6	0.40	11.7	0.18	11.7	0.10	11.2	0.28
AMDR1	7.9	0.01	4.1	0.03	4.0	0.04	4.1	0.03	4.2	0.13	4.1	0.03	4.2	0.05	4.1	0.02
AMDR2	6.3	0.01	7.8	0.02	7.8	0.01	7.9	0.02	7.9	0.03	8.0	0.02	8.0	0.02	8.0	0.03

Table 2
The dissolved reactive phosphorus (DRP) removal (%) for the gradient of initial DRP concentrations for steel slag 1 (SS1), steel slag 2 (SS2), acid mine drainage residuals 1 (AMDR1), and acid mine drainage residuals 2 (AMDR2).

	+100 mg kg^{-1}		+200 mg kg^{-1}		+400 mg kg^{-1}		+600 mg kg^{-1}		+800 mg kg^{-1}		+1000 mg kg^{-1}	
	mean	se	mean	se	mean	se	mean	se	mean	se	mean	se
SS1 <2	99.53	0.07	99.12	0.18	98.48	0.22	93.43	1.52	89.58	3.19	84.32	1.94
SS1 2-4	98.86	0.66	98.58	0.86	92.90	3.22	75.74	5.22	78.91	3.94	63.60	1.94
SS1 4-6.3	97.29	1.45	91.60	4.59	81.89	5.17	65.88	2.94	59.17	6.01	58.02	5.13
SS1 Bulk	99.70	0.07	99.82	0.05	99.73	0.10	93.78	3.97	87.99	1.61	69.80	4.46
SS2 <2	99.96	0.04	99.93	0.03	99.98	0.01	99.99	0.01	99.94	0.06	99.99	0.04
SS2 2-4	99.89	0.11	100.00	0.00	100.00	0.00	100.00	0.00	100.00	0.01	100.00	0.00
SS2 4-6.3	99.86	0.12	99.97	0.01	99.97	0.02	99.99	0.00	99.97	0.02	100.00	0.00
SS2 6.3-8	99.67	0.16	99.50	0.27	99.82	0.11	68.48	18.57	78.24	12.54	99.94	0.25
SS2 8-10	94.36	4.70	98.79	0.39	82.84	9.97	82.73	9.87	52.98	14.03	37.79	2.20
SS2 Bulk	99.82	0.14	99.89	0.04	95.45	4.52	99.93	0.02	99.97	0.02	75.15	24.65
AMDR1	99.93	0.07	100.00	0.00	99.99	0.01	100.00	0.00	100.00	0.00	99.99	0.00
AMDR2	100.00	0.02	100.00	0.01	100.00	0.00	100.00	0.01	100.00	0.00	99.99	0.00

1.3.4 Hydraulic Conductivity (K_{sat})

The K_{sat} of SS_{bulk} was higher than AMDR (Table 3). The K_{sat} of SS_{bulk} was 3,120% greater than that of AMDR. The K_{sat} was 72% lower for AMDR2 than AMDR1. K_{sat} was 13% higher for $SS2_{bulk}$ than $SS1_{bulk}$. Steel slag 2 particle size fractions 2 – 4 mm and 4 – 6.3 mm had a higher K_{sat} than SS1 of the same particle size fractions, but SS1 had a higher K_{sat} for the < 2 mm and bulk particle size fractions. The particle size fractions for SS1 had similar K_{sat} values. The K_{sat} values for $SS2_{<2}$ and $SS2_{bulk}$ were significantly lower than the other SS2 particle size fractions.

Table 3
The saturated hydraulic conductivity of steel slag 1 (SS1), steel slag 2 (SS2), acid mine drainage residuals 1 (AMDR1), and acid mine drainage residuals 2 (AMDR2). Uppercase letter marks significant difference ($p \leq 0.05$) for particle size fractions across PSM types and sources. Lowercase letter marks significant difference ($p \leq 0.05$) within the PSM.

	mean	se	
SS1 <2	0.16	0.06	aA
SS1 2-4	0.14	0.05	aB
SS1 4-6.3	0.13	0.05	aB
SS1 Bulk	0.12	0.04	aA
SS2 <2	0.02	0.01	bB
SS2 2-4	0.23	0.08	aA
SS2 4-6.3	0.22	0.07	aA
SS2 6.3-8	0.22	0.07	a
SS2 8-10	0.26	0.09	a
SS2 Bulk	0.03	0.00	bB
AMDR1	0.00	0.00	C
AMDR2	0.00	0.00	D

1.3.5 Metal Cation

There was a marked difference in total (Table 4), WS, AO, and CBD (Table 4 and 5) concentrations between the two different types of PSM, SS_{bulk} and AMDR. Total Fe was 5-fold greater on average, in AMDR than SS_{bulk}, whereas Mg_{tot} was 64-fold, and Ca_{tot} was 6-fold greater in SS_{bulk}. The Ca_{ws} and Mg_{ws} were 1.6- and 1.8-fold higher in SS_{bulk} than AMDR. Though the water-soluble proportion of Ca_{tot} was similar between AMDR and SS_{bulk} (54.6% and 55.8%, respectively), AMDR had a greater proportion of Mg_{tot} in water soluble form (7.5% vs. 0.2%). The Al_{ao} and Al_{cbd} were higher (15-fold and 5-fold) in SS_{bulk} than AMDR, whereas in AMDR Fe_{ao} and Fe_{cbd} were 2-fold and 9-fold higher. Though Fe_{ao} was 2-fold higher in AMDR than SS_{bulk}, the ammonium-oxalate extractable fraction of Fe_{tot} was 3-fold higher in SS_{bulk}.

The total, WS, AO, and CBD metal cation differences varied more between AMDR sources than SS sources. Total Fe of AMDR1 and AMDR2 differed by approximately 2%, while AMDR2 had 2811% greater Ca_{tot} and 260% greater Mg_{tot}. Although Ca_{ws} was greater in AMDR2, the proportion of Ca_{tot} and Mg_{tot} that was water-soluble was only 19.5% and 3.5%, respectively compared to 89.7% and 11.4% in AMDR1. Both Fe_{ao} and Al_{ao} were greater in AMDR2 than AMDR1 by 1651% and 1273%. Acid mine drainage residuals 2 had greater Fe_{cbd} by 147%, while AMDR1 had 1007% greater Al_{cbd}. The $SS2_{bulk}$ had 130% greater Ca_{tot} than $SS1_{bulk}$. Both Mg_{tot} and Fe_{tot} were greater in $SS1_{bulk}$ than $SS2_{bulk}$ by 134% and 233%. Although Ca_{ws} was greater in $SS2_{bulk}$, the proportion of Ca_{tot} that was water-soluble was negligible (< 0.1%) and similar to that of $SS1_{bulk}$. Similarly, Mg_{ws} of $SS1_{bulk}$ was greater than $SS2_{bulk}$, but the proportion of Mg_{tot} for both were negligible (0.002%). Both Fe_{ao} and Fe_{cbd} was higher in $SS1_{bulk}$ (273% and 362%), but as a proportion of Fe_{tot}, $SS1_{bulk}$ and $SS2_{bulk}$ were similar with 50% vs.

42% as Fe_{ao} and 10% vs 7% as Fe_{cbd}. For Al_{ao}, $SS2_{bulk}$ was 154% higher than $SS1_{bulk}$. The Mg_{cbd} for SS1 and SS2 bulk constituted a small proportion of Mg_{tot} (< 1%) .

The extent of the variation between the smallest and largest particle size fraction for a given PSM depended greatly on the metal cation. With increasing particle size diameter of SS1 (< 2 to 4-6.3 mm), Ca_{tot} and Mg_{tot} decreased by 16.5% and 13.4% with larger decreases in the water-soluble fraction of 47% (Ca_{ws}) and 55% (Mg_{ws}). Opposite to Ca_{tot} and Mg_{tot}, Fe_{tot} increased with SS1 particle size fraction by 118% and 221%. The Fe_{ao} increased with decreasing particle size fraction by up to 137% whereas Al_{ao} exhibited a minor decrease of 12.7%. There was not a clear trend for the particle size fractions of SS1 for Fe_{cbd} and $Al_{cbd.}$ As the particle size fractions for SS2 increased, Mg_{tot} and Ca_{ws} decreased by 22% and 78% respectively from $SS2_{<2}$ to $SS2_{8\text{-}10}$. Water-soluble Mg decreased by 28% from $SS2_{<2}$ to $SS2_{6.3\text{-}8}$, then increased by 34% from $SS2_{6.3\text{-}8}$ to $SS2_{8\text{-}10}$. Both Al_{tot} and Al_{ao} increased with particle size fraction by 440% and 156% from $SS2_{<2}$ to $SS2_{8\text{-}10}$. The Al_{cbd} was similar across all SS2 particle size fractions except for $SS2_{4\text{-}6.3}$, which is 8.3-fold greater than the other particle size fractions. Total Fe was > 90% less for $SS2_{8\text{-}10}$ than the other SS2 particle size fractions which were similar. There was not a clear trend between SS2 particle size fractions Fe_{ao}. The Fe_{cbd} was similar for SS2 particle size fractions < 6.3 mm, then increased for $SS2_{6.3\text{-}8}$ and $SS2_{8\text{-}10}$.

Table 4
The metal cation composition consisting of total Ca, total Mg, total Fe for steel slag 1 (SS1) and 2 (SS1) and acid mine drainage residuals 1 (AMDR1) and 2 (AMDR2) to test the effects of source, type, and particle size fractions. Uppercase letter marks significant difference ($p \leq 0.05$) across PSM with the same particle size fraction. Lowercase letter marks significant difference ($p \leq 0.05$) within the PSM.

	Particle Size Fraction	Total (%)								
		Ca			Mg			Fe		
		mean	se		mean	se		mean	se	
SS1	< 2 mm	14.5	0.5	aB	6.7	0.3	aA	35.5	1.3	bB
	2 - 4 mm	13.3	0.1	abB	6.3	0.2	abA	37.8	0.3	aA
	4 - 6.3 mm	12.1	0.9	bB	5.8	0.2	bA	42.1	0.8	aA
	Bulk	14	0.8	aB	6.6	0.30	aA	17.7	0.4	cC
SS2	< 2 mm	17.6	0.8	bA	6.3	0.2	aA	43.5	2.3	aA
	2 - 4 mm	19.9	0.4	bA	5.9	0.1	bcA	42.9	2.60	aA
	4 - 6.3 mm	20.5	1.6	bA	5.5	0.5	bcA	48.8	3.3	aA
	6.3 - 8 mm	19.0	1.1	b	4.9	0.1	c	44.6	4.1	a
	8 - 10 mm	20.2	2.4	b	4.9	0.5	c	3.7	0.5	bB
	Bulk	18.3	0.7	bA	4.9	0.2	cB	7.6	2.8	bD
AMDR1	< 2 mm	0.18	0.1	D	0.05	0.0	C	65.2	1.1	B
AMDR2	< 2 mm	5.06	0.7	C	0.13	0.0	C	67.20	0.3	A

Table 5

The metal cation composition consisting of water-soluble Ca, water-soluble Mg, ammonium-oxalate Fe, ammonium-oxalate Al, CBD-Fe, and CBD-Al for steel slag 1 (SS1) and 2 (SS2) and acid mine drainage residuals 1 (AMDR1) and 2 (AMDR2) to test the effects of source, type, and particle size fractions. Uppercase letter marks significant difference ($p \leq 0.05$) across PSM with the same particle size fraction. Lowercase letter marks significant difference ($p \leq 0.05$) within the PSM.

		Water soluble (mg/kg)						Ammonium Oxalate (mg/kg)						Dithionite (mg/kg)					
	Particle Size	Ca			Mg			Fe			Al			Fe			Al		
	Fraction	mean	se		mean	se		mean	se		mean	se		mean	se		mean	se	
SS1	< 2 mm	6671	682	aB	67	6.63	bA	76616	3634	cA	3090	246	aA	21274	1607	aA	421	141	aB
	2 - 4 mm	3358	92	bB	40	3.18	cA	101160	4250	aA	2864	174	abA	19584	995	aA	5	0	bA
	4 - 6.3 mm	3561	185	bB	30	6.17	cA	104897	2632	aA	2696	187	abA	22386	2073	aA	15	7	bB
	Bulk	6406	358	aC	101	1.03	aA	88078	1185	bB	2444	91	bB	18057	713	aC	19	10	bD
SS2	< 2 mm	27279	2029	aA	40	1.61	bB	40530	2525	bcB	2337	79	cB	4491	66	cB	518	182	bA
	2 - 4 mm	12860	1748	bA	24	0.50	bcB	50232	1763	aB	2695	117	bcA	4895	307	cB	145	75	bA
	4 - 6.3 mm	5348	400	cA	12	1.07	cB	44907	2835	abB	3251	253	abA	4613	375	cB	5181	955	aA
	6.3 - 8 mm	4495	752	cA	11	1.21	c	25065	1605	d	3237	314	ab	7603	955	b	30	16	b
	8 - 10 mm	5900	964	c	32	2.95	b	24800	2475	d	3644	437	a	9425	612	a	619	572	b
	Bulk	12054	942	bA	89	12.5	aA	32180	4546	cdC	3761	249	aA	4984	251	cD	6323	1074	aA
AMDR1	< 2 mm	1615	94	D	57	2.5	B	12045	196	D	52	3	D	200865	10048	A	117	5	C
AMDR2	< 2 mm	9857	226	B	46	1.21	B	198896	3778	A	662	18	C	136932	9074	B	1178	11	B

1.3.6 FTIR spectroscopy

The vibrational frequencies determined by FTIR spectrum indicate that AMDR mostly consists of goethite-like material and SS mostly consists of calcite-like material (Figure 2). Several of the vibrational frequencies of AMDR1 and AMDR2 correspond to characteristic and prominent bands of goethite (Figure 2c). The prominent peak at 390 cm^{-1} is Fe-O asymmetric stretching [91], the feature at 610 cm^{-1} is Fe-OH stretch [91,92] , the peak at 790 cm^{-1} is O-H bending [93,94], and the band between 3400 – 3000 cm^{-1} encompasses the stretching vibrations of Fe-OH stretch [95]. The feature at 867 cm^{-1} could be goethite [93] or the O-C-O bending modes of calcite [96,97]. The feature at 1006 cm^{-1} likely reflects Si-O bonds [95]. The broader spectral features corresponding to Fe-O bonds of ADMR2 compared to AMDR1 are indicated with a greater degree of amorphous Fe minerals.

Steel slag 1 (Figure 2a) and SS2 (Figure 2b) had several major vibrational frequencies consistent with calcite (1417, 874, 712 cm^{-1}). The relatively low intensity peak at 712 cm^{-1} corresponds to OC-O in-plane bending of CO_3^{2-} [89,98,99]. The peak at 874 cm^{-1} belongs to O-C-O bending modes [97] and asymmetrical CO_3 [100,101]. The broad feature at 1417 cm^{-1} is consistent with C-O stretching of CO_3^{2-} groups for calcite [97,100-102]. Both SS1 and SS2 have bands at 984 cm^{-1} attributable to the asymmetrical stretching of Si-O [103,104]. SS1 and SS2 particle size fractions < 6.3 mm exhibited a peak at 498 cm^{-1} ascribable to the asymmetric stretch of Fe-O of goethite-like Fe oxides [91] or to out of plane vibrations of Si-O of calcium silica hydrate [103]. The particle size fractions of SS2 exhibited more features than SS1 particle size fractions, in particular 927 cm^{-1} of Si-O [105]. The peaks at 378 and 325 cm^{-1} do not correspond to the aforementioned functional groups or minerals; these frequencies partially fit with those associated with Al oxides, but the characteristic OH stretches > 3000 cm^{-1} were not present [106].

$SS2_{8\text{-}10}$ exhibited a unique pattern of higher intensity peaks compared to the other SS2 particle size fractions. There were no spectral features of treated PSM types indicative of bonds associated with P. The treated and untreated AMDR had a peak at 1039 cm^{-1} indicating there was phosphate enrichment within the AMDR, but the subtractions did not show evidence of any metal-P bonds, particularly for Fe-O-P (1012 cm^{-1}) which would be expected if P was binding in AMDR [76].

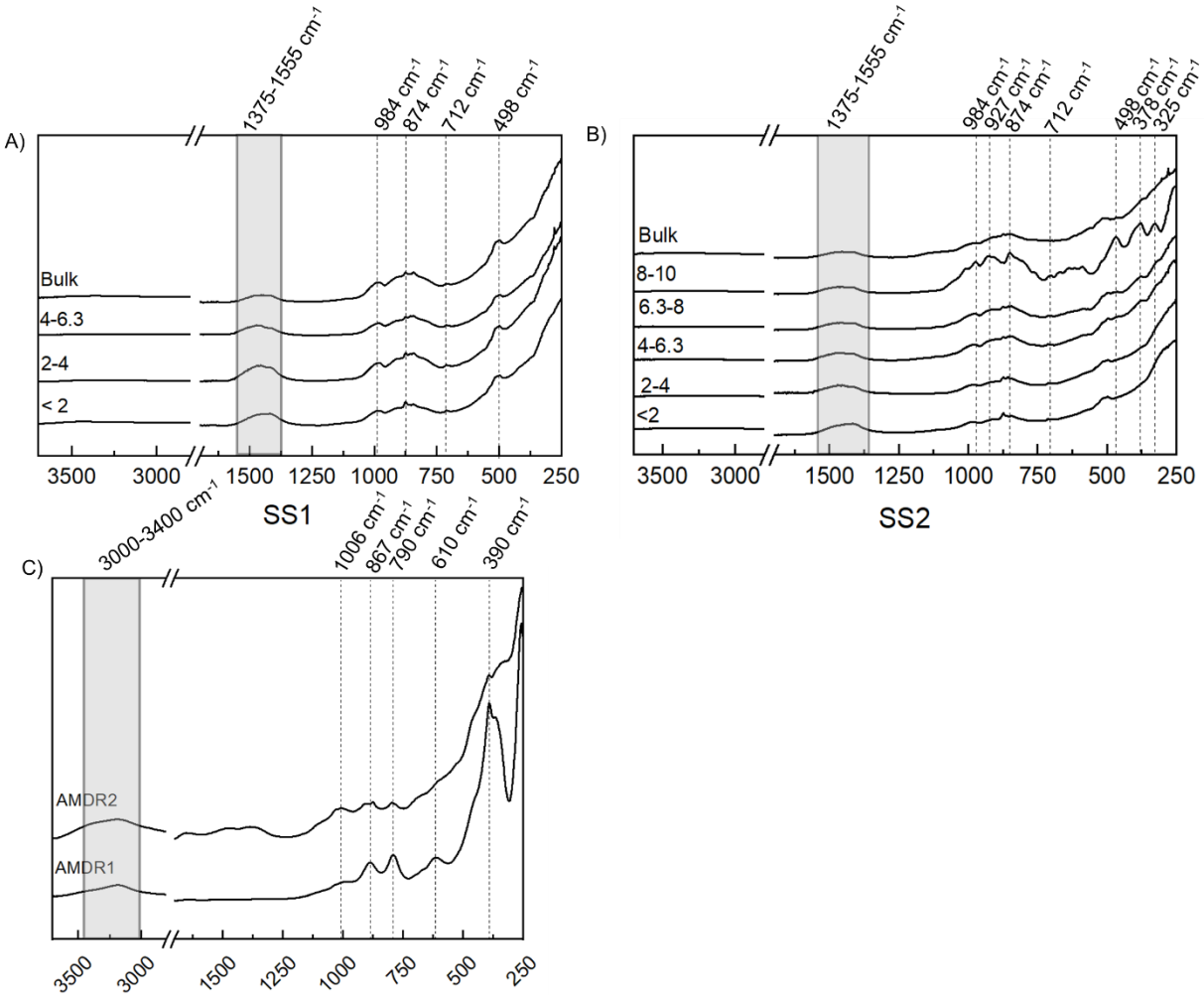

Figure 2. Spectra from Fourier transform infrared spectroscopy highlighting polar bonds for a) steel slag 1 (SS1), b) steel slag 2 (SS2), c) acid mine drainage residuals 1 (AMDR1), and c) acid mine drainage residuals 2 (AMDR2).

1.3.7 P recovery

Recovery of added DRP among P fractions inferred by sequential extraction differed more between PSM type than source and particle size fractions. The DRP added (+100 or 1000 mg kg^{-1}) was not always fully recovered, and for some SS particle size fractions there was negative recovery (e.g., $SS1_{2\text{-}4}$, SS2 < 8 mm) indicating that DRP extracted in the +0 mg kg^{-1} (i.e., inherent) was greater than for +100 or 1000 mg kg^{-1} treated PSM (see section 3.8). All recoveries account for inherent P. DRP recovered as NH_4Cl-P by SS_{bulk} was higher than AMDR for +100 mg kg^{-1} (27% vs 3%) (Figure 3). The DRP recovered as NH_4Cl-P by $SS2_{bulk}$ was higher than $SS1_{bulk}$ for +100 mg kg^{-1} (35% vs 20%), but not for +1000 mg kg^{-1} (7% vs 12%). In SS1 and SS2 particle size fractions, DRP recovered as NH_4Cl-P for +100 mg kg^{-1} was < 10%. Recovery of DRP as NH_4Cl-P in SS particle size fractions for +1000 mg kg^{-1} was < 50%, but consistently higher for SS1 (25 – 49%) than SS2 (< 1 – 45%).

Recovery of DRP as NH_4F-P by SS_{bulk} was higher than AMDR for both P treatments (Figure 4). A negligible amount of DRP was recovered as NH_4F-P by AMDR2 for +1000 mg kg^{-1} and there was no detectable DRP (LOD 20 mg kg^{-1}) recovered for +100 mg kg^{-1} or by AMDR1. The DRP recovered as NH_4F-P by $SS2_{bulk}$ was higher than $SS1_{bulk}$ for +100 mg kg^{-1} (171% vs 9%) and +1000 mg kg^{-1} (24% vs 17%). Across particle size fractions, DRP recovered as NH_4F-P for +1000 mg kg^{-1} ranged from 4 – 35% in SS1 and 11 – 33% in SS2. In SS1 and SS2 particle size fractions, DRP recovered as NH_4F-P for +100 mg kg^{-1} was higher by SS1 (33 – 54%) than SS2 (-65 – 124%). The DRP recovered as NaOH-P was greater by AMDR than SS_{bulk} as both P treatments were not detectable (LOD 20 mg kg^{-1}). A majority of DRP was recovered as NaOH-P by AMDR1 and AMDR2 for +1000 mg kg^{-1}, 62% and 47% respectively, and for +100 mg kg^{-1}, 61% and 80% respectively (Figure 5).

Recovery of DRP as CBD-P by AMDR and SS_{bulk} was negligible for +1000 mg kg^{-1} and 2-fold higher for +1000 mg kg^{-1} by SS_{bulk} than AMDR (Figure 6). Recovery of DRP as CBD-P by AMDR2 was higher for +100 mg kg^{-1} (29%) than +1000 mg kg^{-1} (4%). The DRP recovered as CBD-P by AMDR1 and $SS1_{bulk}$ was negligible for both P treatments. The DRP recovered by $SS2_{bulk}$ was higher for +100 mg kg^{-1} (58%) than +1000 mg kg^{-1} (6%). In SS1 and SS2 particle size fractions, DRP recovered as CBD-P was <10% for +1000 mg kg^{-1}. The DRP recovery was negative for CBD-P in SS1 (-10 to -33%) and SS2 particle size fractions (-1 to -44%) for +100 mg kg^{-1}, except for $SS2_{8\text{-}10}$ (67%). The DRP recovered as H_2SO_4-P by SS_{bulk} was higher than AMDR for +1000 mg kg^{-1} (53% vs 23%) (Figure 7). No DRP was recovered as H_2SO_4-P by AMDR1 for +100 mg kg^{-1}, whereas 65% of DRP added was recovered as H_2SO_4-P by AMDR2. Recovery of DRP as H_2SO_4-P by $SS1_{bulk}$ and $SS2_{bulk}$ was more similar for +1000 mg kg^{-1} (44% and 61%) than +100 mg kg^{-1} (59% and 714%). The DRP recovered as H_2SO_4-P in SS particle size fractions for +1000 mg kg^{-1} were consistently higher for SS2 (51 – 59%) than SS1 (36-48%). Across particle size fractions, DRP recovered as H_2SO_4-P for +100 mg kg^{-1} was -54 – 55% in SS1 and -271 to -178% in SS2, except for $SS2_{8\text{-}10}$ (502%).

Recovery of DRP by AMDR and SS_{bulk} was similar for +1000 mg kg^{-1} (65% and 67%), but not for +100 mg kg^{-1} (118% vs 521%). Recovery of DRP was similar by ADMR1 and AMDR2 (63 vs 66%) for +1000 mg kg^{-1}, but for +100 mg kg^{-1} differed: AMDR1 had 63% recovery whereas AMDR2 over-recovered DRP by 74%. The DRP recovery was higher by $SS2_{bulk}$ than $SS1_{bulk}$ for both +1000 mg kg^{-1} (98% vs 36%) and +100 mg kg^{-1} (956% and 86%). The particle size fractions for SS1 exhibited < 50% recovery for +1000 mg kg^{-1}. The DRP recovery from +100 mg kg^{-1} increased with increasing SS1 particle size fractions (17 – 100%). SS2 particle size fractions did not have any clear trends of DRP recovery from +100 or 1000 mg

kg^{-1}. Except for $SS2_{8-10}$ which had an over-recovery of 595%, there was less DRP recovered from +100 mg kg^{-1} (-168% to -343%) than +0 mg kg^{-1} (inherent) by SS2 particle size fractions. Similarly, $SS2_{8-10}$ over-recovered (19%) from +1000 mg kg^{-1}, whereas the other SS2 particle size fractions recovered < 41%.

1.3.8 Inherent P

Inherent P, measured in the +0 mg kg^{-1} treatment, of the sum of extractable DRP fractions was greater than the DRP recovered from the +1000 mg kg^{-1} for $SS1_{2-4}$ and for +100 mg kg^{-1} for SS2 < 8 mm particle size fractions. Inherent (+0 mg kg^{-1}) P extracted as NH_4Cl-P by SS_{bulk} was 79% of +1000 mg kg^{-1} NH_4Cl-P. Majority of P recovered as NH_4Cl-P was inherent for +100 mg kg^{-1} by AMDR1 (79%) and SS_{bulk} (53%). For +1000 mg kg^{-1}, the majority of P recovered as NH_4Cl-P by $SS1_{bulk}$ (84%) and $SS2_{bulk}$ (73%) was inherent NH_4Cl-P and for +100 mg kg^{-1}, approximately half was inherent NH_4Cl-P by $SS1_{bulk}$ (48%) and $SS2_{bulk}$ (59%). The largest portion of inherent P extracted as NH_4Cl-P by SS1 occurred for $SS1_{2-4}$ for +100 and 1000 mg kg^{-1}, 70% and 84%, respectively. For SS2 particle size fractions, inherent P accounted for the majority of DRP recovered as NH_4Cl-P for +100 mg kg^{-1} (72 – 100%) and for +1000 mg kg^{-1} (61 – 87%). Steel slag 2_{8-10} had the largest portion of inherent P extracted as NH_4Cl-P of +100 and 1000 mg kg^{-1}, 87% and 100%, for SS2. In SS_{bulk}, DRP recovered as NH_4F-P had a greater proportion as inherent for +100 mg kg^{-1} than +1000 mg kg^{-1} (63% vs 42%) and there was no detectable inherent NH_4F-P for either AMDR sources. Inherent P extracted as NH_4F-P for SS1 particle size fractions was > 63% of NH_4F-P for both P treatments, except for $SS1_{<2}$ for +1000 mg kg^{-1} (22%). Inherent P extracted as NH_4F-P in SS2 particle sizes was < 40% of +1000 and 100 mg kg^{-1} NH_4F-P, except for $SS2_{8-10}$ with +1000 mg kg^{-1} (27%). The inherent P extracted as

NaOH-P by AMDR1 was less than AMDR2 for both +100 and 1000 mg kg^{-1} (52% and 10% vs 83% and 46%).

Inherent P extracted as CBD-P (+0 mg kg^{-1}) by all PSM was a significant amount (37-111%) of the extractable P for +100 and 1000 mg kg^{-1}. In AMDR1 and AMDR2, inherent P extracted as CBD-P accounted for a larger portion of +100 mg kg^{-1} (105% and 83%) than +1000 mg/kg (49% and 77%). In $SS1_{bulk}$, inherent P extracted as CBD-P was greater than the DRP recovered as CBD-P for +100 and 1000 mg kg^{-1}. Inherent P extracted as CBD-P by $SS2_{bulk}$ was similar of +100 (55%) and 1000 mg kg^{-1} (56%). In $SS2_{8\text{-}10}$, inherent P extracted as CBD-P was the lowest for +100 and 1000 mg kg^{-1}, 39% and 38% respectively. There was high (52 – 100%) inherent P extracted as H_2SO_4-P by SS_{bulk} and AMDR . There was negligible inherent P extracted as H_2SO_4-P by AMDR1 and was > 88% by AMDR2 for +100 and 1000 mg kg^{-1}. Inherent P extracted as H_2SO_4-P by $SS1_{bulk}$ was greater than $SS2_{bulk}$ for +1000 mg kg^{-1} (83% vs 42%) and +100 mg kg^{-1} (87% vs 39%). In $SS2_{<2}$, inherent P extracted as H_2SO_4-P was greater than DRP recovered for either +100 or 1000 mg kg^{-1} (1.3 and 1.2-fold). In $SS2_{8\text{-}10}$, inherent P extracted as H_2SO_4-P was 75% lower than the other SS2 particle size fractions and was 26% of +1000 mg kg^{-1} H_2SO_4-P and 33% of +100 mg kg^{-1} H_2SO_4-P.

Total inherent P exceeded the sum of the total extractable P for all PSM particle size fractions. Total inherent P was 1.3-fold higher in SS_{bulk} than AMDR. There was a greater relative difference between the two AMDR sources (5.7-fold) than the two SS sources (1.2-fold). Total inherent P was similar among SS1 particle size fractions. Total inherent P was similar among SS2 particle size fractions except for $SS2_{8\text{-}10}$ which was 50% less than the others. Across all PSM, < 55% of total inherent P was extractable (+0 mg kg^{-1}). With AMDR2, 52% of total inherent P was extractable compared to 23% by AMDR1 was. Both $SS1_{bulk}$ and $SS2_{bulk}$ had

similar amount of extractable total inherent P, 42% and 40%, respectively. SS1 particle sizes had 47 – 54% of extractable total inherent P as extractable. Steel slag 2 particle sizes had 38 – 44% of extractable total inherent P as extractable.

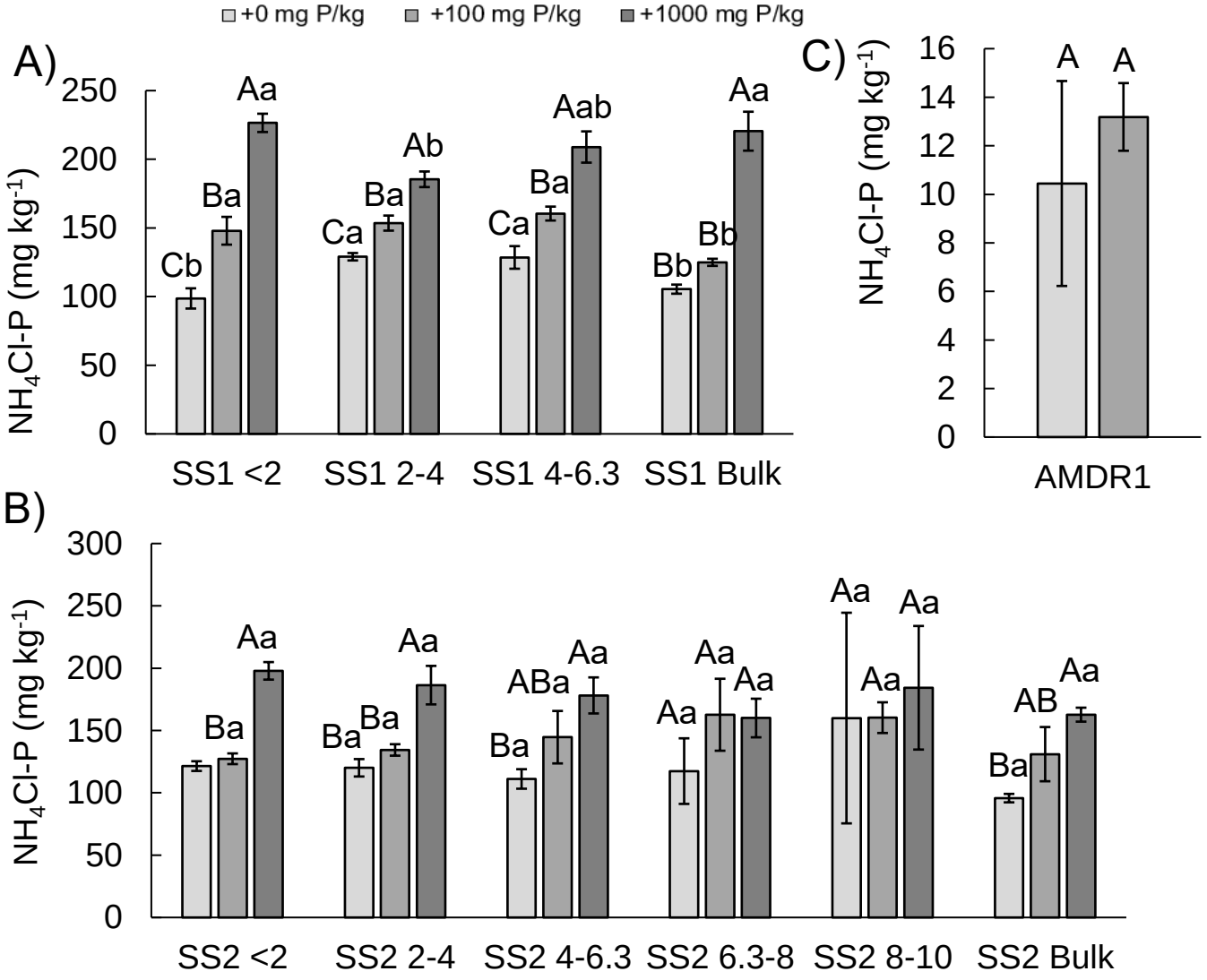

Figure 3. Dissolved reactive phosphorus extracted as NH_4Cl-P for a) steel slag 1 (SS1), b) steel slag 2 (SS2), c) acid mine drainage residuals 1 (AMDR1), and c) acid mine drainage residuals 2 (AMDR2) for +0 mg P kg^{-1} phosphorus-sorbing media (PSM) added, +100 mg P kg^{-1} PSM added, and +1000 mg P kg^{-1} PSM added. Uppercase letter marks significant difference ($p \leq 0.05$) across P treatments within a given particle size fractions. Lowercase letter marks significant difference ($p \leq 0.05$) across particle size fractions within a PSM source for the same P treatment.

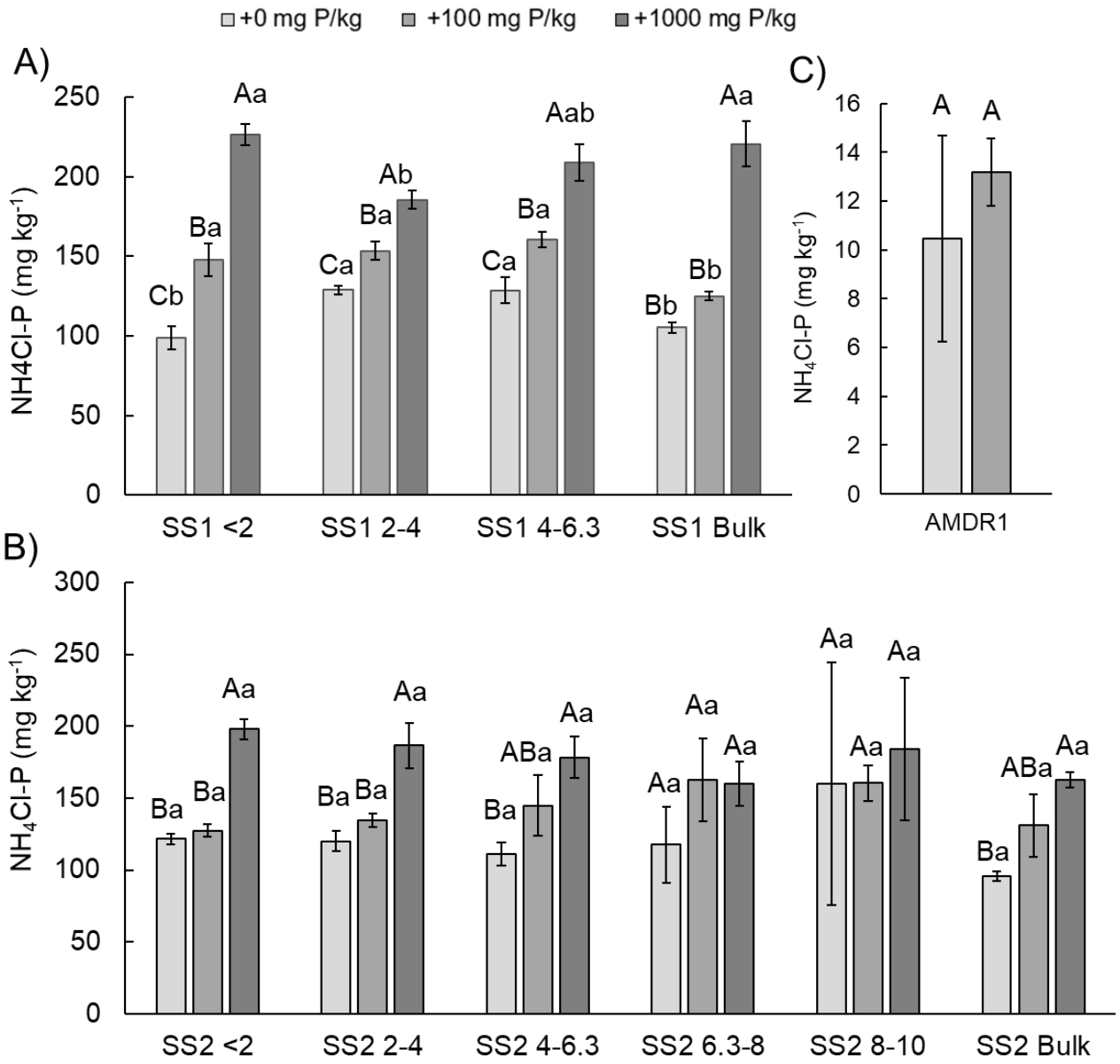

Figure 4. Dissolved reactive phosphorus extracted as NH_4F-P for a) steel slag 1 (SS1), b) steel slag 2 (SS2), c) acid mine drainage residuals 1 (AMDR1), and c) acid mine drainage residuals 2 (AMDR2) for +0 mg P kg^{-1} phosphorus-sorbing media (PSM) added, +100 mg P kg^{-1} PSM added, and +1000 mg P kg^{-1} PSM added. Uppercase letter marks significant difference ($p \leq 0.05$) across P treatments within a given particle size fractions. Lowercase letter marks significant difference ($p \leq 0.05$) across particle size fractions within a PSM source for the same P treatment.

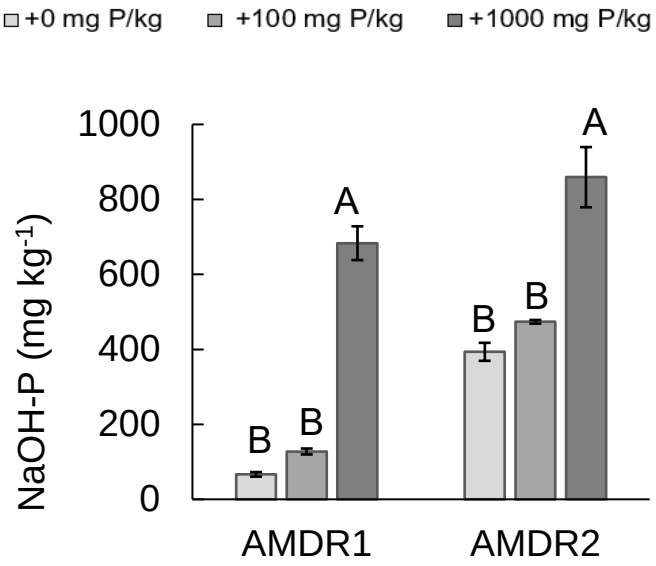

Figure 5. Dissolved reactive phosphorus extracted as NaOH-P for acid mine drainage residuals 1 (AMDR1), and acid mine drainage residuals 2 (AMDR2) for +0 mg P kg^{-1} phosphorus-sorbing media (PSM) added, +100 mg P kg^{-1} PSM added, and +1000 mg P kg^{-1} PSM added. Uppercase letter marks significant difference ($p \leq 0.05$) across P treatments within a given particle size fractions. Lowercase letter marks significant difference ($p \leq 0.05$) across particle size fractions within a PSM source for the same P treatment.

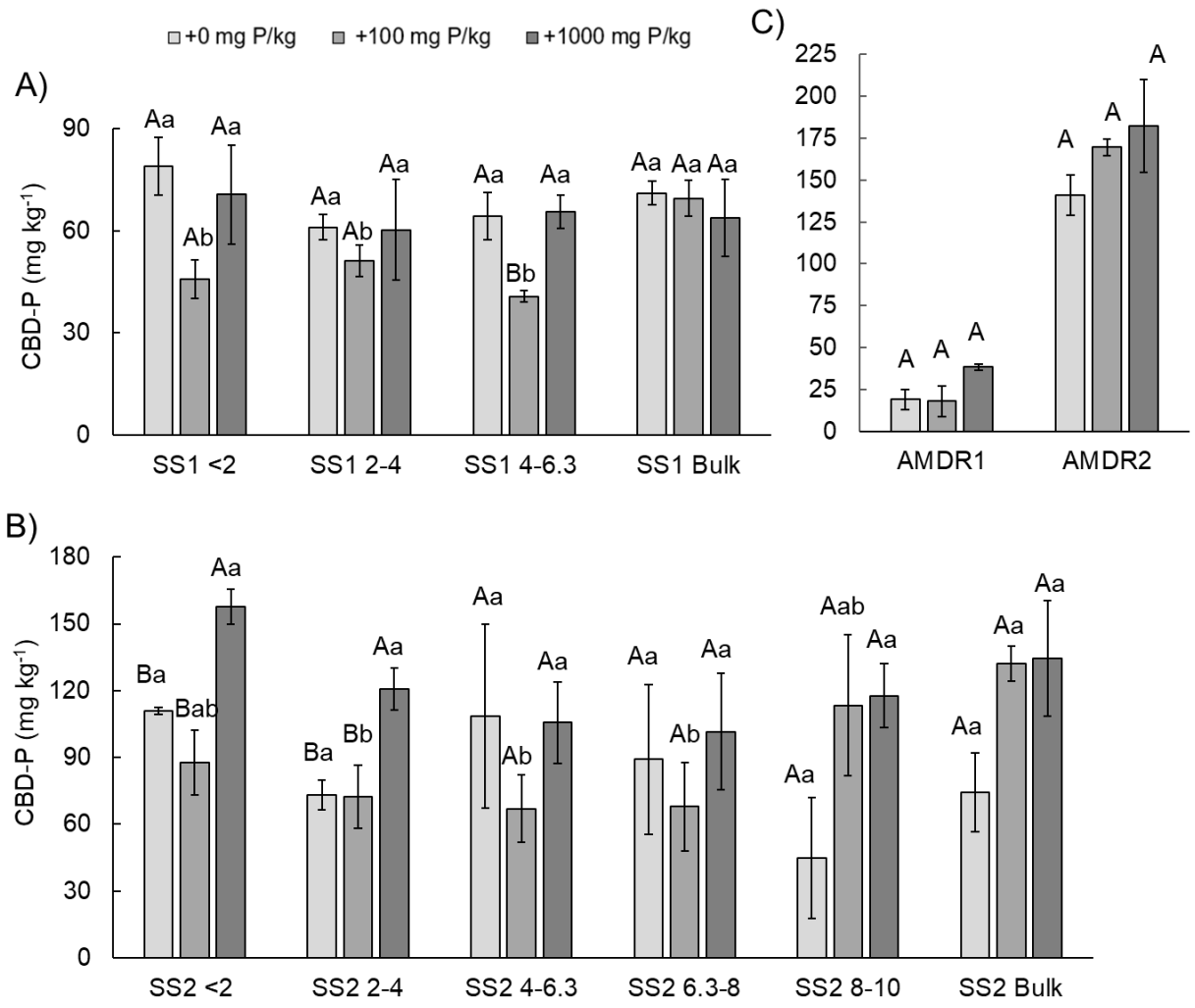

Figure 6. Dissolved reactive phosphorus extracted as CBD-P for a) steel slag 1 (SS1), b) steel slag 2 (SS2), c) acid mine drainage residuals 1 (AMDR1), and c) acid mine drainage residuals 2 (AMDR2) for +0 mg P kg^{-1} phosphorus-sorbing media (PSM) added, +100 mg P kg^{-1} PSM added, and +1000 mg P kg^{-1} PSM added. Uppercase letter marks significant difference ($p \leq 0.05$) across P treatments within a given particle size fractions. Lowercase letter marks significant difference ($p \leq 0.05$) across particle size fractions within a PSM source for the same P treatment.

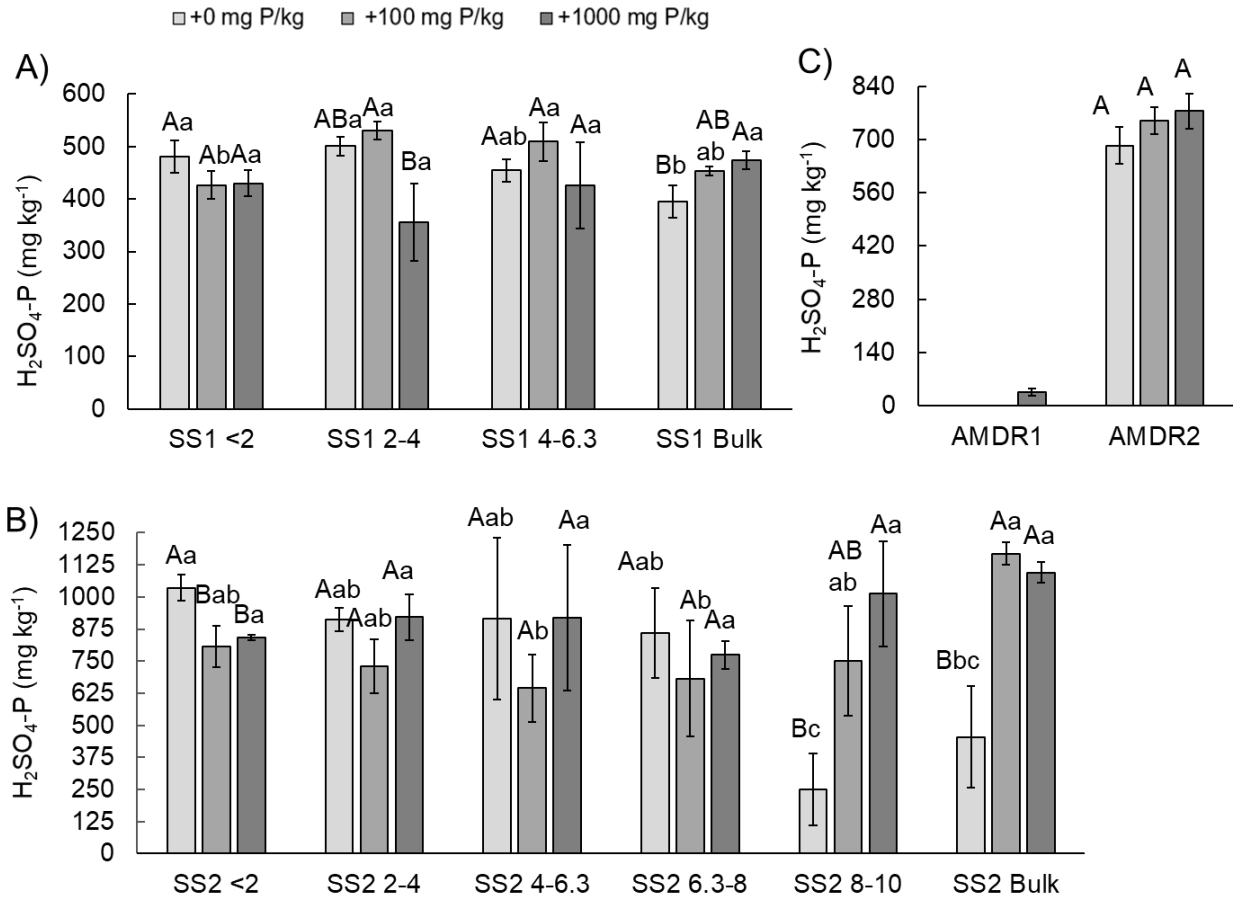

Figure 7. Dissolved reactive phosphorus extracted as H_2SO_4-P for a) steel slag 1 (SS1), b) steel slag 2 (SS2), c) acid mine drainage residuals 1 (AMDR1), and c) acid mine drainage residuals 2 (AMDR2) for +0 mg P kg^{-1} phosphorus-sorbing media (PSM) added, +100 mg P kg^{-1} PSM added, and +1000 mg P kg^{-1} PSM added. Uppercase letter marks significant difference ($p \leq 0.05$) across P treatments within a given particle size fractions. Lowercase letter marks significant difference ($p \leq 0.05$) across particle size fractions within a PSM source for the same P treatment.

1.4 Discussion

1.4.1 Relationship between K_{sat} and particle size fraction

Our results supported the hypothesis that PSM type would have a greater role in DRP removal and K_{sat} than source and particle size diameter. Our results were in mixed support of the hypothesized optimization of DRP removal and flow rate (K_{sat}) trade-offs by the largest particle size fractions (> 4 mm). Although both AMDR sources had near complete DRP removal across

initial concentrations of 100 to 1000 mg kg^{-1}), this PSM type was limited by a low K_{sat} likely to impede water flow through a P removal structure. Similar to both AMDR sources, the low K_{sat} of $SS2_{<2}$ and $SS2_{bulk}$ would preclude effective treatment of water flowing from a field. The K_{sat} informs the retention time and volume needed when designing P removal structures. An acceptable K_{sat} for media in P removal structures is depends on the expected peak runoff flow rate, the DRP concentration, and the DRP removal goal [32]. While there are no clear K_{sat} thresholds for PSM, NRCS hydrologic soil groups can be used to interpret K_{sat} values for PSM in a P removal structure [107]. Four hydrologic soil groups based on the infiltration and percolation of water through soil at maximum yearly saturation. The PSM tested fall within two of the hydrologic soils groups: Group A has the highest K_{sat} of > 0.1 cm s^{-1} and Group D has the lowest $K_{sat} \leq 0.04$ cm s^{-1} [108]. A low K_{sat} would allow a longer retention time [37], but would require a greater quantity of PSM and a larger P removal structure that is a more shallow to sufficiently treat runoff or tile drain effluent [107]. However, low K_{sat} PSM with high DRP removal potential such as AMDR can be pelletized to increase K_{sat} [109]. Pelletization can decrease DRP removal when the particle size diameter is increased [109] likely due to a decrease in binding sites and pelletization could increase costs and undermine the low expense advantage of PSM. In this study, SS differed from AMDR in that SS sources had multiple particle size fractions > 2 mm. For SS1 particle size fractions and SS2 particle size fractions, excluding $SS2_{<2}$ and $SS2_{bulk}$, the K_{sat} was similar so the particle size fraction with the highest DRP removal should be chosen. However, the finest (< 2 mm) particle size fraction has been shown to clog P removal structures in field evaluations [36,107], so it may be prudent to remove this particle size fraction by sieving before use in a P removal structure.

This study followed the initial DRP concentrations typically used in batch isotherms of PSM, with the initial DRP concentration added is generally no more than 1000 mg P kg^{-1} PSM (50 mg L^{-1}) [41,48,110], despite a much higher P sorption maxima of PSM types such as AMDR (up to 157,000 mg P kg^{-1} PSM [37]). On the other hand, DRP concentrations from agricultural fields typically have a maximum flow-weighted average of 1.25 mg P L^{-1} [5,111], therefore the tested DRP concentrations are more similar to field conditions. Batch isotherms can be used to evaluate PSM removal by the percent P removed and also to determine the maximum P sorption (S_{max}) possible. The PSM evaluated were not fully P-saturated and still had near 100% removal of DRP, indicating the S_{max} for these PSM was higher as has been shown in studies that have gone beyond 1000 mg P kg^{-1} PSM [39,41]. Although this range of DRP concentration is more similar to field conditions, it does not allow for S_{max} determination of PSM with high P removal capacity which inhibits the design of the P removal structure and calculation of PSM longevity, but allows for relative comparisons of a set initial DRP solution concentration among PSM.

1.4.2 Metal cations relevant to P removal

Our results supported the hypothesis that metal cation concentrations would vary most by PSM type. The results were in mixed support of the hypothesis that there would be variation between the smallest and largest particle size fraction and that there would be the least difference by source. The difference in metal cation composition between PSM type was due to how these PSM were made and concurrent with compositional differences that have been found with similar PSM in previous studies [38,39,41]. The high concentrations of Fe_{tot} and Fe_{ao} in AMDR are consistent with AMDR evaluated in other studies [38,48]. An inconsistency found in this study was the higher Al_{ao} and Al_{cbd} concentrations in SS which deviates from the known mineralogy of SS of dicalcium silicate, tricalcium silicate, dicalcium ferrite, and lime [77,79].

Fourier transform infrared spectroscopy supports compositional differences between the two SS sources, particularly for peaks < 400 cm^{-1}, which could explain the higher DRP removal in SS2. Testing the relationship of total and reactive metal cation concentrations with DRP removal was not possible for AMDR1 and AMDR2 because complete DRP removal means that variation in composition would be muted by the same magnitude of DRP removed. The FTIR spectra for the two AMDR sources suggest that although similar, the more prominent peaks associated with goethite in ADMR1 may not be as important for DRP removal as the concentration of higher Fe_{ao} in AMDR2. Dissolved reactive P concentrations tested would need to be higher in order to distinguish potential differences in maximum P removal capacity. The lack of detectable metal-P bonds in the FTIR spectra is also likely due to the DRP concentrations not being sufficiently high for the concentration of metal-P bonds to be high enough to be detected.

By coupling sequential P fractionation with routine metal cation composition analyses, we demonstrate that a high concentration of a metal cation does not necessarily indicate that P removal is driven by that metal cation by PSM source, type, or particle size diameter. Sequential P fractionation largely supported previous findings that Ca drives P removal in these Ca-rich PSM [38,65], and this is mostly upheld except for the < 2 mm fraction. The sequential P fractionation for the < 2 mm fraction indicates that the majority of P recovered is loosely bound P, despite there being higher reactive Ca and similar or even lower total Ca and reactive Al concentrations than the larger particle size diameters. The reactive Mg pool is higher in the < 2 mm fraction than the other particle size fractions, which could be loosely bound P, but the sequential P fractionation is not though to specifically isolate Mg- P. Although Mg_{tot} and Mg_{ws} were low in AMDR and SS compared to the other metal cation concentrations, the molar ratio of Mg:P added (0.88:1) for +100 mg kg^{-1} suggests that Mg may have a relatively minor

contribution to P removal. For the two SS sources, the higher Ca_{tot} and Ca_{ws} in SS2 particle size fractions can explain the higher DRP removal for particle size fractions and initial DRP concentration combinations than SS1. In addition to high extractable Ca-P, SS1 and $SS2_{8\text{-}10}$ also exhibited moderate (4%) to high (171%) extractable Al-P, indicating Al may be an appreciable but overlooked metal cation of SS that contributes to DRP removal by this PSM type. The point of zero charge of Al oxides (pH 7-9.4) [112] would be reasonable for some SS (pH > 8), particularly when pH decreases at higher DRP concentrations. Research into spectral identification in the FIR range (< 400 cm^{-1}) is limited making it difficult to determine if the peaks < 400 cm^{-1} for SS2 FTIR spectra are associated with Al oxides or not.

The SS contained highest amounts of total and reactive Fe, but there was very little Fe-P recovered which is likely due to the point of zero charge of Fe oxides (pH 7-8) [113] being lower than that of SS (pH > 8). Although the various particle size fractions of both SS sources showed appreciable amounts of soluble and loosely bound P, desorption batch isotherm experiments from other SS sources have shown once removed, P is unlikely to be lost [114]. For AMDR, P was recovered as Fe-P as hypothesized, consistent with the high levels of Fe_{ao} and in agreement with what has been found before [47,48]. There was an appreciable amount of Ca-P in AMDR2, which corresponds with the elevated Ca_{ws} and the pH of ADMR2 is high enough during batch isotherms for Ca to remove P. Though, this fraction has been shown to extract Fe-P [115] which could also be likely with ADMR due to the high Fe concentrations.

1.4.3 High inherent P in PSM

This study finds that PSM can inherently have a large amount of P. The distribution of inherent P across sequentially extracted P fractions are consistent with the PSM formation process. Differences in the distribution are greater between PSM type than source or particle size

fraction, although ADMR sources differed more in distribution of inherent P than SS. Steel slag is a by-product of steel making when scrap steel is mixed with lime to remove impurities such as P and Fe [116]. The cooling rate of SS is slow enough that crystalline compounds often form which can account for CBD-P [116]. The formation process helps to explain the large (> 43%) concentration of inherent Ca-P, as well as the lower concentration of CBD-P present in SS likely formed from the slow cooling rate which could explain the lack of non-crystalline Fe-P. The Al-P is unique in that typically the composition of total and reactive Al is relatively minor compared to Fe and Ca, yet it can vary depending on the steel used. For AMDR, the inherent P is largely distributed among Fe-P, CBD-P, and Ca-P, consistent with AMDR production. Acid mine drainage residuals are a by-product of the neutralization (~7) of acid mine drainage that is formed by the oxidation of minerals in the mining of coal and metal deposits such as pyrite form dissolved Fe and sulfuric acid [117]. Phosphorus is available in small quantities in coal (< 1%), including as apatite, and other mines [118] to be bound to Fe in acid mine drainage. Then through the neutralization process with an alkaline material, typically with high concentrations of Ca [47], Ca-P can be formed. For both PSM, it is likely that the precipitates formed with Ca, Fe, and the more crystalline CBD-P will not be at risk of loss in P removal structures as the pH of the PSM in the batch isotherms is not conducive to dissolution.

Given the magnitude of inherent P in some fractions, sequentially extracted fractions used to examine DRP recovery by PSM should account for inherent P. A high inherent P means there is potential for the PSM to become a source of P rather than a sink, especially as it was indicated that there was loosely and soluble bound P. Since inherent P is unaffected by DRP concentration, a larger proportion of DRP extracted from the +100 mg kg^{-1} P treatment should be inherent than the +1000 mg kg^{-1} P treatment, unless the +100 mg kg^{-1} P treatment is

recovering more of the added DRP. The minor magnitude of over-recovery relative to total P means that extraction of total inherent P could explain apparent over-recovery of DRP. A negative recovery suggests that the PSM tested contain more P than is retained from the DRP concentration added.

1.5 Conclusions

The results of this study show that both physical and chemical properties impact P removal among PSM type, source, and particle size fractions. The differences in metal cation concentrations between PSM type and source are more important than among particle size fractions for DRP removal. Total concentrations of Ca, Mg, Fe, and Al do not appear to be relevant to how P is removed, but rather the pH of the PSM and reactive pools of metal cations dictate P removal. From this study it appears that Al in SS, along with Ca, may be removing P which would make it more desirable in a P removal structure as it would function as a P remover for a wider pH range. Particle size seems to have the largest role when it comes to designing a P removal structure for the water inflow. Finer sized components of PSM may not be the best for P removal structures due to low flow and a larger particle size fraction such as 4-6.3 mm or 6.3-8 mm should be used. High inherent P in PSM does not appear to impact the ability to remove more P, but is important to quantify to accurately measure which metal cation is responsible for removing P.

References

1. Jarvie, H.P.; Sharpley, A.N.; Flaten, D.; Kleinman, P.J.A.; Jenkins, A.; Simmons, T. The Pivotal Role of Phosphorus in a Resilient Water–Energy–Food Security Nexus. *Journal of Environmental Quality* **2015**, *44*, 1049-1062, doi:https://doi.org/10.2134/jeq2015.01.0030.
2. Liu, W.; Ciais, P.; Liu, X.; Yang, H.; Hoekstra, A.Y.; Tang, Q.; Wang, X.; Li, X.; Cheng, L. Global Phosphorus Losses from Croplands under Future Precipitation Scenarios. *Environmental Science & Technology* **2020**, *54*, 14761-14771, doi:10.1021/acs.est.0c03978.
3. Sharpley, A.N.; Smith, S.J.; Jones, O.R.; Berg, W.A.; Coleman, G.A. The Transport of Bioavailable Phosphorus in Agricultural Runoff. *Journal of Environmental Quality* **1992**, *21*, 30-35, doi:10.2134/jeq1992.00472425002100010003x.
4. McKelvie, I.D.; Peat, D.M.W.; Worsfold, P.J. Analytical perspective. Techniques for the quantification and speciation of phosphorus in natural waters. *Analytical Proceedings including Analytical Communications* **1995**, *32*, 437-445, doi:10.1039/AI9953200437.
5. Gentry, L.E.; David, M.B.; Royer, T.V.; Mitchell, C.A.; Starks, K.M. Phosphorus Transport Pathways to Streams in Tile-Drained Agricultural Watersheds. *Journal of Environmental Quality* **2007**, *36*, 408-415, doi:10.2134/jeq2006.0098.
6. Force, M.R.G.o.M.W.N.T. Gulf Hypoxia Action Plan 2008 for Reducing, Mitigating, and Controlling Hypoxia in the Northern Gulf of Mexico and Improving Water Quality in the Mississippi River Basin. USEPA, Ed. Washington D.C., 2008.
7. Robertson, D.M.; Saad, D.A. SPARROW models used to understand nutrient sources in the Mississippi/Atchafalaya River Basin. *Journal of Environmental Quality* **2013**, *42*, 1422-1440, doi:10.2134/jeq2013.02.0066.
8. Agency, M.P.C. The Minnesota Nutrient Reduction Strategy. **2014**.
9. Stewardship, I.D.o.A.a.L.; Resources, I.D.o.N.; Sciences, I.S.U.C.o.A.a.L. *Iowa Nutrient Reduction Strategy: A science and technology-based framework to assess and reduce nutrients to Iowa waters and the Gulf of Mexico*; 2013.
10. Force, M.R.G.o.M.W.N.T. Mississippi River Gulf of Mexico Watershed Nutrient Task Force New Goal Framework. USEPA, Ed. 2014.
11. Force, M.R.G.o.M.W.N.T. *Looking Forward: The Strategy of the Federal Members of the Hypoxia Task Force*; 2013.
12. Christianson, R.; Christianson, L.; Wong, C.; Helmers, M.; McIsaac, G.; Mulla, D.; McDonald, M. Beyond the nutrient strategies: Common ground to accelerate agricultural water quality improvement in the upper Midwest. *Journal of Environmental Management* **2018**, *206*, 1072-1080, doi:https://doi.org/10.1016/j.jenvman.2017.11.051.
13. Alexander, R.B.; Smith, R.A.; Schwarz, G.E.; Boyer, E.W.; Nolan, J.V.; Brakebill, J.W. Differences in Phosphorus and Nitrogen Delivery to The Gulf of Mexico from the Mississippi River Basin. *Environmental Science & Technology* **2008**, *42*, 822-830, doi:10.1021/es0716103.
14. ILEPA. Illinois Nutrient Loss Reduction Strategy. EPA, Ed. 2014.
15. ILEPA. Illinois Nutrient Loss Reduction Strategy: Biennial Report. EPA, Ed. 2019.
16. Ohio EPA, D.o.S.W.; Ohio Department of Agriculture, L.E.P.P.; Ohio Department of Natural Resources, D.o.S.a.W.R. *Ohio Nutrient Reduction Strategy*; 2013.

17. Kleinman, P.J.A.; Sharpley, A.N.; Saporito, L.S.; Buda, A.R.; Bryant, R.B. Application of manure to no-till soils: phosphorus losses by sub-surface and surface pathways. *Nutrient Cycling in Agroecosystems* **2009**, *84*, 215-227, doi:10.1007/s10705-008-9238-3.
18. Reid, K.; Schneider, K.; McConkey, B. Components of Phosphorus Loss From Agricultural Landscapes, and How to Incorporate Them Into Risk Assessment Tools. *Frontiers in Earth Science* **2018**, *6*, doi:10.3389/feart.2018.00135.
19. Addy, K.; Gold, A.J.; Christianson, L.E.; David, M.B.; Schipper, L.A.; Ratigan, N.A. Denitrifying Bioreactors for Nitrate Removal: A Meta-Analysis. *Journal of Environmental Quality* **2016**, *45*, 873-881, doi:https://doi.org/10.2134/jeq2015.07.0399.
20. Christianson, L.E.; Lepine, C.; Sibrell, P.L.; Penn, C.; Summerfelt, S.T. Denitrifying woodchip bioreactor and phosphorus filter pairing to minimize pollution swapping. *Water Research* **2017**, *121*, 129-139, doi:https://doi.org/10.1016/j.watres.2017.05.026.
21. Mayer, P.M.; Reynolds Jr., S.K.; McCutchen, M.D.; Canfield, T.J. Meta-Analysis of Nitrogen Removal in Riparian Buffers. *Journal of Environmental Quality* **2007**, *36*, 1172-1180, doi:https://doi.org/10.2134/jeq2006.0462.
22. Mankin, K.R.; Ngandu, D.M.; Barden, C.J.; Hutchinson, S.L.; Geyer, W.A. Grass-Shrub Riparian Buffer Removal of Sediment, Phosphorus, and Nitrogen From Simulated Runoff1. *JAWRA Journal of the American Water Resources Association* **2007**, *43*, 1108-1116, doi:https://doi.org/10.1111/j.1752-1688.2007.00090.x.
23. Saunders, D.L.; Kalff, J. Nitrogen retention in wetlands, lakes and rivers. *Hydrobiologia* **2001**, *443*, 205-212, doi:10.1023/A:1017506914063.
24. Uusi-Kämppä, J.; Braskerud, B.; Jansson, H.; Syversen, N.; Uusitalo, R. Buffer Zones and Constructed Wetlands as Filters for Agricultural Phosphorus. *Journal of Environmental Quality* **2000**, *29*, 151-158, doi:https://doi.org/10.2134/jeq2000.00472425002900010019x.
25. Hey, D.L.; Kenimer, A.L.; Barrett, K.R. Water quality improvement by four experimental wetlands. *Ecological Engineering* **1994**, *3*, 381-397, doi:https://doi.org/10.1016/0925-8574(94)00008-5.
26. Kovacic, D.A.; David, M.B.; Gentry, L.E.; Starks, K.M.; Cooke, R.A. Effectiveness of Constructed Wetlands in Reducing Nitrogen and Phosphorus Export from Agricultural Tile Drainage. *Journal of Environmental Quality* **2000**, *29*, 1262-1274, doi:10.2134/jeq2000.00472425002900040033x.
27. Kadlec, R.H. Large Constructed Wetlands for Phosphorus Control: A Review. *Water* **2016**, *8*, 243.
28. Dillaha, T.A.; Sherrard, J.H.; Lee, D.; Mostaghimi, S.; Shanholtz, V.O. Evaluation of Vegetative Filter Strips as a Best Management Practice for Feed Lots. *Journal (Water Pollution Control Federation)* **1988**, *60*, 1231-1238.
29. Lee, K.-H.; Isenhart, T.M.; Schultz, R.C.; Mickelson, S.K. Multispecies Riparian Buffers Trap Sediment and Nutrients during Rainfall Simulations. *Journal of Environmental Quality* **2000**, *29*, 1200-1205, doi:https://doi.org/10.2134/jeq2000.00472425002900040025x.
30. Lowrance, R.; Sheridan, J.M. Surface Runoff Water Quality in a Managed Three Zone Riparian Buffer. *Journal of Environmental Quality* **2005**, *34*, 1851-1859, doi:https://doi.org/10.2134/jeq2004.0291.
31. Uusi-Kämppä, J. Phosphorus purification in buffer zones in cold climates. *Ecological Engineering* **2005**, *24*, 491-502, doi:https://doi.org/10.1016/j.ecoleng.2005.01.013.

32. Penn, C.; McGrath, J.; Bowen, J.; Wilson, S. Phosphorus removal structures: A management option for legacy phosphorus. *Journal of Soil and Water Conservation* **2014**, *69*, 51A-56A, doi:10.2489/jswc.69.2.51A.
33. Shedekar, V.S.; Penn, C.J.; Pease, L.; King, K.W.; Kalcic, M.M.; Livingston, S.J. Performance of a Ditch-Style Phosphorus Removal Structure for Treating Agricultural Drainage Water with Aluminum-Treated Steel Slag. *Water* **2020**, *12*, 2149.
34. Penn, C.; Livingston, S.; Shedekar, V.; King, K.; Williams, M. Performance of Field-Scale Phosphorus Removal Structures Utilizing Steel Slag for Treatment of Subsurface Drainage. *Water* **2020**, *12*, 443.
35. Indiana State Department of Agriculture, D.o.S.C.; Management, I.D.o.E. *Indiana Nutrient Reduction Strategy: A framework to reduce nutrients entering Indiana's waters*; 2016.
36. Penn, C.J.; Bryant, R.B.; Kleinman, P.J.A.; Allen, A.L. Removing dissolved phosphorus from drainage ditch water with phosphorus sorbing materials. *Journal of Soil and Water Conservation* **2007**, *62*, 269-276.
37. Stoner, D.; Penn, C.; McGrath, J.; Warren, J. Phosphorus Removal with By-Products in a Flow-Through Setting. *Journal of Environmental Quality* **2012**, *41*, 654-663, doi:10.2134/jeq2011.0049.
38. Penn, C.J.; Bryant, R.B.; Callahan, M.P.; McGrath, J.M. Use of Industrial By-products to Sorb and Retain Phosphorus. *Communications in Soil Science and Plant Analysis* **2011**, *42*, 633-644, doi:10.1080/00103624.2011.550374.
39. Cucarella, V.; Renman, G. Phosphorus Sorption Capacity of Filter Materials Used for On-site Wastewater Treatment Determined in Batch Experiments–A Comparative Study. *Journal of Environmental Quality* **2009**, *38*, 381-392, doi:10.2134/jeq2008.0192.
40. Ragheb, S.M. Phosphate removal from aqueous solution using slag and fly ash. *HBRC Journal* **2013**, *9*, 270-275, doi:https://doi.org/10.1016/j.hbrcj.2013.08.005.
41. Drizo, A.; Frost, C.A.; Grace, J.; Smith, K.A. Physico-chemical screening of phosphate-removing substrates for use in constructed wetland systems. *Water Research* **1999**, *33*, 3595-3602, doi:https://doi.org/10.1016/S0043-1354(99)00082-2.
42. King, K.W.; Williams, M.R.; Dick, W.A.; LaBarge, G.A. Decreasing Phosphorus Loss in Tile-Drained Landscapes Using Flue Gas Desulfurization Gypsum. *Journal of Environmental Quality* **2016**, *45*, 1722-1730, doi:10.2134/jeq2016.04.0132.
43. Bryant, R.B.; Buda, A.R.; Kleinman, P.J.A.; Church, C.D.; Saporito, L.S.; Folmar, G.J.; Bose, S.; Allen, A.L. Using Flue Gas Desulfurization Gypsum to Remove Dissolved Phosphorus from Agricultural Drainage Waters. *Journal of Environmental Quality* **2012**, *41*, 664-671, doi:10.2134/jeq2011.0294.
44. Gottschall, N.; Edwards, M.; Craiovan, E.; Frey, S.K.; Sunohara, M.; Ball, B.; Zoski, E.; Topp, E.; Khan, I.; Clark, I.D., et al. Amending woodchip bioreactors with water treatment plant residuals to treat nitrogen, phosphorus, and veterinary antibiotic compounds in tile drainage. *Ecological Engineering* **2016**, *95*, 852-864, doi:https://doi.org/10.1016/j.ecoleng.2016.06.011.
45. Leader, J.W.; Dunne, E.J.; Reddy, K.R. Phosphorus Sorbing Materials: Sorption Dynamics and Physicochemical Characteristics. *Journal of Environmental Quality* **2008**, *37*, 174-181, doi:10.2134/jeq2007.0148.

46. Gibbs, M.M.; Hickey, C.W.; Özkundakci, D. Sustainability assessment and comparison of efficacy of four P-inactivation agents for managing internal phosphorus loads in lakes: sediment incubations. *Hydrobiologia* **2010**, *658*, 253-275.
47. Sibrell, P.L.; Montgomery, G.A.; Ritenour, K.L.; Tucker, T.W. Removal of phosphorus from agricultural wastewaters using adsorption media prepared from acid mine drainage sludge. *Water Research* **2009**, *43*, 2240-2250, doi:https://doi.org/10.1016/j.watres.2009.02.010.
48. Sibrell, P.L.; Tucker, T.W. Fixed bed sorption of phosphorus from wastewater using iron oxide-based media derived from acid mine drainage. *Water, Air, & Soil Pollution* **2012**, *223*, 5105-5117, doi:10.1007/s11270-012-1262-x.
49. Penn, C.J.; McGrath, J.M. Predicting Phosphorus Sorption onto Steel Slag Using a Flow-through approach with Application to a Pilot Scale System. *Journal of Water Resource and Protection* **2011**, *Vol.03No.04*, 10, doi:10.4236/jwarp.2011.34030.
50. Penn, C.J.; McGrath, J.M.; Rounds, E.; Fox, G.; Heeren, D. Trapping Phosphorus in Runoff with a Phosphorus Removal Structure. *Journal of Environmental Quality* **2012**, *41*, 672-679, doi:10.2134/jeq2011.0045.
51. Hou, L.; Liang, Q.; Wang, F. Mechanisms that control the adsorption–desorption behavior of phosphate on magnetite nanoparticles: the role of particle size and surface chemistry characteristics. *RSC Advances* **2020**, *10*, 2378-2388, doi:10.1039/C9RA08517C.
52. Liu, D.; Zhu, H.; Wu, K.; Wang, F.; Zhao, X.; Liao, Q. Understanding the effect of particle size of waste concrete powder on phosphorus removal efficiency. *Construction and Building Materials* **2020**, *236*, 117526, doi:https://doi.org/10.1016/j.conbuildmat.2019.117526.
53. Penn, C.; Bowen, J.; McGrath, J.; Nairn, R.; Fox, G.; Brown, G.; Wilson, S.; Gill, C. Evaluation of a universal flow-through model for predicting and designing phosphorus removal structures. *Chemosphere* **2016**, *151*, 345-355, doi:https://doi.org/10.1016/j.chemosphere.2016.02.105.
54. Kostura, B.; Kulveitová, H.; Leško, J. Blast furnace slags as sorbents of phosphate from water solutions. *Water Research* **2005**, *39*, 1795-1802, doi:https://doi.org/10.1016/j.watres.2005.03.010.
55. Sanford, J.R.; Larson, R.A. Evaluation of Phosphorus Filter Media for an Inline Subsurface Drainage Treatment System. *Journal of Environmental Quality* **2016**, *45*, 1919-1925, doi:10.2134/jeq2016.01.0038.
56. Hemwall, J.B. The Fixation of Phosphorus by Soils. In *Advances in Agronomy*, Norman, A.G., Ed. Academic Press: 1957; Vol. 9, pp. 95-112.
57. Dayton, E.A.; Basta, N.T. A Method for Determining the Phosphorus Sorption Capacity and Amorphous Aluminum of Aluminum-Based Drinking Water Treatement Residuals. *Journal of Environmental Quality* **2005**, *34*, 1112-1118.
58. McKeague, J.; Day, J.H. Dithionite and oxalate-extractable Fe and Al as aids in differentiation various classes of soils. *Canadian Journal of Soil Science* **1966**, *46*, 13-22.
59. Zhang, H.; Kovar, J.L. Fractionation of Soil Phosphorus. In *Methods of Phosphorus Analysis for Soils, Sediments, Residuals, and Waters*, Second Edition ed.; Kovar, J.L., Pierzynski, G.M., Eds. SERA-IEG 17: Southern Cooperative Series Bulletin No. 408, 2009.

60. Chang, S.C.; Jackson, M.L. Fractionation of soil phosphorus. *Soil Science* **1957**, *84*, 133-144.
61. Drizo, A.; Comeau, Y.; Forget, C.; Chapuis, R.P. Phosphorus Saturation Potential: A Parameter for Estimating the Longevity of Constructed Wetland Systems. *Environmental Science & Technology* **2002**, *36*, 4642-4648, doi:10.1021/es011502v.
62. Ballantine, D.J.; Tanner, C.C. Substrate and filter materials to enhance phosphorus removal in constructed wetlands treating diffuse farm runoff: a review. *New Zealand Journal of Agricultural Research* **2010**, *53*, 71-95, doi:10.1080/00288231003685843.
63. Mann, R.; Bavor, H.J. Phosphorus Removal in Constructed Wetlands Using Gravel and Industrial Waste Substrata. *Water Science and Technology* **1993**, *27*, 107-113, doi:10.2166/wst.1993.0027.
64. Sakadevan, K.; Bavor, H.J. Phosphate adsorption characteristics of soils, slags and zeolite to be used as substrates in constructed wetland systems. *Water Research* **1998**, *32*, 393-399, doi:https://doi.org/10.1016/S0043-1354(97)00271-6.
65. Drizo, A.; Cummings, J.; Weber, D.; Twohig, E.; Druschel, G.; Bourke, B. New Evidence for Rejuvenation of Phosphorus Retention Capacity in EAF Steel Slag. *Environmental Science & Technology* **2008**, *42*, 6191-6197, doi:10.1021/es800232r.
66. Nancucheo, I.; Bitencourt, J.A.P.; Sahoo, P.K.; Alves, J.O.; Siqueira, J.O.; Oliveira, G. Recent Developments for Remediating Acidic Mine Waters Using Sulfidogenic Bacteria. *BioMed Research International* **2017**, *2017*, 7256582, doi:10.1155/2017/7256582.
67. Kefeni, K.K.; Msagati, T.A.M.; Mamba, B.B. Acid mine drainage: Prevention, treatment options, and resource recovery: A review. *Journal of Cleaner Production* **2017**, *151*, 475-493.
68. Standard, A.; D422. Standard Test Method for Particle-Size Analysis of Soils. West Conshohocken, PA, 1963 (1998).
69. Xu, D.; Xu, J.; Wu, J.; Muhammad, A. Studies on the phosphorus sorption capacity of substrates used in constructed wetland systems. *Chemosphere* **2006**, *63*, 344-352, doi:https://doi.org/10.1016/j.chemosphere.2005.08.036.
70. Murphy, J.; Riley, J.P. A modified single solution method for the determination of phosphate in natural waters. *Analytica Chimica Acta* **1962**, *27*, 31-36, doi:https://doi.org/10.1016/S0003-2670(00)88444-5.
71. EPA, U.S. Method 3050B: Acid digestion of sediments, sludges, and soils. Washington, DC, 1996.
72. Sparks, D.L.; Page, A.; Helmke, P.; Loeppert, R.; Soltanpour, P.; Tabatabai, M.; Johnston, C.; Sumner, M. Methods of soil analysis. Part 3-Chemical methods. *Soil Science Society of America* **1996**.
73. Guan, X.-H.; Liu, Q.; Chen, G.-H.; Shang, C. Surface complexation of condensed phosphate to aluminum hydroxide: An ATR-FTIR spectroscopic investigation. *Journal of Colloid and Interface Science* **2005**, *289*, 319-327, doi:https://doi.org/10.1016/j.jcis.2004.08.041.
74. Margenot, A.J.; Calderón, F.J.; Parikh, S.J. Limitations and Potential of Spectral Subtractions in Fourier-Transform Infrared Spectroscopy of Soil Samples. *Soil Science Society of America Journal* **2015**, *80*, 10-26.
75. Yildirim, I.Z.; Prezzi, M. Steel Slag: Chemistry, Mineralogy, and Morphology. In *IFCEE 2015*, 2015; doi:10.1061/9780784479087.263pp. 2816-2825.

76. Yildirim, I.Z.; Prezzi, M. Chemical, Mineralogical, and Morphological Properties of Steel Slag. *Advances in Civil Engineering* **2011**, *2011*, 463638, doi:10.1155/2011/463638.
77. Geiseler, J. Use of steelworks slag in Europe. *Waste Management* **1996**, *16*, 59-63, doi:https://doi.org/10.1016/S0956-053X(96)00070-0.
78. Reddy, A.S.; Pradhan, R.K.; Chandra, S. Utilization of Basic Oxygen Furnace (BOF) slag in the production of a hydraulic cement binder. *International Journal of Mineral Processing* **2006**, *79*, 98-105, doi:https://doi.org/10.1016/j.minpro.2006.01.001.
79. Tzevelekou, T.; Lampropoulou, P.; Giannakopoulou, P.P.; Rogkala, A.; Koutsovitis, P.; Koukouzas, N.; Petrounias, P. Valorization of Slags Produced by Smelting of Metallurgical Dusts and Lateritic Ore Fines in Manufacturing of Slag Cements. *Applied Sciences* **2020**, *10*, 4670.
80. Wachsmuth, F.; Geiseler, J.; Fix, W.; Koch, K.; Schwerdtfeger, K. Contribution to the Structure of BOF-Slags and its Influence on Their Volume Stability. *Canadian Metallurgical Quarterly* **1981**, *20*, 279-284, doi:10.1179/cmq.1981.20.3.279.
81. Juckes, L.M. The volume stability of modern steelmaking slags. *Mineral Processing and Extractive Metallurgy* **2003**, *112*, 177-197, doi:10.1179/037195503225003708.
82. Tsakiridis, P.E.; Papadimitriou, G.D.; Tsivilis, S.; Koroneos, C. Utilization of steel slag for Portland cement clinker production. *Journal of hazardous materials* **2008**, *152*, 805-811, doi:https://doi.org/10.1016/j.jhazmat.2007.07.093.
83. Tossavainen, M.; Engstrom, F.; Yang, Q.; Menad, N.; Lidstrom Larsson, M.; Bjorkman, B. Characteristics of steel slag under different cooling conditions. *Waste Management* **2007**, *27*, 1335-1344, doi:https://doi.org/10.1016/j.wasman.2006.08.002.
84. Nicolae, M.; Vîlciu, I. X-RAY DIFFRACTION ANALYSIS OF STEEL SLAG AND BLAST FURNACE SLAG VIEWING THEIR USE FOR ROAD CONSTRUCTION.
85. Qian, G.R.; Sun, D.D.; Tay, J.H.; Lai, Z.Y. Hydrothermal reaction and autoclave stability of Mg bearing RO phase in steel slag. *British Ceramic Transactions* **2002**, *101*, 159-164, doi:10.1179/096797802225003415.
86. Masindi, V. Recovery of drinking water and valuable minerals from acid mine drainage using an integration of magnesite, lime, soda ash, CO2 and reverse osmosis treatment processes. *Journal of Environmental Chemical Engineering* **2017**, *5*, 3136-3142, doi:https://doi.org/10.1016/j.jece.2017.06.025.
87. Masindi, V.; Madzivire, G.; Tekere, M. Reclamation of water and the synthesis of gypsum and limestone from acid mine drainage treatment process using a combination of pre-treated magnesite nanosheets, lime, and CO2 bubbling. *Water Resources and Industry* **2018**, *20*, 1-14, doi:https://doi.org/10.1016/j.wri.2018.07.001.
88. Masindi, V.; Osman, M.S.; Shingwenyana, R. Valorization of acid mine drainage (AMD): A simplified approach to reclaim drinking water and synthesize valuable minerals – Pilot study. *Journal of Environmental Chemical Engineering* **2019**, *7*, 103082, doi:https://doi.org/10.1016/j.jece.2019.103082.
89. Blanch, A.J.; Quinton, J.S.; Lenehan, C.E.; Pring, A. The crystal chemistry of Al-bearing goethites: an infrared spectroscopic study. *Mineralogical Magazine* **2008**, *72*, 1043-1056, doi:10.1180/minmag.2008.072.5.1043.
90. Ruan, H.D.; Frost, R.L.; Kloprogge, J.T. The behavior of hydroxyl units of synthetic goethite and its dehydroxylated product hematite. *Spectrochimica Acta Part A:*

Molecular and Biomolecular Spectroscopy **2001**, *57*, 2575-2586, doi:https://doi.org/10.1016/S1386-1425(01)00445-0.
91. Cui, H.; Ren, W.; Lin, P.; Liu, Y. Structure control synthesis of iron oxide polymorph nanoparticles through an epoxide precipitation route. *Journal of Experimental Nanoscience* **2013**, *8*, 869–875, doi:10.1080/17458080.2011.616541.
92. Cambier, P. Infrared study of goethites of varying crystallinity and particle size: I. Interpretation of OH and lattice vibration frequencies. *Clay Minerals* **1986**, *21*, 191-200, doi:10.1180/claymin.1986.021.2.08.
93. Margenot, A.J.; Calderón, F.J.; Goyne, K.W.; Mukome, F.N.D.; Parikh, S.J. IR Spectroscopy, Soil Analysis Applications. In *Encyclopedia of Spectroscopy and Spectrometry (Third Edition)*, Lindon, J.C., Tranter, G.E., Koppenaal, D.W., Eds. Academic Press: Oxford, 2017; https://doi.org/10.1016/B978-0-12-409547-2.12170-5pp. 448-454.
94. Vahur, S.; Teearu, A.; Peets, P.; Joosu, L.; Leito, I. ATR-FT-IR spectral collection of conservation materials in the extended region of 4000-80 cm–1. *Analytical and Bioanalytical Chemistry* **2016**, *408*, 3373-3379, doi:10.1007/s00216-016-9411-5.
95. Frost, R.L.; Kloprogge, J.T. Infrared emission spectroscopic study of brucite. *Spectrochimica Acta Part A: Molecular and Biomolecular Spectroscopy* **1999**, *55*, 2195-2205, doi:https://doi.org/10.1016/S1386-1425(99)00016-5.
96. Reig, F.B.; Adelantado, J.V.G.; Moya Moreno, M.C.M. FTIR quantitative analysis of calcium carbonate (calcite) and silica (quartz) mixtures using the constant ratio method. Application to geological samples. *Talanta* **2002**, *58*, 811-821, doi:https://doi.org/10.1016/S0039-9140(02)00372-7.
97. Campbell, S.; Poduska, K.M. Incorporating Far-Infrared Data into Carbonate Mineral Analyses. *Minerals* **2020**, *10*, 628.
98. Toffolo, M.B.; Regev, L.; Dubernet, S.; Lefrais, Y.; Boaretto, E. FTIR-Based Crystallinity Assessment of Aragonite–Calcite Mixtures in Archaeological Lime Binders Altered by Diagenesis. *Minerals* **2019**, *9*, 121.
99. Rodriguez-Blanco, J.; Shaw, S.; Benning, L. The Kinetics and Mechanisms of Amorphous Calcium Carbonate (ACC) Crystallization to Calcite, Via Vaterite. *Nanoscale* **2010**, *3*, 265-271, doi:10.1039/c0nr00589d.
100. Zuleta, F.; Murciano, A.; Gehrke, S.A.; Maté-Sánchez de Val, J.E.; Calvo-Guirado, J.L.; De Aza, P.N. A New Biphasic Dicalcium Silicate Bone Cement Implant. *Materials (Basel)* **2017**, *10*, 758, doi:10.3390/ma10070758.
101. Horgnies, M.; Chen, J.J.; Bouillon, C. Overview about the use of Fourier Transform Infrared spectroscopy to study cementitious materials. *WIT Transactions on Engineering Sciences* **2013**, *77*.
102. Parikh, S.J.; Goyne, K.W.; Margenot, A.J.; Mukome, F.N.D.; Calderón, F.J. Chapter One - Soil Chemical Insights Provided through Vibrational Spectroscopy. In *Advances in Agronomy*, Sparks, D.L., Ed. Academic Press: 2014; Vol. 126, pp. 1-148.
103. Yasipourtehrani, S.; Strezov, V.; Evans, T. Investigation of Phosphate Removal Capability of Blast Furnace Slag in Wastewater Treatment. *Scientific Reports* **2019**, *9*, 7498, doi:10.1038/s41598-019-43896-y.
104. Ruan, H.D.; Frost, R.L.; Kloprogge, J.T.; Duong, L. Far-infrared spectroscopy of alumina phases. *Spectrochimica Acta Part A: Molecular and Biomolecular Spectroscopy* **2002**, *58*, 265-272, doi:https://doi.org/10.1016/S1386-1425(01)00532-7.

105. Penn, C.; Bowen, J. *Design and Construction of Phosphorus Removal Structures for Improving Water Quality*; 2018; 10.1007/978-3-319-58658-8.
106. NRCS, U. Part 630 Hydrology National Engineering Handbook. Washington, D.C., 2007.
107. Li, S.; Cooke, R.A.; Huang, X.; Christianson, L.; Bhattarai, R. Evaluation of fly ash pellets for phosphorus removal in a laboratory scale denitrifying bioreactor. *Journal of Environmental Management* **2018**, *207*, 269-275, doi:https://doi.org/10.1016/j.jenvman.2017.11.040.
108. Boujelben, N.; Bouzid, J.; Elouear, Z.; Feki, M.; Jamoussi, F.; Montiel, A. Phosphorus removal from aqueous solution using iron coated natural and engineered sorbents. *Journal of hazardous materials* **2008**, *151*, 103-110, doi:https://doi.org/10.1016/j.jhazmat.2007.05.057.
109. Hertzberger, A.; Pittelkow, C.; Harmel, R.; Christianson, L. Analysis of the MANAGE Drain Concentration Database to Evaluate Agricultural Management Effects on Drainage Water Nutrient Concentrations. *Transactions of the ASABE* **2019**, *62*, 929-939, doi:10.13031/trans.13230.
110. Scholtz, E.C.; Feldkamp, J.R.; White, J.L.; Hem, S.L. Point of zero charge of amorphous aluminum hydroxide as a function of adsorbed carbonate. *Journal of Pharmaceutical Sciences* **1985**, *74*, 478-481, doi:https://doi.org/10.1002/jps.2600740423.
111. Parks, G.A.; Bruyn, P.L.d. The Zero Point of Charge of Oxides. *The Journal of Physical Chemistry* **1962**, *66*, 967-973, doi:10.1021/j100812a002.
112. Mann, R.A. Phosphorus adsorption and desorption characteristics of constructed wetland gravel and steelworks by-products. *Australian Journal of Soil Research* **1997**, *35*, 375-384.
113. Barrow, N.J.; Sen, A.; Roy, N.; Debnath, A. The soil phosphate fractionation fallacy. *Plant and Soil* **2020**, 10.1007/s11104-020-04476-6, doi:10.1007/s11104-020-04476-6.
114. Administration, F.H. User Guidelines for Waste and Byproduct Materials in Pavement Construction. Transportation, U.D.o., Ed. Washington, DC, 2016.
115. USEPA. Technical Document: Acid Mine Drainage Prediction. USEPA, Ed. Washington, DC, 1994.
116. Mahony, B.; Moulson, I.; Wilkinson, H.C. Study of the relation between the phosphorus content of coal and coke. *Fuel* **1981**, *60*, 355-358, doi:https://doi.org/10.1016/0016-2361(81)90206-4.

CHAPTER 2: ASSESSING METHODOLOGIES USED TO EVALUATE DISSOLVED PHOSPHORUS REMOVAL OF PHOSPHORUS-SORBING MATERIAL

2.1 Introduction

Phosphorus (P) losses from agricultural fields to surface waters continue to contribute to eutrophication globally [1]. Export of P to surface waters from soils occurs as particulate and soluble forms, the latter known as dissolved reactive P (DRP) [3]. Particulate P loss can be reduced by erosion control measures, but some commonly utilized best management practices (e.g. cover crops, reduced tillage, buffers) are not specifically designed to mitigate DRP losses [119] and therefore can vary in effectiveness of decreasing DRP losses [27,31,120]. Phosphorus removal structures are a relatively underutilized management practice [12] that target DRP removal from agricultural surface runoff [32,39]. Phosphorus removal structures are targeted to hydrologically active areas on the edge of agricultural fields where surface runoff will pass through the structure. Phosphorus removal structures are filled with P-sorbing media (PSM), waste by-products with high P removal potential. Before P removal structures can be designed and constructed, the PSM are generally chosen based on laboratory experiments to determine the DRP removal potential. Multiple studies have evaluated DRP removal across diverse PSM [39], but differing methodologies challenge comparisons [61].

Two methods frequently used to evaluate DRP removal potential of PSM are batch sorption isotherm experiments and flow-through columns. Batch sorption isotherm experiments are utilized to estimate DRP removal potential by yielding a maximum P sorption capacity. This in turn can be used in tandem with the PSM mass of the P removal structure to predict its lifespan [61]. For batch isotherm experiments evaluating P sorption by soil, a set of methodological procedures has been proposed [121,122], but for PSM the recommendations on

batch sorption parameters are not strictly followed for every experiment [39]. Key batch isotherm parameters include the solid to solution ratio, contact time, DRP concentrations used, and whether an electrolyte is present in the background matrix [122,123]. The solid to solution ratio affects DRP removal potential because a lower ratio requires a longer equilibration time and also can lead to higher concentration of DRP removed, potentially introducing discrepancies between P removal determined by batch isotherms of PSM versus field-scale P removal structures [39,124]. The contact time of solution to solid needs to be sufficient for equilibrium to be reached, and this time can vary greatly depending on PSM particle size [125,126]. The range of DRP concentration is typically lower (< 50 mg L^{-1}) [41,48] to simulate the concentration of surface runoff (typically ≤ 1.25 mg L^{-1} for surface and subsurface flow in the US) [5,111] or an arbitrarily higher DRP concentration (e.g. 1,000 or 3,200 mg L^{-1}) [38,71]. Using DRP concentrations of up to 1000 mg L^{-1} can still be insufficient to saturate certain PSM , and preventing the calculation of S_{max} as a metric of maximum DRP removal potential [127]. The background matrix for batch isotherms in general requires the use of an electrolyte solution (e.g., 0.01 M KCl), but in PSM evaluations the use of an electrolyte is inconsistent. The value of using an electrolyte is to maintain ionic strength as P is removed from solution to offset the potassium counterion effect of the potassium monophosphate added to not overestimate P removal. Electrolytes are known to interfere with the P sorption process and thus sorption capacity [39].

Flow-through columns are another method used to evaluate DRP removal potential by PSM. The effect of retention time and P concentration on DRP removal potential can be tested using flow-through columns. Columns are meant to simulate an inflow DRP concentration and retention time similar to what PSM would experience in a P removal structure [107]. The inflow DRP concentrations for flow-through columns (0.5 – 15 mg L^{-1} [37,49,128]) are typically closer to

DRP concentrations in agricultural runoff (maximum flow-weighted average of 1.25 mg P L^{-1}) [5,111]. In batch isotherms, the concentration of DRP added decreases as P is sorbed by PSM, thereby reducing the DRP concentration in contact with the PSM as time elapses. For flow-through columns, a constant inflow solution DRP concentration is maintained which lowers the DRP removal potential the PSM has to sorb DRP from the starting solution concentration every new cycle of the retention time [107]. Retention time has been shown in one study to have little impact on DRP removal potential for diverse PSM, including AMDR, slag fines, fly ash, flue gas desulfurization gypsum, water treatment residuals, and Excell Minerals [37]. Retention times for flow-through columns (0.5 – 10 min [37,49,128]) represent the limited contact time (< 20 min [50]) DRP-loaded water has with PSM when flowing through a P removal structure. The limited retention time (< 20 min for flow-through columns vs 24 h for batch isotherms) along with the maintained inflow DRP concentrations lower the ability of DRP removal in flow-through columns, therefore flow-through columns typically yield lower magnitudes of DRP removal than batch isotherms [49].

Phosphorus-sorbing materials are commonly classified by two hypothesized elemental mechanisms of DRP removal: 1) slower (> 1 h [129]) precipitation by Ca and/or Mg (pH > 7) and 2) more rapid (< 1 h [130,131]) precipitation by Fe and/or Al (pH < 6.5) [38,56]. As flow-through columns have a retention time < 1 h, the metal cation or mechanism responsible for P removal may be different than previously thought or change as retention time is shortened. Sequential chemical fractionation of P can be used to test the metal cation that is responsible for DRP removal by PSM as retention time is shortened. Sequentially extracted P fractions can be interpreted to approximate P pools based on solubility-based extraction of Al, Fe, and Ca [59]. A standard method for sequential chemical fractionation of inorganic P is that of Chang and

Jackson [60] as modified by Zhang and Kovar [59], which separates P into five fractions NH_4Cl-P (soluble and loosely bound P), NH_4F-P (Al-P), NaOH-P (Fe-P), $Na_3C_6H_5O_7$, $NaHCO_3$, $Na_2S_2O_4$ or CBD-P) (reductant-soluble P), or H_2SO_4-P (Ca-P) [59]. For Ca- and Mg-rich PSM, it would be expected to have DRP recovered as NH_4Cl-P (soluble and loosely bound P) and H_2SO_4-P (Ca-P) and for Al- and Fe-rich PSM, DRP recovered as NH_4Cl-P (soluble and loosely bound P), NH_4F-P (Al-P), NaOH-P (Fe-P), $Na_3C_6H_5O_7$, $NaHCO_3$, $Na_2S_2O_4$ or CBD-P) (reductant-soluble P) [59].

This study examined how the parameters of batch isotherms and flow-through columns as well as the difference between the two methods affected the DRP removal potential of PSM. The first objective was to evaluate to what extent the presence of an electrolyte and DRP concentration range interactively determine the measured DRP removal potential of SS and AMDR. We hypothesized that presence of KCl would lead to a lower DRP removal potential, constraining the DRP concentration to ≤ 1000 mg kg^{-1} may overestimate the DRP removal potential for PSM, and that the effect of DRP concentration range on DRP removal potential would depend on whether an electrolyte solution was used. The second objective was to determine to what extent retention time and influent DRP concentration influence DRP removal in flow-through columns, using a subset of PSM (steel slag). We hypothesized the combinations of retention time and DRP concentration would have the same DRP removal on a mass basis. The third objective was to determine if the metal cation removing DRP is consistent across the DRP concentration and retention time combinations for a subset of PSM in flow-through columns, using a subset of PSM (steel slag). We hypothesized that the majority of DRP removed would be recovered as NH_4Cl-P (soluble and loosely bound P), H_2SO_4-P (Ca-P), and NH_4F-P (Al-P) in flow-through columns, within an increased proportion of DRP recovered as NH_4F-P as retention time decreased. The final objective was to determine to what extent DRP removal

potential was similar for flow-through columns and batch isotherms for a subset of PSM. We hypothesized batch isotherms (no electrolyte, ≤ 20,000 mg kg^{-1}) would lead to greater DRP removal potential for a subset of PSM than flow-through columns, whereas batch isotherms (no electrolyte, ≤ 1000 mg kg^{-1}) would underestimate DRP removal potential.

2.2 Materials & Methods

2.2.1 Filter Media and General Characterization

This study examined four different PSM with recognized potential for DRP removal [39,62]: steel slag 1 (SS1), steel slag 2 (SS2), acid mine drainage residuals 1 (AMDR1) and acid mine drainage residuals 2 (AMDR2) (Table 6). Steel slag is a granular by-product of steel production. For this study, there were two sources of SS and one particle size fraction chosen from each source (< 2 mm for SS1 and 4 – 6.3 mm for SS2) based on the highest combination of P removal and K_{sat} [127]. Steel slag 1 was sourced from TMS International Corporation in Parkhill, PA and SS2 was sourced from US Steel Corporation in Granite City, IL. Acid mine drainage treatment residuals (AMDR) are a fine (< 2 mm diameter) by-product of neutralizing mine drainage waste. The two AMDRs tested were sourced from the Pennsylvania EPA (AMDR1) and the Blue Valley Mine Drainage Treatment and Fish Culture Station in Brandy Camp, PA (AMDR2).

Table 6

Elemental concentrations and pH for steel slag 1 (SS1), steel slag 2 (SS2) and acid mine drainage residuals 1 (AMDR1), and acid mine drainage residuals 2 (AMDR2).

			Total (%)						Water soluble (mg/kg)				Ammonium Oxalate (mg/kg)				Dithionite (mg/kg)			
	pH (1:1)		Ca		Mg		Fe		Ca		Mg		Fe		Al		Fe		Al	
	mean	se	mean	se	mean	se	mean	se	mean	se	mean	se	mean	se	mean	se	mean	se	mean	se
SS1	11	0	15	1	7	0	36.0	1	6671	682	67	6.6	76616	3634	3090	246	21274	1607	421	141
SS2	12	0	21	2	6	1	49.0	3	5348	400	12	1.1	44907	2835	3251	253	4613	375	5181	955
AMDR1	8	0	0	0	0	0	65.0	1	1615	94	57	2.5	12045	196	52	3	200865	10048	117	5
AMDR2	6	0	5	1	0	0	67.0	0	9857	226	46	1.2	198896	3778	662	18	136932	9074	1178	11

2.2.2 Batch isotherms

Phosphorus removal by PSM was quantified via batch sorption isotherm experiments. A solid to solution ratio of 1:20 with 1.50 ± 0.05 g air-dry PSM mass to 30 mL of increasing concentration of PO_4^{3-}-P L^{-1} with an equilibration time of 24 h was selected for consistency with previous evaluations [39]. Batch sorption isotherm tests were conducted in quadruplicate for a factorial of two background combinations by two ranges of DRP concentrations as KH_2PO_4 . The two different background matrices were 18.2 MΩ·cm water and 0.01 M KCl and the two ranges of DRP concentrations used were 0, 100, 200, 400, 600, 800, and 1000 mg kg^{-1} (0 – 50 mg L^{-1}) as and 0, 100, 200, 400, 600, 800, 1000, 1500, 2000, 4000, 6000, 10000, 20000 mg kg^{-1} (0 – 1000 mg L^{-1}) as KH_2PO_4 . The supernatant was immediately filtered (0.45 µm cellulosic filter) after the end of equilibration, DRP was quantified as molybdate reactive phosphorus by colorimetry [72] to calculate the filtrate concentration of P (mg kg^{-1}). With the initial DRP concentration added and the final DRP concentration remaining in the filtrate known, the percent DRP removal was calculated:

$$\text{Percent DRP removed: } \left(\frac{DRP\ added - Final\ DRP\ Concentration}{DRP\ added}\right) * 100 \quad (4)$$

Maximum P sorption capacity (S_{max}) was quantified from the difference between the initial solution P concentration and the equilibrium concentration in the supernatant. The maximum P sorption capacity was determined using the Langmuir equation:

$$S = \frac{S_{max}KC}{1+KC} \quad (5)$$

where S is the sorbed P concentration (mg kg^{-1}), S_{max} is the maximum sorption capacity of the PSM (mg kg^{1}), K is the Langmuir binding strength coefficient (L mg^{-1}), and C is the equilibrium concentration (mg L^{-1}) [132]. The goodness of fit (R^2) was used to determine the fit of the Langmuir model, with a fit above 0.90 deemed an acceptable fit.

2.2.3 Flow-through columns

Flow-through columns were conducted to test the effect of P concentration and retention time on P removal for PSM. Steel slag 1 and SS2 were chosen as a subset of the PSM tested for batch isotherms due to the higher hydraulic conductivity than AMDR1 and AMDR2 [127]. The triplicate columns were constructed of schedule 40 PVC, 2.5 cm diameter, 10.2 cm length packed with either SS1 (~ 110 g per column) or SS2 (~ 80 g per column) and connected to an eight-channel peristaltic pump (Masterflex L/S Variable-Speed Digital Drive Pump with Masterflex L/S Multichannel Cartridge Pump Head for Microbore and Precision Tubing, 8-channels, 4-rollers) that maintained a constant flow of P solution from tanks the columns. A barrier of corrugated plastic with 10, 6-mm holes and three layers of 100% cotton cheese cloth were both cut to the diameter of the columns and placed at both the base and top of the column. The corrugated plastic was closest to the PSM with the cheesecloth on the outside to prevent loss of fine particles. Ten treatments resulted from the combination of retention times and inflow solution DRP concentrations were tested: 1) 2 min RT, 3 mg P L-1, 2) 2 min RT, 1 mg P L^{-1}, 3) 2 min, 0.5 mg P L^{-1}, 4) 1 min, 3 mg P L^{-1}, 5) 1 min, 1 mg P L^{-1}, 6) 1 min, 0.5 mg P L^{-1}, 7) 20 s RT, 3 mg P L^{-1}, 8) 20 s RT, 1 mg P L^{-1}, 9) 20 s RT, 0.5 mg P L^{-1}, and 10) 20 s, 0.05 mg P L^{-1} ($SS2_{4\text{-}6.3}$ only used one column for this combination). Dissolved reactive P solutions were made using potassium monophosphate. Flow rates needed to achieve RT for SS1 were 12 mL min^{-1} (2 min RT), 24 mL min^{-1} (1 min RT), 73 mL min^{-1} (20 s RT) and for SS2, 15 mL min^{-1} (2 m RT), 29 mL min^{-1} (1 m RT), 89 mL min^{-1} (20 s RT). Sampling frequency is shown in Table 7.

Table 7
The sampling frequency (h) for flow-through column experiments. The 'x' indicates that samples were taken at h timepoints from the Day 8 to termination, which varied depending on the steel slag (SS) and treatment.

Day 1	Day 2	Day 3	Day 4	Day 5	Day 6	Day 7	Day 8 to Termination
0.5	24	48	72	96	120	144	x
2	26	50					
4	28	52	76	100	124		
6	30	54					
8	32	56	80	104	128	152	x
12	36	60					

2.2.4 Sequential Fractionation

Sequential fractionation was performed for PSM after completion in flow-through columns. The remaining PSM from the columns were air-dried and ground to < 2 mm. The Chang and Jackson [60] sequential fractionation as modified by Zhang and Kovar [59] was used to estimate 1) NH_4Cl-P (soluble and loosely bound P), 2) NH_4F-P (Al-P), 3) NaOH-P (Fe-P), 4) $Na_3C_6H_5O_7$, $NaHCO_3$, $Na_2S_2O_4$ or CBD-P) (reductant-soluble P), and 5) H_2SO_4-P (Ca-P). First, 0.4 g of air-dried, ground PSM were extracted in 20 mL 1 M NH_4Cl for 30 min, centrifuged, and decanted. Twenty mL 0.5 M NH_4F were added to the residuals, shaken for 1 h, centrifuged, decanted, and washed twice with 10 mL 6.8M NaCl that was combined with the extract. Then, 20 mL 0.1 M NaOH was added to the residuals, shaken for 17 h, centrifuged, decanted, and washed twice with 10 mL 6.8 M NaCl that was combined with the extract. Next, 10 mL 0.3M $Na_3C_6H_5O_7$and 2 mL 1 M $NaHCO_3$ were added to the residuals and heated for 15 min at 85°C. Next, 0.4 g $Na_2S_2O_4$ was added with rapid stirring to mix and heated at 85°C for another 15 min. The samples were then centrifuged, decanted, and washed twice with 10 mL 6.8 M NaCl that was combined with the extract. Finally, 20 mL 0.25 M H_2SO_4 were added to the residuals,

shaken for 1 h, centrifuged, decanted, and the residuals washed twice with 10 mL 6.8 M NaCl that was combined with the extract. The P in the extracts was quantified via ICP-MS (carrier gas Argon). The LOD for NH_4Cl-P was 10 mg kg^{-1}, 17 mg kg^{-1} for CBD-P, and 20 mg kg^{-1} for NH_4F-P, NaOH-P, and H_2SO_4-P.

The NH_4Cl-P was interpreted as soluble and loosely bound P and the metal cation responsible could be Fe, Al, Ca, or Mg (total and/or water-soluble). The NH_4F-P was interpreted as Al-P, corresponding to the metal cation composition of Al_{ao}, the reactive pool of Al. The NaOH-P was interpreted as Fe-P, corresponding to Fe_{ao}. The CBD-P was interpreted as reductant-soluble P or occluded P, corresponding to Fe_{cbd} and Al_{cbd}. The H_2SO_4-P was interpreted as Ca-P, corresponding to the insoluble Ca_{tot} and Mg_{tot}. Total Mg is included here as there is not a fraction that is interpreted specifically for Mg, but fits most closely with Ca.

2.2.5 Statistical Analyses

Analyses were performed using SAS v9.4 (Cary Institute, NC). Response variables were evaluated for the assumptions of normality of residuals and homogeneity of variances. A two-way ANOVA was performed for each PSM on the percent DRP removal for batch isotherms to determine if there was a significant interaction. Mean differences for each PSM between percent DRP removal of batch isotherms for the two-way interaction of the presence of an electrolyte solution and the DRP concentration range were evaluated using Tukey's test with significance at $p \leq 0.05$.

For the flow-through columns, a three-way ANOVA was performed on each sequentially extracted fractions as well as the slopes of the removal curves. Mean differences for percent DRP recovered as NH_4Cl for the effect of PSM type and inflow solution DRP concentration were evaluated using Tukey's test with significance at $p \leq 0.05$. Mean differences for percent DRP

recovered as NH_4F for the effect of PSM type and inflow solution DRP concentration as well as the effect of retention time and inflow solution DRP concentration were evaluated using Tukey's test with significance at $p \leq 0.05$. Mean differences for percent DRP recovered as CBD for the effect of PSM type and inflow solution DRP concentration were evaluated using Tukey's test with significance at $p \leq 0.05$. For the flow-through columns, exponential models, percent DRP removal was log-transformed to create a linear model of percent DRP removal as a function of cumulative DRP added for which the slope was calculated. Mean differences for the slopes of the flow-through column linear models for the effect of PSM type, retention time, and inflow solution DRP concentration were evaluated using Tukey's test with significance at $p \leq 0.05$.

2.3 Results

2.3.1 Batch Sorption Isotherms

The S_{max} was greater for the DRP range $\leq$ 20,000 mg kg^{-1} than $\leq$ 1000 mg kg^{-1} for both the presence and absence of KCl, except for ADMR2 excluding KCl (Table 8). The S_{max} of AMDR2, in the absence of KCl, was 1.5-fold greater for $\leq$ 1000 mg kg^{-1} than $\leq$ 20,000 mg kg^{-1}. The S_{max} was not always less with an electrolyte solution. For SS1, the KCl background decreased the S_{max} for both DRP ranges. S_{max} of SS2, was 4.0-fold greater for $\leq$ 20,000 mg kg^{-1} for KCl inclusion than exclusion. For AMDR1, S_{max} was 4.6-fold greater for $\leq$ 1000 mg kg^{-1} in the presence of KCl than the absence. The S_{max} of AMDR2, was 58.3-fold greater for $\leq$ 20,000 mg kg^{-1} for KCl inclusion than exclusion. None of the PSM exhibited a saturation curve needed to model P removal from solution by the method of Langmuir (Figure 8). The Langmuir model fit (R^2) exceeded 0.90 for six of the sixteen factorial combinations. There was no consistency in which combination of DRP range and electrolyte inclusion or exclusion provided an R^2 above 0.90 for all PSM.

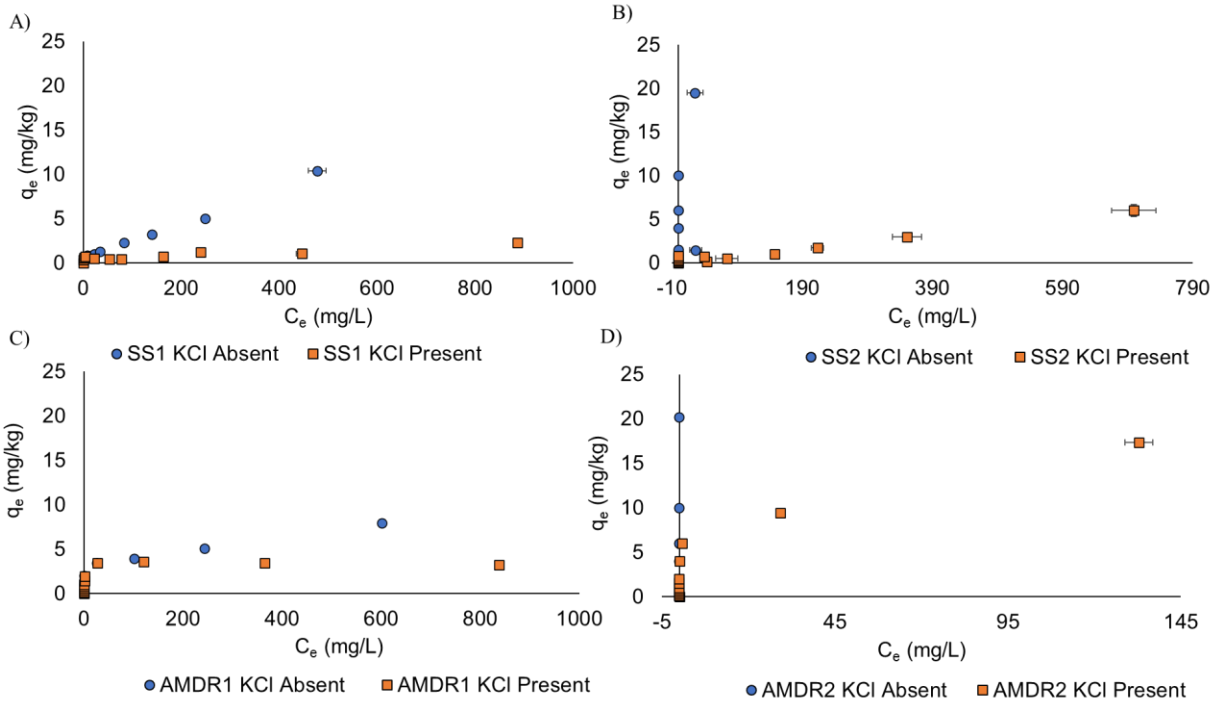

Figure 8.
The batch isotherm Langmuir models showing the DRP in solution at equilibrium on a mass basis (C_e) and the P removed by PSM on a mass basis (q_e) for: a) steel slag 1 (SS1), b) steel slag 2 (SS2), c) acid mine drainage residuals 1 (AMDR1), and d) acid mine drainage residuals 2 (AMDR2).

The proportion of initial solution DRP removed by AMDR1 and AMDR2 was not significantly different for the inclusion of the KCl or not at 1000 mg kg^{-1}, but was greater without KCl when initial DRP concentration was increased to 20,000 mg kg^{-1} (Table 8). The exclusion of KCl increased the percent DRP removal for all PSM at both DRP ranges. Without KCl, the percent DRP removal was similar for both DRP ranges for SS2 and AMDR2. SS1 and AMDR1 had a greater percent DRP removed for 1000 mg kg^{-1} added than 20,000 mg kg^{-1} in the absence of KCl. The percent DRP removed by SS1, AMDR1, and AMDR2 was greater for 1000 mg kg^{-1} added than 20,000 mg kg^{-1} with the inclusion of KCl, but not SS2. Percent DRP removal for SS2 was > 90% for both DRP ranges without KCl. AMDR1 and AMDR2 had > 90% DRP removal for 1000 mg kg^{-1} added with and without KCl.

Table 8

The S_{max} and percent DRP removed for steel slag 1 (SS1, <2 mm), steel slag 2 (SS2, 4-6.3 mm), acid mine drainage residuals 1 (AMDR1), and acid mine drainage residuals 2 (AMDR2) for the factorial combinations of KCl absent ≤1000 mg kg^{-1}, KCl absent ≤ 20,000 mg kg^{-1}, KCl present ≤ 1000 mg kg^{-1}, and KCl present ≤ 20,000 mg kg^{-1}.

	Initial DRP Concentration (mg/kg)	KCl Absent		KCl Present		% DRP Removed	
		S_{max} (mg/kg)	R^2	S_{max} (mg/kg)	R^2	Water	KCl
SS1	1000	909	0.98	714	0.94	84 a	54 b
	20,000	10000	0.61	2500	0.82	52 b	11 c
SS2	1000	294	0.15	133	0.99	100 a	13 c
	20,000	2500	0.56	10000	0.1	97 a	30 b
AMDR1	1000	313	0.14	1429	0.07	100 a	99 a
	20,000	10000	0.95	3333	0.99	40 b	16 c
AMDR2	1000	435	0.05	263	0.18	100 a	100 a
	20,000	286	0.15	16667	0.91	100 a	87 b

Lowercase letter denotes significant difference ($p \leq 0.05$) within PSM type by factorial

The percent DRP removed depended on the DRP concentration range and whether an electrolyte solution was used, for SS1, AMDR1, and AMDR2 (Table 9). For SS2, the percent DRP removed was only dependent on whether an electrolyte solution was used.

Table 9

The F statistic from a two-way ANOVA for steel slag 1 (SS1), steel slag 2 (SS2), acid mine drainage residuals 1 (AMDR1), and acid mine drainage residuals 2 (AMDR2).

	F_{stat}			
Source	SS1	SS2	AMDR1	AMDR2
DRP Range	245.0*	4.3	4624.8*	1002.0*
Electrolyte Solution	233.5*	34.2*	544.7*	902.3*
Range x Electrolyte	67.8*	4.6	521.6*	952.8*

* Denotes significance at ($p \leq 0.001$)

2.3.2 Flow-through Column Breakthrough Curves

The slopes of DRP removal curves for flow-through columns depended on PSM type, retention time and inflow solution DRP concentration (three-way interaction $p < 0.001$) (Figure

9). The slope of the removal curve indicates the percent DRP removed per unit (mg DRP per kg PSM) addition of inflow DRP solution. The slopes are either negative or very close to zero due to the DRP removal curves being an exponential decay equation in which less DRP is removed as the cumulative DRP added increases.

There were only four combinations of retention time and inflow solution DRP concentration at which the slopes of the DRP removal curves differed between PSM type. All of the retention times at 0.5 mg L^{-1} and the 20 s retention time at 1 mg L^{-1}. SS2 DRP removal curves had a 4-fold greater slope than SS1 at the 20 s retention times at 1 mg L^{-1} (-0.0018 vs -0.007) and 6-fold greater at 0.5 mg L^{-1} (-0.0013 vs -0.0074). Steel slag 1 DRP removal curves had a 91-fold greater slope than SS2 at the 2 min (-0.0004 vs -0.0363) and 20-fold greater at 1 min (-0.0008 vs -0.0156) retention time at 0.5 mg L^{-1}. For SS1, the slopes of the DRP removal curves were similar or decreased as the inflow solution DRP concentration decreased from 3 mg L^{-1} to 0.5 mg L^{-1} for 2 min (-0.0004 to -0.0002) and 20 s (-0.0074 to -0.0024) retention time. At 1 min retention time, the DRP removal curves slope was greatest at 1 mg L^{-1} (0.0010) vs 3 mg L^{-1} (-0.0024) or 0.5 mg L^{-1} (-0.0074) for SS1. The slopes of the SS2 DRP removal curves were similar or decreased as the inflow solution DRP concentration decreased from 3 mg L^{-1} to 0.5 mg L^{-1} for all retention times. For the 2 min retention time, both PSM type and all DRP concentrations were similar (slopes -0.0015 to -0.0002) except for SS2 0.5 mg L^{-1} (slope of -0.0363). At 1 min retention time, the slopes of the DRP removal curves for SS1 and SS2 were similar at 3 mg L^{-1} (-0.0002 vs -0.0032) and 1 mg L^{-1} (-0.0015 vs -0.0020). Steel slag 1 and SS2 DRP removal curve slopes at 1 min retention time at 0.5 mg L^{-1} were not similar, -0.0004 vs -0.0363 respectively. The slopes of the DRP removal curves at 20 s retention time were similar for SS1 and SS2 at 3 mg L^{-1} (-0.0024 and -0.0029), SS2 1 mg L^{-1} (-0.0018), and SS2 at 0.5 mg L^{-}

^{1} (-0.0013). Steel slag 1 DRP removal curves had a similar, smaller slope at 20 s retention time at 1 and 0.5 mg L^{-1} (-0.0070 and -0.0074) when compared to 20 s retention time at 3 mg L^{-1}.

The retention time within each inflow DRP concentration either did not affect the slope of the DRP removal curve or the fastest retention time (20 s) decreased the slope of the DRP removal curves for both SS1 and SS2, except at 0.5 mg L^{-1} for SS2. All slopes of the DRP removal curves for SS1 and SS2 at 3 mg L^{-1} were similar across retention times within and across the type of PSM (-0.0046 to -0.0002). At 1 mg L^{-1}, the slopes of the DRP removal curves for all retention times were similar for both SS1 and SS2 (-0.0020 to 0.00104), except at 20 s retention time for SS1 (-0.0070). The slopes of the DRP removal curves for SS1 and SS2 at 0.5 mg L^{-1} across retention times were not as similar at the other DRP concentrations. The 2 and 1 min retention time slopes for SS1 DRP removal curves were similar at 0.5 mg L^{-1} (-0.0004 vs -0.0008), but were greater than the 20 s retention time (-0.0074) or the SS2 2 and 1 min retention time (-0.0363 and -0.0156). For SS2, the slope of the DRP removal curves at 0.5 mg L^{-1} increased as retention times increased.

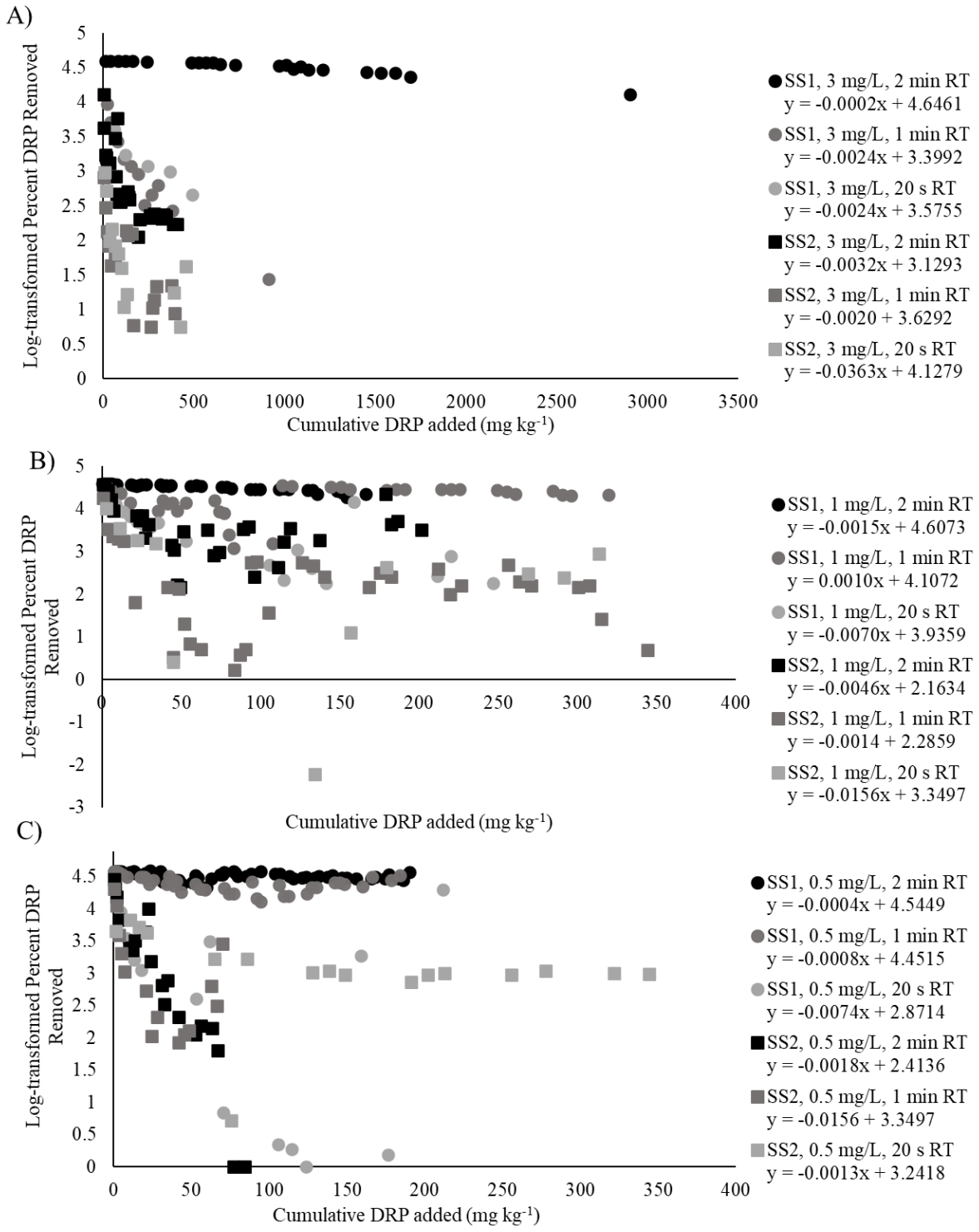

Figure 9. The flow-through column log-transformed percent DRP removed vs the cumulative DRP added (mg kg^{-1}) for each retention time (min) and initial solution DRP concentration (mg kg^{-1}) for both steel slag 1 (SS1) and steel slag 2 (SS2). Steel slag 1 is represented by circles and steel slag 2 is represented by squares. Each panel is for an initial solution DRP concentration of a) 3 mg L^{-1}, b) 1 mg L^{-1}, and c) 0.5 mg L^{-1}.

2.3.3 Flow-through column Sequential Fractionation for Al-, Fe-, and Ca-P

The percent DRP recovered by sequential extraction varied by fraction. DRP recovered as NH_4Cl was highly sensitive to PSM type and DRP concentration (Table 10). For NH_4Cl-P, all PSM type and DRP concentrations were similar (7 – 43% NH_4Cl-P) except for SS2 at 3 mg L^{-1} which was only similar to SS1 at 0.5 mg L^{-1} with -53% and 7% NH_4Cl-P respectively. Recovery of DRP as NH_4F was significantly affected by PSM type and DRP concentration as well as retention time and DRP concentration. For NH_4F-P, all PSM type and DRP concentrations were similar (6 – 56% NH_4F-P) except for SS2 at 3 mg L^{-1} which was only similar to SS2 at 1 mg L^{-1} with -129% and 6% NH_4F-P respectively. Retention time and DRP concentrations were all similar for DRP recovered as NH_4F (4 – 81%) except for the 2 min retention time at 3 mg L^{-1} (-210%). NaOH-P was similar for all PSM types, retention times, and DRP concentrations. Recovery of DRP as CBD was significantly affected by PSM type and DRP concentration. Steel slag 1 at 0.5 mg L^{-1} had greater CBD-P than SS2 at 0.5 mg L^{-1}, 7% vs -9% respectively. The CBD-P was similar for both SS1 and SS2 at 1 mg L^{-1} (2% and -3%) and at 3 mg L^{-1} (-13% and -3%). The H_2SO_4-P was similar for all PSM types, retention times, and DRP concentrations.

The sum of the percent of DRP recovered was used to indicate how much DRP was recovered across all sequentially extracted fractions. Steel slag 1 recovered 19 – 139% of the DRP that was removed by the PSM. For SS1 and SS2, the highest sum of percent DRP recovered occurred at 20 s retention time at 3 mg L^{-1}, 30% and 139% respectively. The lowest sum of percent DRP recovered for SS1 occurred at 1 min retention time at 1 mg L^{-1} (20%) and for SS1 at 2 min retention time at 3 mg L^{-1} (-491%). The sum of percent DRP recovered for SS2 ranged from -491 – 30% of the DRP that was removed in the flow-through columns. Inherent P was higher than DRP recovered for SS2 a majority of the retention time and DRP concentration

combinations, resulting in a negative recovery. There was a negative recovery for the combinations of 3 mg L^{-1} at 2 min retention time (-491%), 3 mg L^{-1} at 1 min retention time (-9%), 1 mg L^{-1} at 1 min retention time (-33%), 1 mg L^{-1} at 20 s retention time (-65%), and 0.5 mg L^{-1} at 2 min retention time (-122%).

Table 10.

The percent DRP recovered by steel slag 1 (SS1) and steel slag 2 (SS2) for each combination of DRP concentration (mg L^{-1}) and retention time (min) sequential fractionation after flow-through column experiment. Lowercase letter denotes significant difference ($p \leq 0.05$) of PSM type*DRP concentration. Uppercase letter denotes significant difference ($p \leq 0.05$) of retention time* DRP concentration. No letter denotes no significant difference ($p \leq 0.05$).

NH_4Cl-P

	3 mg L^{-1}						1 mg L^{-1}						0.5 mg L^{-1}					
	2 min		1 min		20 s		2 min		1 min		20 s		2 min		1 min		20 s	
	mean	se	mean	se	mean	se	mean	se	mean	se	mean	se	mean	se	mean	se	mean	se
SS1	11 a	1	59 a	21	60 a	15	18 a	0	6 a	0	8 a	2	6 ab	1	2 ab	1	14 ab	2
SS2	-170 b	140	-14 b	3	26 b	22	2 a	0	12 a	1	14 a	5	10 a	6	27 a	6	32 a	16

NH_4F-P

	3 mg L^{-1}						1 mg L^{-1}						0.5 mg L^{-1}					
	2 min		1 min		20 s		2 min		1 min		20 s		2 min		1 min		20 s	
	mean	se	mean	se	mean	se	mean	se	mean	se	mean	se	mean	se	mean	se	mean	se
SS1	12 aB	2	71 aA	20	87 aA	27	15 aA	1	8 aA	1	13 aA	2	14 aA	3	12 aA	1	20 aA	2
SS2	-433 bB	295	-30 bA	23	75 bA	66	1 bA	2	-1 bA	10	17 bA	15	-2 bA	11	50 bA	25	32 bA	4

NaOH-P

	3 mg L^{-1}						1 mg L^{-1}						0.5 mg L^{-1}					
	2 min		1 min		20 s		2 min		1 min		20 s		2 min		1 min		20 s	
	mean	se	mean	se	mean	se	mean	se	mean	se	mean	se	mean	se	mean	se	mean	se
SS1	0	0	0	0	0	0	0	0	1	0	4	2	1	1	0	0	2	2
SS2	-64	61	6	3	-34	18	-1	1	-2	1	-12	2	-10	5	-12	6	-16	8

CBD-P

	3 mg L^{-1}						1 mg L^{-1}						0.5 mg L^{-1}					
	2 min		1 min		20 s		2 min		1 min		20 s		2 min		1 min		20 s	
	mean	se	mean	se	mean	se	mean	se	mean	se	mean	se	mean	se	mean	se	mean	se
SS1	7 c	1	-16 c	11	-30 c	8	3 ab	2	1 ab	0	1 ab	2	9 a	1	13 a	0	0 a	2
SS2	-8 abc	17	11 abc	8	-13 abc	6	0 abc	1	-4 abc	5	-6 abc	7	-7 bc	10	-16 bc	13	-4 bc	7

H_2SO_4-P

	3 mg L^{-1}						1 mg L^{-1}						0.5 mg L^{-1}					
	2 min		1 min		20 s		2 min		1 min		20 s		2 min		1 min		20 s	
	mean	se	mean	se	mean	se	mean	se	mean	se	mean	se	mean	se	mean	se	mean	se
SS1	5	2	-87	26	22	48	3	2	3	0	-2	3	18	6	14	3	-4	4
SS2	184	348	18	48	-25	45	5	8	-38	17	-78	11	-114	37	-34	37	-25	30

Sum of Percent DRP Recovered

	3 mg L^{-1}						1 mg L^{-1}						0.5 mg L^{-1}					
	2 min		1 min		20 s		2 min		1 min		20 s		2 min		1 min		20 s	
	mean	se	mean	se	mean	se	mean	se	mean	se	mean	se	mean	se	mean	se	mean	se
SS1	35 B	4	27 B	11	139 B	88	39 A	4	20 A	1	24 A	8	47 A	9	40 A	4	32 A	5
SS2	-491 B	211	-9 B	85	30 B	108	8 A	10	-33A	28	-65 A	9	-122 A	56	14 A	51	19 A	37

2.3.4 DRP removal potential comparison for flow-through vs batch isotherm

SS1 removal of DRP was consistently higher than SS2 when evaluated by batch isotherms (S_{max}) or flow-through column experiments (cumulative removal). Batch isotherms showed DRP removal by SS2 continuing to increase with increasing initial DRP concentration, but in the flow-through columns at 3 mg L^{-1}, the opposite was shown. Cumulative DRP removed increased to a peak at 50 h (2 min retention time), 2 h (1 min retention time), and 8 h (20 s retention time) and then decreased until the end of the experiment and resulted in a net loss of P for the 2 min and 1 min retention time. The S_{max} for SS1 was 4-fold higher than SS2. Cumulative DRP removal from the flow-through columns for SS1 and SS2 was approximately only 10% of the S_{max} for 20,000 mg kg^{-1} determined by the batch isotherms. The S_{max} for 1000 mg kg^{-1} for SS1 was 16% less than the cumulative DRP removed for SS1 in the flow through columns and 19% higher for SS2. Steel slag 1 cumulative DRP removal was 4.4-fold higher than SS2 when averaged across all retention times and DRP concentrations. Steel slag 1 cumulative DRP removal was greater than SS2 at 3 mg L^{-1} (832 mg kg^{-1} vs -10 mg kg^{-1}), 2.3-fold greater at 1 mg L^{-1}, and 6.5-fold greater at 0.5 mg L^{-1}. At 2 min retention time, SS1 cumulative DRP removal was 3.8-fold greater than SS2 at 2 min retention time, 10.5-fold greater at 1 min retention time, and 2-fold greater at 20 s retention time.

2.4 Discussion

2.4.1 Batch sorption isotherm parameters

Our results were in mixed support of the hypothesis that omitting KCl from batch isotherms will have a higher DRP removal potential than KCl presence and in mixed support that constraining the DRP concentration to ≤ 1000 mg kg^{-1} will overestimate the DRP removal potential of PSM. There was higher percent DRP removal in the absence of KCl for both DRP concentration ranges, except for the PSM that still had 100% removal (AMDR1 ≤ 1000 mg kg^{-1}

and AMDR2 ≤ 1000 mg kg^{-1}). With a higher DRP concentration, the expected lower percent DRP removal as PSM approaches P-saturation [41,45] is observed for most of the factorial combinations.

The S_{max} from batch isotherms was not consistently higher with the use of an electrolyte solution vs not using an electrolyte solution for either DRP concentrations across the PSM. This is in contrast with the percent DRP removal that was consistently lower for the use of an electrolyte for both DRP concentrations. The lack of trends for S_{max} for KCl presence or absence can mostly be explained due to the lack of fit with the model. The fit of the Langmuir model is poor for many of the PSM factorial combinations studied, which is contrary to what other studies have found when evaluating SS and AMDR [45,47,133]. The S_{max} was sometimes lower than expected when compared to the percent DRP removal, particularly with SS2, AMDR1, and AMDR2 at ≤ 1000 mg kg^{-1}, KCl absence where there was 100% removal, but the S_{max} was below 1000 mg kg^{-1}. This discrepancy also indicates that the Langmuir model from which S_{max} is derived is not necessarily suitable for all PSM.

2.4.2 Flow-through Column Breakthrough Curves

Our results were in mixed support of the hypothesis that the combinations of retention time and inflow solution DRP concentration would have the same DRP removal on a mass basis for SS1 and SS2. As slopes of the removal curves were mostly only different between PSM type at 0.5 mg L^{-1} for all retention times, the best way to minimize discrepancies in estimated DRP removal potential between PSM types would be to use an inflow solution DRP concentration that is greater than 0.5 mg L^{-1} and less than 3 mg L^{-1}. Minimizing discrepancies is beneficial because in a P removal structure, each batch of PSM may be slightly different than before so it is pertinent that the design of the structure can provide conditions optimal for DRP removal for

multiple PSM. Other researchers have suggested that DRP concentration should be above 0.2 mg L^{-1} due to the inability of PSM to remove low DRP concentrations over an extended period of time [32]. Within PSM type, particularly SS1, the decrease in slope and DRP removal potential with faster retention time was due to shorter contact time of the PSM with the inflow solution DRP concentration. A retention time > 20 s and inflow solution DRP concentration > 0.5 mg L^{-1} would provide the most effective DRP removal on a mass basis for both types of PSM type for a P removal structure in the field. The same stipulations should be used for accessing and comparing DRP removal potential for PSM in flow-through columns to decrease the number of flow-through column experiments needed.

Although the comparison of slopes to test DRP removal potential is effective in determining differences in the removal curves of the flow-through columns, it does not have the ability to indicate if a PSM is losing P, as was the case with SS2 at 2 min and 1 min retention time at 3 mg L^{-1}. The outflow DRP concentration was greater than the inflow DRP concentration for these two flow-through combinations, eventually resulting in a negative cumulative DRP removed, indicating that the SS2 was not only releasing DRP already sorbed, but was also losing DRP that present in the PSM (inherent P). The loss of this P could be due to anaerobic conditions from the long retention time and resulting in Fe-P selective dissolution from inherent Fe-P. This occurrence is only present for SS2 though, not SS1 even though SS1 has a greater concentration of ammonium-oxalate extractable Fe and citrate-bicarbonate-dithionite extractable Fe. It also does not occur for the lower inflow solution DRP concentrations for SS2 indicating that this may only be an issue when there is higher DRP concentrations, which could be an issue in a field scenario if there is a high DRP loss event (e.g. rainfall event after fertilization).

2.4.3 Flow-Through Columns DRP Recovered by Sequentially Extracted Fraction

We found support for the hypothesis that the majority of DRP removed for SS in flow-through columns would be recovered primarily as NH_4Cl-P (soluble and loosely bound P), H_2SO_4-P (Ca-P), and NH_4F-P (Al-P), but not for the hypothesized increase in relative DRP recovery as NH_4F-P with decreasing retention time. As hypothesized, NH_4Cl-P, NH_4F-P, and H_2SO_4-P had the largest proportion of DRP recovered for SS1 and SS2 flow-through columns across all retention times and inflow solution DRP concentrations. DRP recovered as NH_4F, often interpreted as Al-P [59], was the only P fraction for which the effect of retention time depended on the inflow solution DRP concentration which supports the hypothesis, but only for 3 mg L^{-1}. This was likely due to the negative recovery by SS2 at 3 mg L^{-1} for 2 min and 1 min retention times decreasing the average percent DRP recovered as NH_4F and why the effect of retention time for NH_4F-P was not seen at the other two inflow solution DRP concentrations. Negative DRP recovery by SS2 at the highest DRP concentration (3 mg L^{-1}) and longer retention times (1 and 2 min) evaluated suggests under higher flow of more P-rich water, this particular SS released P. The majority of DRP recovered was as H_2SO_4 (Ca-P) for all flow-through column combinations which is in agreement with other studies [38,65]. It has been asserted that DRP removal by Ca-rich PSM such as SS occurs by precipitation [38], but this is an assumption that overlooks (relatively more rapid) P adsorption to Ca minerals. Studies evaluating P removal by Ca-rich minerals such as dolomite and calcite, which are present in SS [127], show that Ca adsorption can occur within 20 min to 3 h [129,134], whereas precipitation occurs at > 24 h [129]. The high percentage of DRP recovered as loosely and soluble-bound P would indicate that Ca removal with SS may occur as adsorption along with Fe and Al. The low NaOH-P is in alignment with results from [127], but is contrary to a higher level of NaOH-P for SS [61],[65],

indicating that Fe may be playing a larger role in DRP removal even for Ca-rich PSM. These two studies did not account for the inherent P, which has been shown to account for up to 100% of DRP recovered [127], of SS which could explain the higher NaOH-P. It is important to account for inherent P when performing sequentially extracted fractions in order to determine the magnitude of DRP recovered from what was removed and not P already present in the PSM.

2.4.4 Comparisons among DRP Removal Potential of Flow-through Columns vs Batch Isotherms

Our results support the hypothesis that batch isotherms (no electrolyte, $\leq$ 20,000 mg kg^{-1}) would lead to greater estimated DRP removal potential for SS1 and SS2 than flow-through columns, but were in mixed support that batch isotherms (no electrolyte, $\leq$ 1000 mg kg^{-1}) would underestimate DRP removal potential. These results support [49] findings that the S_{max} from batch isotherms did not match the S_{max} from flow-through columns at a retention time of 30 s. The batch isotherms with a DRP range $\leq$ 1000 mg kg^{-1} more closely estimated the DRP removal potential of the SS in the flow-through columns. It is difficult to compare the DRP removal potential, whether by S_{max} or percent DRP removal, between batch isotherms and flow-through column experiments as some PSM won't reach saturation, some PSM will experience desorption after saturation, and the initial DRP concentrations are typically not the same for the two methods. Although the DRP removal potential varies between the two methods, for every combination of retention time and initial solution DRP concentration, SS1 has a greater cumulative DRP removed than SS2, similar to the greater S_{max} of batch isotherms of both $\leq$ 1000 and $\leq$ 20,000 mg kg^{-1} without an electrolyte solution. For these PSM studied, the one with the greatest DRP removal potential remains the same.

One study [49] found that modeling flow-through columns better predicted DRP removal in a P removal structure than batch isotherms, thereby concluding that flow-through columns

should be used in the design of a P removal structure. Batch isotherms are still needed to screen PSM for DRP removal potential [107]. Columns are costly and time-consuming so being able to narrow down the PSM selection by DRP removal potential is necessary. Flow-through columns better simulate realistic conditions than batch isotherms but they still pose unrealistic conditions such as continuous flow until saturation instead of the wetting and drying that would come with intermittent rainfall events and the DRP solution used in the laboratory is distilled water which is not representative of agricultural runoff that contains other ions such as Ca, Mg, K, and Na [36].

2.5 Conclusions

The results of this study show that the methodology used to assess DRP removal potential can affect the measured DRP removal potential and comparability of PSM DRP removal potential. The use of an electrolyte solution decreased the percent DRP removed, but did not always lower S_{max} as expected when compared to a non-electrolyte solution. Additionally, S_{max} may not be an accurate metric when evaluating P-saturation capacity as some PSM had a greater DRP removal than the S_{max} indicated which could be due the some PSM batch sorption data having a poor fit to the Langmuir model. A standardized protocol is needed to improve the comparability of PSM DRP removal potential which should include a water solution (no electrolyte) and a DRP concentration range $\leq$ 1000 mg kg^{-1}. Based on the SS evaluated here, a retention time > 20 s and inflow solution DRP concentration > 0.5 mg L^{-1} would provide the most comparable DRP removal potential on a mass basis for both types of PSM type. Although a limited number of PSM were evaluated, the highest DRP removing PSM remained the same between batch isotherms and flow-through columns, but more efficiently (time, cost, effort) determined with batch isotherms. Batch isotherms should be used to determine the highest DRP removing PSM before any further testing in flow-through columns.

References

1. Jarvie, H.P.; Sharpley, A.N.; Flaten, D.; Kleinman, P.J.A.; Jenkins, A.; Simmons, T. The Pivotal Role of Phosphorus in a Resilient Water–Energy–Food Security Nexus. *Journal of Environmental Quality* **2015**, *44*, 1049-1062, doi:https://doi.org/10.2134/jeq2015.01.0030.
2. Liu, W.; Ciais, P.; Liu, X.; Yang, H.; Hoekstra, A.Y.; Tang, Q.; Wang, X.; Li, X.; Cheng, L. Global Phosphorus Losses from Croplands under Future Precipitation Scenarios. *Environmental Science & Technology* **2020**, *54*, 14761-14771, doi:10.1021/acs.est.0c03978.
3. Sharpley, A.N.; Smith, S.J.; Jones, O.R.; Berg, W.A.; Coleman, G.A. The Transport of Bioavailable Phosphorus in Agricultural Runoff. *Journal of Environmental Quality* **1992**, *21*, 30-35, doi:10.2134/jeq1992.00472425002100010003x.
4. McKelvie, I.D.; Peat, D.M.W.; Worsfold, P.J. Analytical perspective. Techniques for the quantification and speciation of phosphorus in natural waters. *Analytical Proceedings including Analytical Communications* **1995**, *32*, 437-445, doi:10.1039/AI9953200437.
5. Gentry, L.E.; David, M.B.; Royer, T.V.; Mitchell, C.A.; Starks, K.M. Phosphorus Transport Pathways to Streams in Tile-Drained Agricultural Watersheds. *Journal of Environmental Quality* **2007**, *36*, 408-415, doi:10.2134/jeq2006.0098.
6. Force, M.R.G.o.M.W.N.T. Gulf Hypoxia Action Plan 2008 for Reducing, Mitigating, and Controlling Hypoxia in the Northern Gulf of Mexico and Improving Water Quality in the Mississippi River Basin. USEPA, Ed. Washington D.C., 2008.
7. Robertson, D.M.; Saad, D.A. SPARROW models used to understand nutrient sources in the Mississippi/Atchafalaya River Basin. *Journal of Environmental Quality* **2013**, *42*, 1422-1440, doi:10.2134/jeq2013.02.0066.
8. Agency, M.P.C. The Minnesota Nutrient Reduction Strategy. **2014**.
9. Stewardship, I.D.o.A.a.L.; Resources, I.D.o.N.; Sciences, I.S.U.C.o.A.a.L. *Iowa Nutrient Reduction Strategy: A science and technology-based framework to assess and reduce nutrients to Iowa waters and the Gulf of Mexico*; 2013.
10. Force, M.R.G.o.M.W.N.T. Mississippi River Gulf of Mexico Watershed Nutrient Task Force New Goal Framework. USEPA, Ed. 2014.
11. Force, M.R.G.o.M.W.N.T. *Looking Forward: The Strategy of the Federal Members of the Hypoxia Task Force*; 2013.
12. Christianson, R.; Christianson, L.; Wong, C.; Helmers, M.; McIsaac, G.; Mulla, D.; McDonald, M. Beyond the nutrient strategies: Common ground to accelerate agricultural water quality improvement in the upper Midwest. *Journal of Environmental Management* **2018**, *206*, 1072-1080, doi:https://doi.org/10.1016/j.jenvman.2017.11.051.
13. Alexander, R.B.; Smith, R.A.; Schwarz, G.E.; Boyer, E.W.; Nolan, J.V.; Brakebill, J.W. Differences in Phosphorus and Nitrogen Delivery to The Gulf of Mexico from the Mississippi River Basin. *Environmental Science & Technology* **2008**, *42*, 822-830, doi:10.1021/es0716103.
14. ILEPA. Illinois Nutrient Loss Reduction Strategy. EPA, Ed. 2014.
15. ILEPA. Illinois Nutrient Loss Reduction Strategy: Biennial Report. EPA, Ed. 2019.
16. Ohio EPA, D.o.S.W.; Ohio Department of Agriculture, L.E.P.P.; Ohio Department of Natural Resources, D.o.S.a.W.R. *Ohio Nutrient Reduction Strategy*; 2013.

17. Kleinman, P.J.A.; Sharpley, A.N.; Saporito, L.S.; Buda, A.R.; Bryant, R.B. Application of manure to no-till soils: phosphorus losses by sub-surface and surface pathways. *Nutrient Cycling in Agroecosystems* **2009**, *84*, 215-227, doi:10.1007/s10705-008-9238-3.
18. Reid, K.; Schneider, K.; McConkey, B. Components of Phosphorus Loss From Agricultural Landscapes, and How to Incorporate Them Into Risk Assessment Tools. *Frontiers in Earth Science* **2018**, *6*, doi:10.3389/feart.2018.00135.
19. Addy, K.; Gold, A.J.; Christianson, L.E.; David, M.B.; Schipper, L.A.; Ratigan, N.A. Denitrifying Bioreactors for Nitrate Removal: A Meta-Analysis. *Journal of Environmental Quality* **2016**, *45*, 873-881, doi:https://doi.org/10.2134/jeq2015.07.0399.
20. Christianson, L.E.; Lepine, C.; Sibrell, P.L.; Penn, C.; Summerfelt, S.T. Denitrifying woodchip bioreactor and phosphorus filter pairing to minimize pollution swapping. *Water Research* **2017**, *121*, 129-139, doi:https://doi.org/10.1016/j.watres.2017.05.026.
21. Mayer, P.M.; Reynolds Jr., S.K.; McCutchen, M.D.; Canfield, T.J. Meta-Analysis of Nitrogen Removal in Riparian Buffers. *Journal of Environmental Quality* **2007**, *36*, 1172-1180, doi:https://doi.org/10.2134/jeq2006.0462.
22. Mankin, K.R.; Ngandu, D.M.; Barden, C.J.; Hutchinson, S.L.; Geyer, W.A. Grass-Shrub Riparian Buffer Removal of Sediment, Phosphorus, and Nitrogen From Simulated Runoff1. *JAWRA Journal of the American Water Resources Association* **2007**, *43*, 1108-1116, doi:https://doi.org/10.1111/j.1752-1688.2007.00090.x.
23. Saunders, D.L.; Kalff, J. Nitrogen retention in wetlands, lakes and rivers. *Hydrobiologia* **2001**, *443*, 205-212, doi:10.1023/A:1017506914063.
24. Uusi-Kämppä, J.; Braskerud, B.; Jansson, H.; Syversen, N.; Uusitalo, R. Buffer Zones and Constructed Wetlands as Filters for Agricultural Phosphorus. *Journal of Environmental Quality* **2000**, *29*, 151-158, doi:https://doi.org/10.2134/jeq2000.00472425002900010019x.
25. Hey, D.L.; Kenimer, A.L.; Barrett, K.R. Water quality improvement by four experimental wetlands. *Ecological Engineering* **1994**, *3*, 381-397, doi:https://doi.org/10.1016/0925-8574(94)00008-5.
26. Kovacic, D.A.; David, M.B.; Gentry, L.E.; Starks, K.M.; Cooke, R.A. Effectiveness of Constructed Wetlands in Reducing Nitrogen and Phosphorus Export from Agricultural Tile Drainage. *Journal of Environmental Quality* **2000**, *29*, 1262-1274, doi:10.2134/jeq2000.00472425002900040033x.
27. Kadlec, R.H. Large Constructed Wetlands for Phosphorus Control: A Review. *Water* **2016**, *8*, 243.
28. Dillaha, T.A.; Sherrard, J.H.; Lee, D.; Mostaghimi, S.; Shanholtz, V.O. Evaluation of Vegetative Filter Strips as a Best Management Practice for Feed Lots. *Journal (Water Pollution Control Federation)* **1988**, *60*, 1231-1238.
29. Lee, K.-H.; Isenhart, T.M.; Schultz, R.C.; Mickelson, S.K. Multispecies Riparian Buffers Trap Sediment and Nutrients during Rainfall Simulations. *Journal of Environmental Quality* **2000**, *29*, 1200-1205, doi:https://doi.org/10.2134/jeq2000.00472425002900040025x.
30. Lowrance, R.; Sheridan, J.M. Surface Runoff Water Quality in a Managed Three Zone Riparian Buffer. *Journal of Environmental Quality* **2005**, *34*, 1851-1859, doi:https://doi.org/10.2134/jeq2004.0291.
31. Uusi-Kämppä, J. Phosphorus purification in buffer zones in cold climates. *Ecological Engineering* **2005**, *24*, 491-502, doi:https://doi.org/10.1016/j.ecoleng.2005.01.013.

32. Penn, C.; McGrath, J.; Bowen, J.; Wilson, S. Phosphorus removal structures: A management option for legacy phosphorus. *Journal of Soil and Water Conservation* **2014**, *69*, 51A-56A, doi:10.2489/jswc.69.2.51A.
33. Shedekar, V.S.; Penn, C.J.; Pease, L.; King, K.W.; Kalcic, M.M.; Livingston, S.J. Performance of a Ditch-Style Phosphorus Removal Structure for Treating Agricultural Drainage Water with Aluminum-Treated Steel Slag. *Water* **2020**, *12*, 2149.
34. Penn, C.; Livingston, S.; Shedekar, V.; King, K.; Williams, M. Performance of Field-Scale Phosphorus Removal Structures Utilizing Steel Slag for Treatment of Subsurface Drainage. *Water* **2020**, *12*, 443.
35. Indiana State Department of Agriculture, D.o.S.C.; Management, I.D.o.E. *Indiana Nutrient Reduction Strategy: A framework to reduce nutrients entering Indiana's waters*; 2016.
36. Penn, C.J.; Bryant, R.B.; Kleinman, P.J.A.; Allen, A.L. Removing dissolved phosphorus from drainage ditch water with phosphorus sorbing materials. *Journal of Soil and Water Conservation* **2007**, *62*, 269-276.
37. Stoner, D.; Penn, C.; McGrath, J.; Warren, J. Phosphorus Removal with By-Products in a Flow-Through Setting. *Journal of Environmental Quality* **2012**, *41*, 654-663, doi:10.2134/jeq2011.0049.
38. Penn, C.J.; Bryant, R.B.; Callahan, M.P.; McGrath, J.M. Use of Industrial By-products to Sorb and Retain Phosphorus. *Communications in Soil Science and Plant Analysis* **2011**, *42*, 633-644, doi:10.1080/00103624.2011.550374.
39. Cucarella, V.; Renman, G. Phosphorus Sorption Capacity of Filter Materials Used for On-site Wastewater Treatment Determined in Batch Experiments–A Comparative Study. *Journal of Environmental Quality* **2009**, *38*, 381-392, doi:10.2134/jeq2008.0192.
40. Ragheb, S.M. Phosphate removal from aqueous solution using slag and fly ash. *HBRC Journal* **2013**, *9*, 270-275, doi:https://doi.org/10.1016/j.hbrcj.2013.08.005.
41. Drizo, A.; Frost, C.A.; Grace, J.; Smith, K.A. Physico-chemical screening of phosphate-removing substrates for use in constructed wetland systems. *Water Research* **1999**, *33*, 3595-3602, doi:https://doi.org/10.1016/S0043-1354(99)00082-2.
42. King, K.W.; Williams, M.R.; Dick, W.A.; LaBarge, G.A. Decreasing Phosphorus Loss in Tile-Drained Landscapes Using Flue Gas Desulfurization Gypsum. *Journal of Environmental Quality* **2016**, *45*, 1722-1730, doi:10.2134/jeq2016.04.0132.
43. Bryant, R.B.; Buda, A.R.; Kleinman, P.J.A.; Church, C.D.; Saporito, L.S.; Folmar, G.J.; Bose, S.; Allen, A.L. Using Flue Gas Desulfurization Gypsum to Remove Dissolved Phosphorus from Agricultural Drainage Waters. *Journal of Environmental Quality* **2012**, *41*, 664-671, doi:10.2134/jeq2011.0294.
44. Gottschall, N.; Edwards, M.; Craiovan, E.; Frey, S.K.; Sunohara, M.; Ball, B.; Zoski, E.; Topp, E.; Khan, I.; Clark, I.D., et al. Amending woodchip bioreactors with water treatment plant residuals to treat nitrogen, phosphorus, and veterinary antibiotic compounds in tile drainage. *Ecological Engineering* **2016**, *95*, 852-864, doi:https://doi.org/10.1016/j.ecoleng.2016.06.011.
45. Leader, J.W.; Dunne, E.J.; Reddy, K.R. Phosphorus Sorbing Materials: Sorption Dynamics and Physicochemical Characteristics. *Journal of Environmental Quality* **2008**, *37*, 174-181, doi:10.2134/jeq2007.0148.

46. Gibbs, M.M.; Hickey, C.W.; Özkundakci, D. Sustainability assessment and comparison of efficacy of four P-inactivation agents for managing internal phosphorus loads in lakes: sediment incubations. *Hydrobiologia* **2010**, *658*, 253-275.
47. Sibrell, P.L.; Montgomery, G.A.; Ritenour, K.L.; Tucker, T.W. Removal of phosphorus from agricultural wastewaters using adsorption media prepared from acid mine drainage sludge. *Water Research* **2009**, *43*, 2240-2250, doi:https://doi.org/10.1016/j.watres.2009.02.010.
48. Sibrell, P.L.; Tucker, T.W. Fixed bed sorption of phosphorus from wastewater using iron oxide-based media derived from acid mine drainage. *Water, Air, & Soil Pollution* **2012**, *223*, 5105-5117, doi:10.1007/s11270-012-1262-x.
49. Penn, C.J.; McGrath, J.M. Predicting Phosphorus Sorption onto Steel Slag Using a Flow-through approach with Application to a Pilot Scale System. *Journal of Water Resource and Protection* **2011**, *Vol.03No.04*, 10, doi:10.4236/jwarp.2011.34030.
50. Penn, C.J.; McGrath, J.M.; Rounds, E.; Fox, G.; Heeren, D. Trapping Phosphorus in Runoff with a Phosphorus Removal Structure. *Journal of Environmental Quality* **2012**, *41*, 672-679, doi:10.2134/jeq2011.0045.
51. Hou, L.; Liang, Q.; Wang, F. Mechanisms that control the adsorption–desorption behavior of phosphate on magnetite nanoparticles: the role of particle size and surface chemistry characteristics. *RSC Advances* **2020**, *10*, 2378-2388, doi:10.1039/C9RA08517C.
52. Liu, D.; Zhu, H.; Wu, K.; Wang, F.; Zhao, X.; Liao, Q. Understanding the effect of particle size of waste concrete powder on phosphorus removal efficiency. *Construction and Building Materials* **2020**, *236*, 117526, doi:https://doi.org/10.1016/j.conbuildmat.2019.117526.
53. Penn, C.; Bowen, J.; McGrath, J.; Nairn, R.; Fox, G.; Brown, G.; Wilson, S.; Gill, C. Evaluation of a universal flow-through model for predicting and designing phosphorus removal structures. *Chemosphere* **2016**, *151*, 345-355, doi:https://doi.org/10.1016/j.chemosphere.2016.02.105.
54. Kostura, B.; Kulveitová, H.; Leško, J. Blast furnace slags as sorbents of phosphate from water solutions. *Water Research* **2005**, *39*, 1795-1802, doi:https://doi.org/10.1016/j.watres.2005.03.010.
55. Sanford, J.R.; Larson, R.A. Evaluation of Phosphorus Filter Media for an Inline Subsurface Drainage Treatment System. *Journal of Environmental Quality* **2016**, *45*, 1919-1925, doi:10.2134/jeq2016.01.0038.
56. Hemwall, J.B. The Fixation of Phosphorus by Soils. In *Advances in Agronomy*, Norman, A.G., Ed. Academic Press: 1957; Vol. 9, pp. 95-112.
57. Dayton, E.A.; Basta, N.T. A Method for Determining the Phosphorus Sorption Capacity and Amorphous Aluminum of Aluminum-Based Drinking Water Treatement Residuals. *Journal of Environmental Quality* **2005**, *34*, 1112-1118.
58. McKeague, J.; Day, J.H. Dithionite and oxalate-extractable Fe and Al as aids in differentiation various classes of soils. *Canadian Journal of Soil Science* **1966**, *46*, 13-22.
59. Zhang, H.; Kovar, J.L. Fractionation of Soil Phosphorus. In *Methods of Phosphorus Analysis for Soils, Sediments, Residuals, and Waters*, Second Edition ed.; Kovar, J.L., Pierzynski, G.M., Eds. SERA-IEG 17: Southern Cooperative Series Bulletin No. 408, 2009.

60. Chang, S.C.; Jackson, M.L. Fractionation of soil phosphorus. *Soil Science* **1957**, *84*, 133-144.
61. Drizo, A.; Comeau, Y.; Forget, C.; Chapuis, R.P. Phosphorus Saturation Potential: A Parameter for Estimating the Longevity of Constructed Wetland Systems. *Environmental Science & Technology* **2002**, *36*, 4642-4648, doi:10.1021/es011502v.
62. Ballantine, D.J.; Tanner, C.C. Substrate and filter materials to enhance phosphorus removal in constructed wetlands treating diffuse farm runoff: a review. *New Zealand Journal of Agricultural Research* **2010**, *53*, 71-95, doi:10.1080/00288231003685843.
63. Mann, R.; Bavor, H.J. Phosphorus Removal in Constructed Wetlands Using Gravel and Industrial Waste Substrata. *Water Science and Technology* **1993**, *27*, 107-113, doi:10.2166/wst.1993.0027.
64. Sakadevan, K.; Bavor, H.J. Phosphate adsorption characteristics of soils, slags and zeolite to be used as substrates in constructed wetland systems. *Water Research* **1998**, *32*, 393-399, doi:https://doi.org/10.1016/S0043-1354(97)00271-6.
65. Drizo, A.; Cummings, J.; Weber, D.; Twohig, E.; Druschel, G.; Bourke, B. New Evidence for Rejuvenation of Phosphorus Retention Capacity in EAF Steel Slag. *Environmental Science & Technology* **2008**, *42*, 6191-6197, doi:10.1021/es800232r.
66. Nancucheo, I.; Bitencourt, J.A.P.; Sahoo, P.K.; Alves, J.O.; Siqueira, J.O.; Oliveira, G. Recent Developments for Remediating Acidic Mine Waters Using Sulfidogenic Bacteria. *BioMed Research International* **2017**, *2017*, 7256582, doi:10.1155/2017/7256582.
67. Kefeni, K.K.; Msagati, T.A.M.; Mamba, B.B. Acid mine drainage: Prevention, treatment options, and resource recovery: A review. *Journal of Cleaner Production* **2017**, *151*, 475-493.
68. Gavlak, R.; Horneck, D.; Miller, R. Particle Size Analysis: Hydrometer Method. In *Soil, plant and water reference methods for the Western Region*, WERA-103 Technical Committee: Western Regional Extension Publication (WREP) 125, 2005.
69. Standard, A.; D422. Standard Test Method for Particle-Size Analysis of Soils. West Conshohocken, PA, 1963 (1998).
70. Peters, J.B.; Nathan, M.V.; Laboski, C.A.M. Chapter 4: pH and Lime Requirement. In *Recommended Chemical Soil Test Procedures for the North Central Region* North Central Regional Research Publication 221 (Revised), 2015.
71. Xu, D.; Xu, J.; Wu, J.; Muhammad, A. Studies on the phosphorus sorption capacity of substrates used in constructed wetland systems. *Chemosphere* **2006**, *63*, 344-352, doi:https://doi.org/10.1016/j.chemosphere.2005.08.036.
72. Murphy, J.; Riley, J.P. A modified single solution method for the determination of phosphate in natural waters. *Analytica Chimica Acta* **1962**, *27*, 31-36, doi:https://doi.org/10.1016/S0003-2670(00)88444-5.
73. EPA, U.S. Method 3050B: Acid digestion of sediments, sludges, and soils. Washington, DC, 1996.
74. Sparks, D.L.; Page, A.; Helmke, P.; Loeppert, R.; Soltanpour, P.; Tabatabai, M.; Johnston, C.; Sumner, M. Methods of soil analysis. Part 3-Chemical methods. *Soil Science Society of America* **1996**.
75. Guan, X.-H.; Liu, Q.; Chen, G.-H.; Shang, C. Surface complexation of condensed phosphate to aluminum hydroxide: An ATR-FTIR spectroscopic investigation. *Journal of Colloid and Interface Science* **2005**, *289*, 319-327, doi:https://doi.org/10.1016/j.jcis.2004.08.041.

76. Margenot, A.J.; Calderón, F.J.; Parikh, S.J. Limitations and Potential of Spectral Subtractions in Fourier-Transform Infrared Spectroscopy of Soil Samples. *Soil Science Society of America Journal* **2015**, *80*, 10-26.
77. Yildirim, I.Z.; Prezzi, M. Steel Slag: Chemistry, Mineralogy, and Morphology. In *IFCEE 2015*, 2015; doi:10.1061/9780784479087.263pp. 2816-2825.
78. Yildirim, I.Z.; Prezzi, M. Chemical, Mineralogical, and Morphological Properties of Steel Slag. *Advances in Civil Engineering* **2011**, *2011*, 463638, doi:10.1155/2011/463638.
79. Geiseler, J. Use of steelworks slag in Europe. *Waste Management* **1996**, *16*, 59-63, doi:https://doi.org/10.1016/S0956-053X(96)00070-0.
80. Reddy, A.S.; Pradhan, R.K.; Chandra, S. Utilization of Basic Oxygen Furnace (BOF) slag in the production of a hydraulic cement binder. *International Journal of Mineral Processing* **2006**, *79*, 98-105, doi:https://doi.org/10.1016/j.minpro.2006.01.001.
81. Tzevelekou, T.; Lampropoulou, P.; Giannakopoulou, P.P.; Rogkala, A.; Koutsovitis, P.; Koukouzas, N.; Petrounias, P. Valorization of Slags Produced by Smelting of Metallurgical Dusts and Lateritic Ore Fines in Manufacturing of Slag Cements. *Applied Sciences* **2020**, *10*, 4670.
82. Wachsmuth, F.; Geiseler, J.; Fix, W.; Koch, K.; Schwerdtfeger, K. Contribution to the Structure of BOF-Slags and its Influence on Their Volume Stability. *Canadian Metallurgical Quarterly* **1981**, *20*, 279-284, doi:10.1179/cmq.1981.20.3.279.
83. Juckes, L.M. The volume stability of modern steelmaking slags. *Mineral Processing and Extractive Metallurgy* **2003**, *112*, 177-197, doi:10.1179/037195503225003708.
84. Tsakiridis, P.E.; Papadimitriou, G.D.; Tsivilis, S.; Koroneos, C. Utilization of steel slag for Portland cement clinker production. *Journal of hazardous materials* **2008**, *152*, 805-811, doi:https://doi.org/10.1016/j.jhazmat.2007.07.093.
85. Tossavainen, M.; Engstrom, F.; Yang, Q.; Menad, N.; Lidstrom Larsson, M.; Bjorkman, B. Characteristics of steel slag under different cooling conditions. *Waste Management* **2007**, *27*, 1335-1344, doi:https://doi.org/10.1016/j.wasman.2006.08.002.
86. Nicolae, M.; Vîlciu, I. X-RAY DIFFRACTION ANALYSIS OF STEEL SLAG AND BLAST FURNACE SLAG VIEWING THEIR USE FOR ROAD CONSTRUCTION.
87. Qian, G.R.; Sun, D.D.; Tay, J.H.; Lai, Z.Y. Hydrothermal reaction and autoclave stability of Mg bearing RO phase in steel slag. *British Ceramic Transactions* **2002**, *101*, 159-164, doi:10.1179/096797802225003415.
88. Masindi, V. Recovery of drinking water and valuable minerals from acid mine drainage using an integration of magnesite, lime, soda ash, CO2 and reverse osmosis treatment processes. *Journal of Environmental Chemical Engineering* **2017**, *5*, 3136-3142, doi:https://doi.org/10.1016/j.jece.2017.06.025.
89. Masindi, V.; Madzivire, G.; Tekere, M. Reclamation of water and the synthesis of gypsum and limestone from acid mine drainage treatment process using a combination of pre-treated magnesite nanosheets, lime, and CO2 bubbling. *Water Resources and Industry* **2018**, *20*, 1-14, doi:https://doi.org/10.1016/j.wri.2018.07.001.
90. Masindi, V.; Osman, M.S.; Shingwenyana, R. Valorization of acid mine drainage (AMD): A simplified approach to reclaim drinking water and synthesize valuable minerals – Pilot study. *Journal of Environmental Chemical Engineering* **2019**, *7*, 103082, doi:https://doi.org/10.1016/j.jece.2019.103082.

91. Blanch, A.J.; Quinton, J.S.; Lenehan, C.E.; Pring, A. The crystal chemistry of Al-bearing goethites: an infrared spectroscopic study. *Mineralogical Magazine* **2008**, *72*, 1043-1056, doi:10.1180/minmag.2008.072.5.1043.
92. Ruan, H.D.; Frost, R.L.; Kloprogge, J.T. The behavior of hydroxyl units of synthetic goethite and its dehydroxylated product hematite. *Spectrochimica Acta Part A: Molecular and Biomolecular Spectroscopy* **2001**, *57*, 2575-2586, doi:https://doi.org/10.1016/S1386-1425(01)00445-0.
93. Cui, H.; Ren, W.; Lin, P.; Liu, Y. Structure control synthesis of iron oxide polymorph nanoparticles through an epoxide precipitation route. *Journal of Experimental Nanoscience* **2013**, *8*, 869–875, doi:10.1080/17458080.2011.616541.
94. Cambier, P. Infrared study of goethites of varying crystallinity and particle size: I. Interpretation of OH and lattice vibration frequencies. *Clay Minerals* **1986**, *21*, 191-200, doi:10.1180/claymin.1986.021.2.08.
95. Margenot, A.J.; Calderón, F.J.; Goyne, K.W.; Mukome, F.N.D.; Parikh, S.J. IR Spectroscopy, Soil Analysis Applications. In *Encyclopedia of Spectroscopy and Spectrometry (Third Edition)*, Lindon, J.C., Tranter, G.E., Koppenaal, D.W., Eds. Academic Press: Oxford, 2017; https://doi.org/10.1016/B978-0-12-409547-2.12170-5pp. 448-454.
96. Vahur, S.; Teearu, A.; Peets, P.; Joosu, L.; Leito, I. ATR-FT-IR spectral collection of conservation materials in the extended region of 4000-80 cm–1. *Analytical and Bioanalytical Chemistry* **2016**, *408*, 3373-3379, doi:10.1007/s00216-016-9411-5.
97. Frost, R.L.; Kloprogge, J.T. Infrared emission spectroscopic study of brucite. *Spectrochimica Acta Part A: Molecular and Biomolecular Spectroscopy* **1999**, *55*, 2195-2205, doi:https://doi.org/10.1016/S1386-1425(99)00016-5.
98. Reig, F.B.; Adelantado, J.V.G.; Moya Moreno, M.C.M. FTIR quantitative analysis of calcium carbonate (calcite) and silica (quartz) mixtures using the constant ratio method. Application to geological samples. *Talanta* **2002**, *58*, 811-821, doi:https://doi.org/10.1016/S0039-9140(02)00372-7.
99. Campbell, S.; Poduska, K.M. Incorporating Far-Infrared Data into Carbonate Mineral Analyses. *Minerals* **2020**, *10*, 628.
100. Toffolo, M.B.; Regev, L.; Dubernet, S.; Lefrais, Y.; Boaretto, E. FTIR-Based Crystallinity Assessment of Aragonite–Calcite Mixtures in Archaeological Lime Binders Altered by Diagenesis. *Minerals* **2019**, *9*, 121.
101. Rodriguez-Blanco, J.; Shaw, S.; Benning, L. The Kinetics and Mechanisms of Amorphous Calcium Carbonate (ACC) Crystallization to Calcite, Via Vaterite. *Nanoscale* **2010**, *3*, 265-271, doi:10.1039/c0nr00589d.
102. Zuleta, F.; Murciano, A.; Gehrke, S.A.; Maté-Sánchez de Val, J.E.; Calvo-Guirado, J.L.; De Aza, P.N. A New Biphasic Dicalcium Silicate Bone Cement Implant. *Materials (Basel)* **2017**, *10*, 758, doi:10.3390/ma10070758.
103. Horgnies, M.; Chen, J.J.; Bouillon, C. Overview about the use of Fourier Transform Infrared spectroscopy to study cementitious materials. *WIT Transactions on Engineering Sciences* **2013**, *77*.
104. Parikh, S.J.; Goyne, K.W.; Margenot, A.J.; Mukome, F.N.D.; Calderón, F.J. Chapter One - Soil Chemical Insights Provided through Vibrational Spectroscopy. In *Advances in Agronomy*, Sparks, D.L., Ed. Academic Press: 2014; Vol. 126, pp. 1-148.

105. Yasipourtehrani, S.; Strezov, V.; Evans, T. Investigation of Phosphate Removal Capability of Blast Furnace Slag in Wastewater Treatment. *Scientific Reports* **2019**, *9*, 7498, doi:10.1038/s41598-019-43896-y.
106. Ruan, H.D.; Frost, R.L.; Kloprogge, J.T.; Duong, L. Far-infrared spectroscopy of alumina phases. *Spectrochimica Acta Part A: Molecular and Biomolecular Spectroscopy* **2002**, *58*, 265-272, doi:https://doi.org/10.1016/S1386-1425(01)00532-7.
107. Penn, C.; Bowen, J. *Design and Construction of Phosphorus Removal Structures for Improving Water Quality*; 2018; 10.1007/978-3-319-58658-8.
108. NRCS, U. Part 630 Hydrology National Engineering Handbook. Washington, D.C., 2007.
109. Li, S.; Cooke, R.A.; Huang, X.; Christianson, L.; Bhattarai, R. Evaluation of fly ash pellets for phosphorus removal in a laboratory scale denitrifying bioreactor. *Journal of Environmental Management* **2018**, *207*, 269-275, doi:https://doi.org/10.1016/j.jenvman.2017.11.040.
110. Boujelben, N.; Bouzid, J.; Elouear, Z.; Feki, M.; Jamoussi, F.; Montiel, A. Phosphorus removal from aqueous solution using iron coated natural and engineered sorbents. *Journal of hazardous materials* **2008**, *151*, 103-110, doi:https://doi.org/10.1016/j.jhazmat.2007.05.057.
111. Hertzberger, A.; Pittelkow, C.; Harmel, R.; Christianson, L. Analysis of the MANAGE Drain Concentration Database to Evaluate Agricultural Management Effects on Drainage Water Nutrient Concentrations. *Transactions of the ASABE* **2019**, *62*, 929-939, doi:10.13031/trans.13230.
112. Scholtz, E.C.; Feldkamp, J.R.; White, J.L.; Hem, S.L. Point of zero charge of amorphous aluminum hydroxide as a function of adsorbed carbonate. *Journal of Pharmaceutical Sciences* **1985**, *74*, 478-481, doi:https://doi.org/10.1002/jps.2600740423.
113. Parks, G.A.; Bruyn, P.L.d. The Zero Point of Charge of Oxides. *The Journal of Physical Chemistry* **1962**, *66*, 967-973, doi:10.1021/j100812a002.
114. Mann, R.A. Phosphorus adsorption and desorption characteristics of constructed wetland gravel and steelworks by-products. *Australian Journal of Soil Research* **1997**, *35*, 375-384.
115. Barrow, N.J.; Sen, A.; Roy, N.; Debnath, A. The soil phosphate fractionation fallacy. *Plant and Soil* **2020**, 10.1007/s11104-020-04476-6, doi:10.1007/s11104-020-04476-6.
116. Administration, F.H. User Guidelines for Waste and Byproduct Materials in Pavement Construction. Transportation, U.D.o., Ed. Washington, DC, 2016.
117. USEPA. Technical Document: Acid Mine Drainage Prediction. USEPA, Ed. Washington, DC, 1994.
118. Mahony, B.; Moulson, I.; Wilkinson, H.C. Study of the relation between the phosphorus content of coal and coke. *Fuel* **1981**, *60*, 355-358, doi:https://doi.org/10.1016/0016-2361(81)90206-4.
119. Thomas Sims, J.; Kleinman, P.J.A. Managing Agricultural Phosphorus for Environmental Protection. In *Phosphorus: Agriculture and the Environment*, 2005; https://doi.org/10.2134/agronmonogr46.c31pp. 1021-1068.
120. Liu, J.; Macrae, M.L.; Elliott, J.A.; Baulch, H.M.; Wilson, H.F.; Kleinman, P.J.A. Impacts of Cover Crops and Crop Residues on Phosphorus Losses in Cold Climates: A Review. *Journal of Environmental Quality* **2019**, *48*, 850-868, doi:https://doi.org/10.2134/jeq2019.03.0119.

121. Graetz, D.A.; Nair, V.D. Phosphorus Sorption Isotherm Determination. In *Methods of Phosphorus Analysis for Soils, Sediments, Residuals, and Waters*, Kovar, J.L., Pierzynski, G.M., Eds. SERA-IEG 17: Southern Cooperative Series Bulletin No. 408, 2009.
122. Nair, P.S.; Logan, T.J.; Sharpley, A.N.; Sommers, L.E.; Tabatabai, M.A.; Yuan, T.L. Interlaboratory Comparison of a Standardized Phosphorus Adsorption Procedure. *Journal of Environmental Quality* **1984**, *13*, 591-595, doi:https://doi.org/10.2134/jeq1984.00472425001300040016x.
123. Barrow, N.J. The Description of Phosphate Adsorption Curves. *Journal of Soil Science* **1978**, *29*, 447-462, doi:https://doi.org/10.1111/j.1365-2389.1978.tb00794.x.
124. Søvik, A.K.; Kløve, B. Phosphorus retention processes in shell sand filter systems treating municipal wastewater. *Ecological Engineering* **2005**, *25*, 168-182, doi:https://doi.org/10.1016/j.ecoleng.2005.04.007.
125. Agyei, N.M.; Strydom, C.A.; Potgieter, J.H. The removal of phosphate ions from aqueous solution by fly ash, slag, ordinary Portland cement and related blends. *Cement and Concrete Research* **2002**, *32*, 1889-1897, doi:https://doi.org/10.1016/S0008-8846(02)00888-8.
126. Bellier, N.; Chazarenc, F.; Comeau, Y. Phosphorus removal from wastewater by mineral apatite. *Water Research* **2006**, *40*, 2965-2971, doi:https://doi.org/10.1016/j.watres.2006.05.016.
127. Berkshire, T.; Christianson, R.; Christianson, L.; Margenot, A.J. Evaluating relationships among physical and chemical properties of phosphorus-sorbing material to optimize phosphorus removal for edge-of-field phosphorus filters. **In Prep**.
128. Lyngsie, G.; Penn, C.J.; Pedersen, H.L.; Borggaard, O.K.; Hansen, H.C.B. Modelling of phosphate retention by Ca- and Fe-rich filter materials under flow-through conditions. *Ecological Engineering* **2015**, *75*, 93-102, doi:https://doi.org/10.1016/j.ecoleng.2014.11.009.
129. Li, Z.; Sun, X.; Huang, L.; Liu, D.; Yu, L.; Wu, H.; Wei, D. Phosphate adsorption and precipitation on calcite under calco-carbonic equilibrium condition. *Chemosphere* **2017**, *183*, 419-428, doi:https://doi.org/10.1016/j.chemosphere.2017.05.139.
130. Strauss, R.; Brümmer, G.W.; Barrow, N.J. Effects of crystallinity of goethite: II. Rates of sorption and desorption of phosphate. *European Journal of Soil Science* **1997**, *48*, 101-114, doi:https://doi.org/10.1111/j.1365-2389.1997.tb00189.x.
131. Luengo, C.; Brigante, M.; Antelo, J.; Avena, M. Kinetics of phosphate adsorption on goethite: Comparing batch adsorption and ATR-IR measurements. *Journal of Colloid and Interface Science* **2006**, *300*, 511-518, doi:https://doi.org/10.1016/j.jcis.2006.04.015.
132. Olsen, S.R.; Watanabe, F.S. A Method to Determine a Phosphorus Adsorption Maximum of Soils as Measured by the Langmuir Isotherm1. *Soil Science Society of America Journal* **1957**, *21*, 144-149, doi:10.2136/sssaj1957.03615995002100020004x.
133. Cheung, K.C.; Venkitachalam, T.H.; Scott, W.D. Selecting soil amendment materials for removal of phosphorus. *Water Science and Technology* **1994**, *30*, 247-256, doi:10.2166/wst.1994.0275.
134. Yuan, X.; Xia, W.; An, J.; Yin, J.; Zhou, X.; Yang, W. Kinetic and Thermodynamic Studies on the Phosphate Adsorption Removal by Dolomite Mineral. *Journal of Chemistry* **2015**, *2015*, 853105, doi:10.1155/2015/853105.